UNIVERSITAT DE
BARCELONA

Improving islet-graft revascularization

Hugo Jorge Alves Figueiredo

This page is intentionally left in blank

UNIVERSITAT DE
BARCELONA

FACULTAT DE FARMÀCIA I CIÈNCIES DE L'ALIMENTACIÓ

PROGRAMA DE DOCTORAT EN BIOMEDICINA

Improving islet-graft revascularization

Thesis presented by Hugo Jorge Alves Figueiredo

for the degree of Ph.D. at the University of Barcelona

Hugo Jorge Alves Figueiredo

2018

UNIVERSITAT DE
BARCELONA

FACULTAT DE FARMÀCIA I CIÈNCIES DE L'ALIMENTACIÓ

PROGRAMA DE DOCTORAT EN BIOMEDICINA

Improving islet-graft revascularization

Thesis presented by **Hugo Jorge Alves Figueiredo**

for the degree of Ph.D. at the University of Barcelona

Supervisors

Prof. Ramon Gomis de Barbarà

Dra. Rita M. Martins de Sousa Maia Malpique

Barcelona, 2018

This work was developed at the Diabetes and Obesity Research Laboratory, at the Institut d'Investigacions Biomèdiques August Pi i Sunyer (IDIBAPS), Barcelona, Spain

IDIBAPS

Institut
D'Investigacions
Biomèdiques
August Pi i Sunyer

Acknowledgments

Se han pasado casi 7 años, y ahora se cierra el ciclo. Llevo conmigo, muchas alegrías, mucho crecimiento personal y profesional y muchas amistades. Quiero agradecer en especial a mis directores. Al Dr. Ramón Gomis, por haber apostado y acreditado en mí, por haber exigido y sacado lo mejor que hay en mí. A él le debo, en gran parte mi crecimiento como científico y como persona. Gracias, Ramón! A la Dra. Rita Malpique, responsable por mí llegada a Barcelona y que me acogió en su casa, cuando llegué a Barcelona, sin conocer a nadie ni saber una única palabra de español. Como Ramón nos dijo tantas veces, formamos un buen equipo. Gracias por tu amistad y por tus enseñanzas.

[PT] O culminar deste trabalho, representa mais do que um esforço profissional e individual, reflete o apoio e o amor dos que empurram dia a dia e espelha todo o carácter, toda a força e valentia da minha família. Aos meus pais e à minha esposa dedico esta tese, sem nunca esquecer os que já só vivem no nosso e de quem sinto saudade incessantemente. Ana, minha companheira de viagem e minha grande fonte de força. A ti devo a minha alegria e felicidade e a minha determinação. Juntos iniciámos e terminámos este ciclo, onde crescemos, lutamos, vencemos batalhas e nos emocionamos, tantas e tantas vezes. Agora, novos horizontes nos esperam e a vontade de partilhar a viagem contigo é imensa.

[ES] A todos mis compañeros de laboratorio, con quien compartí risas, conversas, "sanas" discusiones, carreras y birras. Oscar Iñigo, Sara R, Alicia, Julia, Juan, Gemma, Berta, Marta, Diana, Alex, Valeria, Sara de P., Macarena, Daniela, Guillermo, Carlos, Xavi, Miguel Angél, Kim, Marta Julia, Belen, Marc, Joan Marc y Marce. Y a los que ya no están, Marc, Alba G, Alba M, Merce Obac, Joel, Pau y Pablo. Gracias por haber

compartido todos estos años, os llevaré en mi memoria con la esperanza de un día poder encontrar gente como vosotros. Un especial agradecimiento a Rebeca, Yaiza y Ainhoa, les quiero agradecer por toda la ayuda y amistad a lo largo de éstos años. Y a Rosa Gasa por toda la ayuda, consejos y enseñamientos. Rosa, muchas gracias!

A mis amigos más cercanos, Cascais, Fil, Joan, Iris, Katerina, Elena, Liz, Rita, Lisa, Luca, Saverio, Adriá, Joana, Norberto, Rosa, Carles, Sami, Georgina y Jonas. Gracias por me acompañaren en ésta aventura, por darme fuerza, por hacerme olvidar de los problemas, y por compartir risas, comidas, cenas, confesiones, pasiones y alegrías.

[CAT] Per fi. Als Laton Kings. Laura i Vir, els portaré al cor, gràcies per compartir moments, alegries i emocions. A Santi, per ser juntament amb la meva família el que més força m'ha donat. Gràcies per escoltar i animar i treure el màxim de mi, però sobretot, gràcies a compartir tantes i tantes hores d'emocions, viatges, victòrias i derrotes a la sorra i fora della. Gràcies, nen! I, finalment, agraeixo a Enric i Krishna, la meva família de Barcelona, gràcies pel vostre suport i per tots els grans i inoblidables moments que continuaran amb mi per sempre.

Table of content

Figure index

Table index

List of abbreviations

ACC1   Acetyl-CoA carboxylase

ACE   Anterior chamber of the eye

AgRP   Agouti-related protein

Akt   Protein kinase B

AMPK   Activated protein kinase

aP2   Adipocyte protein 2 LPL

Bnip3   BCL2 interacting protein 3

BSA   Bovine serum albumin

C/EBP- α   CCAAT/enhancer-binding protein alpha

C/EBP-β   CCAAT/enhancer-binding protein beta

CART   Cocaine- and amphetamine-regulated transcript *protein*

CD31   see PECAM1

CFDA SE   Carboxyfluorescein-succinimidyl ester

c-fos   Cellular fos oncogene

c-jun   Cellular jun oncogene

DNA   Deoxyribonucleic acid

EDTA   Ethylenediaminetetraacetic acid

EGF   Endothelial growth factor

eIF4E   1Eukaryotic translation initiation factor 4E

eIF4E-BP1   Eukaryotic translation initiation factor 4E-binding protein 1

Ep   Edmonton protocol

Eph RTKs   Ephrin receptor tyrosine kinase and their

ER   Endoplasmic reticulum

ERK1/2   Extracellular signal–regulated kinases

ESRRA	Estrogen-related receptor alpha
ETOH	Ethanol
FAS	Fatty acid synthase
FBS	Fetal bovine serum
FGF2	Fibroblast growth factor 2
FOXO3	Forkhead box O3
GFAP	Glial fibrillary acidic protein
GLUT2	Glucose transporter 2
GLUT4	Glucose transporter type 4
GPCR	G protein–coupled receptors
GS	Glycogen synthase
GSK3β	Glycogen synthase kinase 3 i
GTPase	G protein hydrolase enzymes
Gαi2	Guanine nucleotide-binding protein 2
Gβγ	G protein beta-gamma complex
Hbss	Hank's balanced salt solution
HIF1	Hypoxia inducible factor 1
HLA	Human leukocyte antigen
HPC-1	Syntaxin-1Aerk
i.d.	inner diameter
IBMIR	Blood-mediated inflammatory reaction
iEC	Intra-islet endthelial cells
ieq	islet equivalent
IGF1	Insulin growth factor 1
INS	Insulin
IP	Inorganic phosphate

IR	Insulin receptor
IRS2	Insulin receptor substrate 2
JAK2	Janus kinase 2
Kdr	Kinase insert domain protein receptor
KRBH	Krebs-Ringer bicarbonate buffer solution
LADA	Autoimmune Diabetes of Adulthood
LepRb	Leptin receptor long isoform
LV	Lentivirus
MAPK	Mitogen-activated protein kinase
mCPT-1	Mast cell protease 1
Mef2	Myocyte enhancer factor-2
MEK1/2	Mitogen-activated protein kinase
MHC	Major histocompatibility complex
MODY	Maturity Onset Diabetes of the Young
MTOR	Mammalian target of rapamycin
n.a.	Not aplicable
Na_2WO_4	Sodium tungstate
NDM	Neonatal Diabetes Mellitus
NeuroD1	Neurogenic differentiation-1
NeuroD1	Neurogenic differentiation-1
o.d.	Outer diameter
O/N	Overnight
P38	Mitogen-activated protein *38*
p90rsk	p90 ribosomal protein S6 kinase
PBS	Phosphate buffer solution
PCR	Polymerase chain reaction

PDX1	Pancreatic and duodenal homeobox 1 transcription factor
PECAM1	Platelet/endothelial cell adhesion molecule-1
PFA	Paraformaldehyde
PGC-1 α	Peroxisome proliferator-activated receptor gamma coactivator 1 α
PI3K	Phosphatidylinositol-4,5-bisphosphate 3-kinase
PKB/AKT	*Protein* kinase B pathway
PKM2	Pyruvate kinase M2
PLD	Phospholipase D
POMC	Pro-opiomelanocortin
PP1	Protein phosphatase 1
PPARγ2	Peroxisome Proliferator Activated Receptor Gamma 2
PTP-1B	Protein tyrosine phosphatase 1B
PTPs	Protein tyrosine phosphatases
Raf-1	RAF proto-oncogene serine/threonine-protein kinase
Rkip	Raf kinase inhibitory protein
RNA	Ribonucleic acid
SDS	Sodium dodecyl sulfate
shRNA LV	Short hairpin RNA lentiviral particles
SNAP-25	Synaptosomal-associated protein 25
SOS1	Son of sevenless homolog 1
ß-cell	Pancreatic beta cell
STAT3	Signal transducer and activator of transcription 3
STZ	Streptozotocin
T1DM	Type 1 diabetes Mellitus
T2DM	Type 2 diabetes Mellitus

TBS	Tris buffered saline
TBST	Tris buffered saline – tween20
TSC2	Tuberous Sclerosis Complex 2
UCP-2	Mitochondrial uncoupling protein 2
VEGFA	Vascular endothelial growth factor A
VEGFR1	Vascular endothelial growth factor A
VEGFR2	see Kdr
ZDF	Zucker diabetic fatty rats
α-cell	Pancreatic alfa cell
δ-cell	Pancreatic delta cell

Introduction

Diabetes Mellitus

Diabetes mellitus is by definition, "(…) a chronic disease caused by inherited and acquired deficiency in the production of insulin by the pancreas, or by the ineffectiveness of the insulin produced. Such a deficiency results in increased concentrations of glucose in the blood, which in turn damage many of the body's systems"[1] (World Health Organization – WHO). It affects over 400 million people, with age between 20 and 79 years, around the world, and the prediction is that this number will dangerously rise over the next decades[2]. In Spain Diabetes affects approximately 10% of its population and the tendency is the exponential growth of diagnosed and undiagnosed cases of this burden disease[2].

Table 1: Spain Country report 2017 in Diabetes[2].

Spain	2017	2045
Diabetes estimates (20-79 years)		
Country prevalence (%)	10 (8-15)	13 (10-18)
Number of people with diabetes, million	3.584	4.2
Undiagnosed cases (%)	28.4	28.4
Number of deaths due to diabetes	15,600	
The proportion of death due to diabetes, < 60years (%)	36.3	
Healthcare expenditure due to diabetes (20-79 years)		
Total expenditure millions eur	9,310	9,200
Health expenditures per person with diabetes, EUR	2,580	2,190
Type 1 diabetes (0-19 years)		
Number of children and adolescents with type 1 diabetes	15,770	
Number of newly diagnosed children and adolescents each year, per 100 000 children	18	

Of all types of classified Diabetes there are three major groups that account for worldwide prevalence: Type 1 Diabetes Mellitus (T1DM), formally known as Insulin Dependent Diabetes Mellitus, Type 2 Diabetes Mellitus (T2DM) or formally known as non-Insulin Dependent Diabetes Mellitus and gestational diabetes, which was first, recognized during pregnancy and is temporary in the majority of cases. At is all forms, diabetes is characterized by hyperglycemia, due to defects in insulin secretion, insulin action on peripheral target tissues, or both, but their etiology and therefore treatment are quite distinct.

T2DM is by far the most common form of diabetes (approximately 80 percent of cases), which is usually associated with obesity and therefore an inability of the insulin-producing β-cells to match the demand for insulin. Ultimately, obesity can cause insulin resistance in peripheral tissues, such as the liver, muscle, and adipose tissue[3], which eventually leads to β-cell failure. T1DM accounts for approximately ten percent of cases worldwide and has a complex etiology. T1DM is a chronic autoimmune disease in which destruction or damaging of the beta-cells in the pancreatic islets results in insulin deficiency and hyperglycemia. Until now it is only known that autoimmunity is the principal effector mechanism of T1DM, but may not be its primary cause, as T1DM can be caused in genetically susceptible individuals, very likely as a result of an environmental trigger. The incidence of T1DM is rising[3], alarmingly, the most significant increase in T1DM is that seen in children under 5[4], with no known way of preventing this pandemic[5]. The other characterized forms of diabetes are the Autoimmune Diabetes of Adulthood (LADA) when the body slowly stops producing insulin, generally, at adulthood, it may be misdiagnosed with T2DM. Therefore a proper diagnose requires the use of antibodies. The Maturity Onset Diabetes of the Young (Mody), a rare form of diabetes caused by a mutation or change in a single gene; nowadays there are up to 11 type of MODYs and diagnosis will

determine different treatment. Neonatal Diabetes Mellitus (NDM), is a monogenic form of diabetes, it is diagnosed in the first six months of life after birth, and it can be temporary or permanent; 20 different genes can induce NDM[6–8].

Etiology of type 1 diabetes

Type 1 diabetes (T1D) is an autoimmune disease resulting from T cell-mediated β cell destruction in the pancreas of genetically susceptible individuals; Briefly, T1DM is characterized by an invasion of macrophages and T-cells in pancreatic islets as an inflammatory reaction also known as insulitis. Where CD4+ T-cells enhance the ability of CD8+ T-cells to kill the islet β-cells[9–11]. Furthermore cognate interactions between T cells and B cells occur that can lead to islet-targeting autoantibody formation (Figure 1). However, the triggering event is unknown, but the appearance of the first islet-targeting autoantibody reflects autoantigen presentation by dendritic cells and the subsequent responses of autoantigen-specific CD4+ and CD8+ T cells.

Disease progression and development of overt diabetes often take some months to years; clinical symptoms do not arise until 70-80 percent of the β-cells have been destroyed[12,13], resulting in an insufficient secretion of insulin and the need for exogenous insulin therapy to maintain glucose homeostasis[3,5,12]. Preclinical autoimmunity in T1DM occurs naturally and spontaneously just as soon as the immune system, by about 12 months after birth, is sufficiently mature to mount an autopathogenic response, with exogenous (environmental) factors serving as a trigger, but not being necessary. A child could carry well above the average number of the susceptibility alleles for T1D but be living in a very protective environment and, therefore, not develop the disease[3,14]. Characteristic autoantibodies

associated with T1DM are those that target insulin, 65 kDa glutamic acid decarboxylase (GAD65; also known as glutamate decarboxylase 2), insulinoma-associated protein 2 (IA2) or zinc transporter 8 (ZNT8); and the most described predisposing genetic variants of T1DM genes include the human leukocyte antigen (HLA) genes[10,15,16], and the variants of the insulin (INS) gene[15,17]. HLAs are a family of homologous proteins that encode major histocompatibility complex protein (MHC), which present antigenic peptides to both effectors- and regulatory- T-cells[15,18] The HLA variants HLADR and HLADQ have an increased risk of developing two or more autoantibodies.
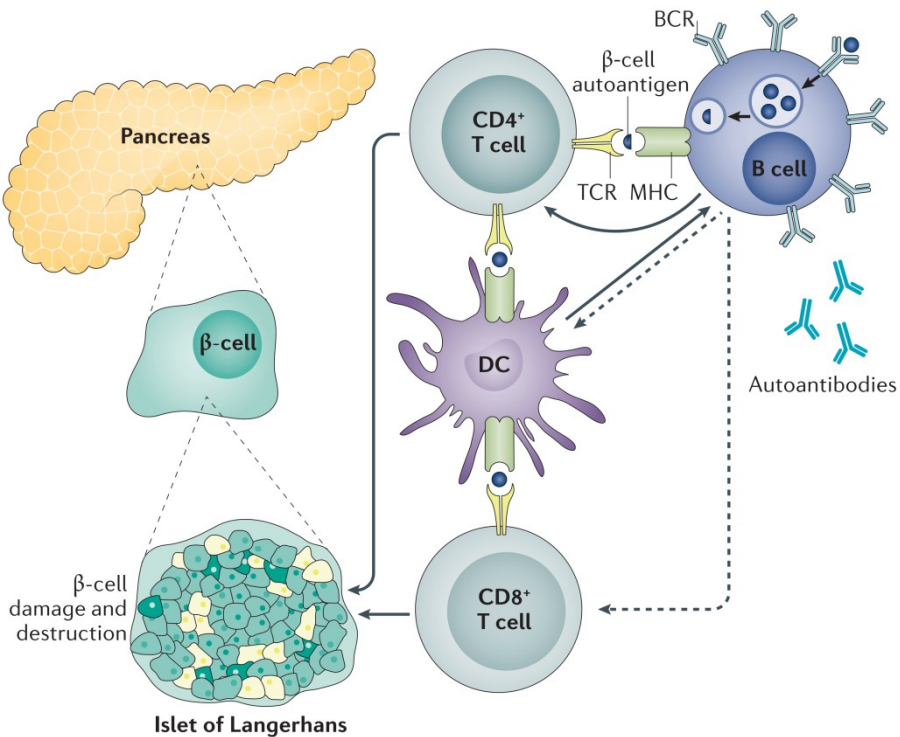
Figure 1: A Model for the Pathogenesis of Type 1 Diabetes Based on Genetic Etiological Studies in Humans. Adapt from[5,18].

Numerous environmental influences such as infections, diet, and toxins that affect children in utero, perinatally, or during early childhood, viral infections, the timing of the first introduction of food and gestational events like gestational infections have been proposed as candidate aetiological factors[19–27]. The epidemiology of T1DM may also provide information regarding the etiology of diabetes, with differences in both genetic and environmental components likely to contribute to the higher incidence of diabetes in northern European countries compared to those on the Mediterranean[5,17,18]. At present, exogenous insulin therapy is the primary treatment for patients with T1DM, although continued research efforts into improving allo and xenogeneic and islet transplantation may potentially enable the more widespread application of this as a treatment for the disease.

Islets of Langerhans

The pancreas is divided into two major components, endocrine, and exocrine tissue. The exocrine tissue constitutes around 98% of all pancreas, serving as the primary source of digestive enzymes in the body and ensures the breakdown of lipids, proteins, and polysaccharides[28]. On another hand the endocrine tissue is characterized by clusters of cells called islets of Langerhans (first described by Paul Langerhans in 1869), closely heterogeneity distributed along vessels and microvessels in the pancreas[29,30]. Islets are high vascularized "micro-organs" constituted. Pancreatic islets are highly vascularized and contain about five times more capillaries than exocrine pancreatic tissue[31,32], receiving 5–15% of the entire pancreatic blood supply, even though they represent only 1–2% of the pancreatic mass[33]. Each islet consists of 1,000-3,000 endocrine cells (Feldman, 1979). Approximately 65–80 percent of the endocrine cells in rodent islets are insulin secreting β-cells, 15-20 percent glucagon secreting

α-cells, 3-10 percent somatostatin secreting δ-cells and 3-5 percent pancreatic polypeptide-secreting PP cells[31,32]. Islet architecture differs from species[31,32]: in rodents ß-cells, are surrounded by α-, δ- and PP cells favoring the physical contact between ß-cells and therefore promoting insulin gene expression, insulin content and glucose-stimulated insulin secretion; in human islets the distribution of endocrine cells is more heterogeneous [34]; β-cells, α-cells, and somatostatin-containing δ cells were found scattered throughout the human islet. Moreover, human β cells were not clustered, showing associations with other endocrine cells, suggesting unique paracrine interactions in human islets[34,35] (Figure 2). Contrary to rodent islets, human islets contained fewer β cells and more α and most β, α, and δ cells were localized along blood vessels with no particular arrangement[34–36] (Figure 2). For both rodent and human islets, β-cells there is a complex interaction between the endocrine cells within the islets which involves several secreted hormones that guarantee the blood glucose homeostasis. The architecture of islets suggests a coupling between morphology and function and the existence of two mechanisms that contribute to cell communication. The first is via paracrine interactions, in which a secretory product from one cell moves a short distance through the interstitial fluid to reach a target cell, and the second mechanism is via the islet vascular system, for sensing and maintenance of an optimal blood glucose homeostasis[37].
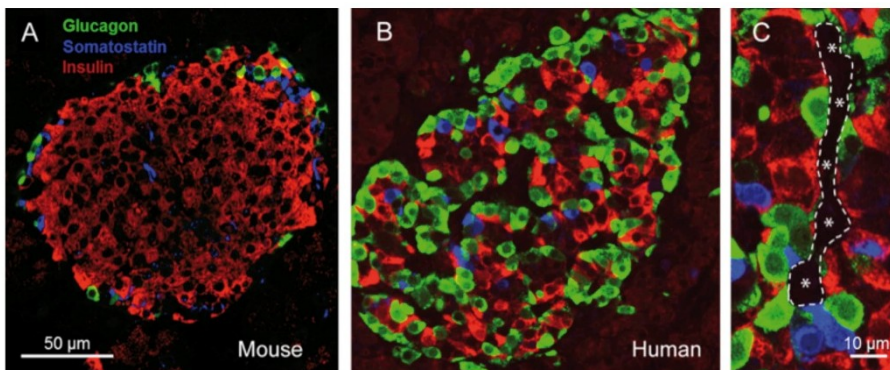
Figure 2: Cytoarchitecture of the human pancreatic islet. Mouse (A) and Human (B) pancreatic islet. Human islets contain less ß- cells and a higher number of α-cells compared to mouse islets. C, Human alpha, beta, and delta cells are distributed in the islet with no particular order of distribution along islet blood vessels (outlined). Adapt from[38].

Islet microvasculature

The pancreatic β-cells are closely associated with the islet microvasculature, where the pancreatic development ensures that each ß-cell is no more than one cell away from a capillary[37,39,40]. The close association between β-cells and intra-islet endothelial cells (iECs), ensures that β-cells can sense fluctuations in blood glucose levels and secrete insulin for maintaining glucose homeostasis. Although highly controversial, the pattern of blood flow that perfuses the islets is "inner-outer," meaning that ß-cells are perfused before α- and δ-cells, in mouse[31,41,42].

The islets contain fenestrated capillaries, which constitute 8%–10% of the islet volume, and are organized into a glomerular-like network[33,41,43]. The number of fenestrae is approximately ten times higher than in exocrine pancreatic capillaries and is induced by the high local production of vascular endothelial growth factor-A (VEGF-A) from the islet β-cells[44]. Fenestrations facilitate hormonal passage into the circulation as well as participate in draining extracellular fluid analogous to functions usually performed by lymphatic capillaries[45]. Besides being fenestrated, islet capillaries are wider than those in the exocrine pancreas, having a 20%–30% larger diameter, and their vascular density is much higher [43,46,47] (Figure 3).
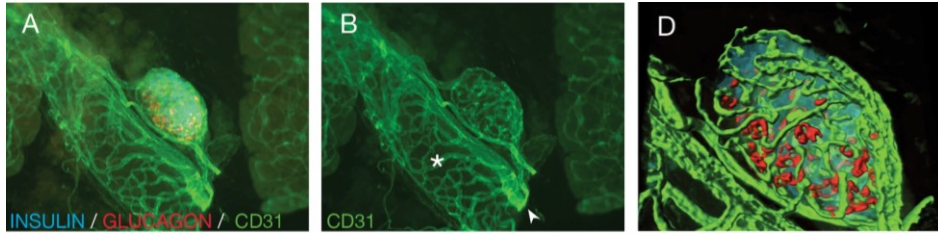
Figure 3: Islet vascular network (A) Merge image of the mouse hypervascular microcapillary network of the islet with glucagon, insulin, and CD31 (vascular marker). Image of the pancreatic islet vascular network with CD31 staining. (D) three-dimensional reconstruction of (A); adapt from[38].

This high vascular density (Figure4) is essential for the adequate provision of oxygen and nutrients, as well as continuous glucose sensing and dispersion of hormones to target tissues. The dense vascularization of the islets is also crucial for β-cell replication, which is particularly crucial at times of increased demand for insulin, such as during pregnancy or obesity[33,39,40,48].
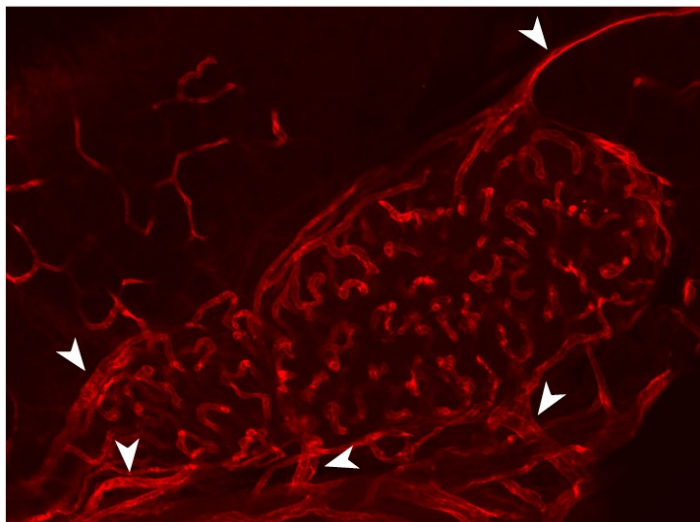
Figure 4: Mouse pancreatic islet microvasculature. Copied from[38].

The role of VEGFA in pancreatic ß-cells

In the pancreas, VEGF-A is cytokine highly produced in islets compared with exocrine cells. The formation pancreas vascular system requires the participation of VEGF-A that is a crucial regulator of vasculogenesis, angiogenesis, vascular permeability, and endothelial fenestration formation[49–51]. The importance of VEGF-A has been shown by the studies where RIP-Cre:Vegf^{fl/fl} mice show reduced vascularization with a reduced fenestration in islets[49,52]. Moreover, in the model of pancreatic-specific deletion of VEGF-A (PDX1-Cre:Vegf^{fl/fl}) islets present reduced vascularization and fenestration [53]. These results indicate that in the family of the vascular endothelial growth factors, expressed in ß-cells VEGF-A plays an essential role in the formation of the tortuous and dense fenestrated capillaries in the islets[52]. VEGF-A is known to bind to VEGF receptor 1 (VEGFR1) and VEGFR2 or Kdr (kinase insert domain protein receptor, which expression is restricted to endothelial cells. The RIP-Cre:Vegf^{fl/fl} mouse is a useful model to investigate the role of vascular structure on beta-cell function. These mice are characterized by a modest glucose intolerance with impaired glucose-stimulated insulin secretion as judged by glucose tolerance test in vivo[54]. However, *in vitro* insulin secretion, where the secretagogues can directly infiltrate beta cells, showed high levels of secretion when compared to controls. These data reflect that a normal islet vascular system is indispensable for normal hormone release from islets into the bloodstream. However, the abnormality of vascular structure does not result in substantial failure of beta-cell function by itself[54].

Endocrine pancreatic organogenesis, the early postnatal development, and transplantation require islet angiogenesis and innervation to establish a viable micro-organ. The two major processes involved in embryonic and extra-embryonic blood vessel formation are angiogenesis (growth of blood vessels from the existing vasculature) and vasculogenesis (the process of

blood vessel formation occurring by a de novo production of endothelial cells)[40,53,55]. Pancreatic vascularization occurs mainly by angiogenesis. Where VEGFA plays a unique role in islet vascularization and is expressed by developing endocrine cells as early as e13.5, and is required for the formation of the normal vasculature within the islet, moreover aftertransplantation[49]. One model of the relationship between vascular endothelial cells and islet development postulates that endothelial cells first stimulate islet development from the pancreatic epithelium. After then, islet cells stimulate endothelial cells to form a branching network of capillaries in the growing islet, and vascular endothelial cells secrete mitogens, such as hepatocyte growth factor, which seems to stimulate beta-cell replication. After the developmental stage of islets, an increase in islet mass is viewed as an essential adaptive reaction to insulin resistance[55]. On the other hand, considering the islet tumor, a mouse model of islet tumor reported that VEGF-A expression in beta cells correlated with tumor mass[52]. Moreover, previous studies indicated that the mass of normal adipose tissue depends on the rate of angiogenesis[55]. These data suggest a tight relation between the number of islet endothelial cells and beta-cell mass.

VEGFA expression

Reciprocal endothelial-endocrine signaling and formation of functional blood vessels appear to guide pancreatic differentiation and morphogenesis. Adult rodent islet endocrine cells produce VEGF-A. Up-regulation of VEGFA under physiological situations allows for adaptation to hypoxic stress, to ischemia, to nutrient deprivation, to transient inflammatory processes, and to wounding. VEGFA is a model of gene regulation as its expression is controlled at many levels including transcription. One of the best-characterized inducers of VEGFA secretion is hypoxia. Hypoxia-

induced VEGF production serves as a "driving force" for the development of neo-vessels during embryonic development and the vascularization of solid tumors, by activation of the hypoxia-inducible factor signaling cascade[49,51,56,57]. All conditions known to activate HIF-1 will have an impact on the expression of VEGFA. Hypoxia activates HIF-1 by stabilizing the limiting subunit, HIF-1α This action is triggered by inhibiting HIF prolyl-4 hydrolysate 2 or PHD2, the key enzyme involved in the instability of HIF-1α[58]. A 47-bp sequence located 985 to 939 bp 5' to the VEGF transcription initiation site-mediated hypoxia-inducible reporter gene expression[59–62]. Besides this significant stimulus, a variety of growth factors and cytokines including EGF, heregulin, FGF2, insulin, IGF1 and 2, and IL-1 increase HIF-1α protein levels and induce HIF-1 dependent genes under non-hypoxic conditions[59,63].

Another VEGFA inducer is nutrient deprivation or ischemia, driven by the upregulation of the estrogen-related receptor alpha (ERRα) and peroxisome proliferator-activated receptor gamma, coactivator 1 alpha (PGC1α)[64–66]. The induction of VEGFA by PGC1α does not involve the canonical hypoxia response pathway and hypoxia-inducible factor (HIF)[66]. In its place, PGC1α coactivates the orphan nuclear receptor ERRα (estrogen-related receptor-α)[66,67,68]. Estrogen-related receptor alpha (ERRα) is an orphan member of the nuclear receptor family of transcription factors, using the coactivator PGC-1α as a protein ligand to regulate ERRα activity. The induction of VEGF results from the interaction of ERRα with specific ERR-responsive elements within the VEGF promoter[64,65]. ERRα is known to interact physically and functionally with PGC1α and is involved in the activation of programs of fatty acid oxidation and oxidative phosphorylation[66,68–70]. It was also found that the first intron of the Vegfa gene contains a putative enhancer region in which several conserved Erra-binding sites are recognized by Erra and coactivated by PGC1α to elicit the robust induction of Vegfa transcription. Studies revealed the existence of 11 such sites; of

these 11 sites, 6 are perfectly conserved between human, mice, and rat. Strikingly, 5 of them are clustered within regions of high homology in the first intron of the Vegfa gene[66]

Intra-islet endothelial cells

ECs line all blood vessels forming a continuous monolayer layer between the blood and interstitial fluid. They are adapted to meet the individual needs of each organ and are therefore both phenotypically and functionally heterogeneous[55]. All ECs function as an immunological and physical barrier between the blood and tissues and play an essential role in angiogenesis[71,72]. Increasing evidence suggests that IECs do not function solely as a transport system, but they are exposed to their own derived molecules including laminins, Hepatocyte Growth Factor thrombospondin-1 and endothelin-1 have been shown to be essential for β-cell function[72,73]; insulin is also a major signal for endothelial cell function, for example, it is required for phosphorylation (activation) of endothelial nitric oxide synthase (NOS3), which catalyses production of the vasodilator nitric oxide (NO) (Figure5).

VEGF-A secreted by ß-cells mainly acts on VEGFR-2 on endothelial cells[74]. VEGFR2 is highly expressed in intra-islet capillaries, while in the microvasculature of exocrine tissue, and even in islet arterioles and venules, it is downregulated[49]. When VEGF-A binds to VEGFR-2, the activating mechanism of signal transductions are multiple. It results in autophosphorylation of tyrosine residues, activate protein kinase C (PKC)-Ras pathway, which induces mitogen-activated protein kinase (MAPK) /extracellular regulated kinase (ERK) pathway activating transcription factors, causing cells proliferation[75]; It activates phosphatidylinositol (PI) 3-kinase (PI3K)/protein kinase B (Akt/PKB) pathway, through increasing lipid

phosphatidylinositol (3,4,5) P3, activates downstream protein kinase B (PKB /Akt) pathway and endothelial nitric oxide synthase, promotes cells survival and increase of vascular permeability and cellular migration[75]; It activates p38MAPK and focal adhesion kinase, inducing cytoskeletal reorganization ad cell migration[75]; and it can activate signal transducer and activator of transcription 3 (STAT3) signaling, developing pancreatic microvasculature[76].
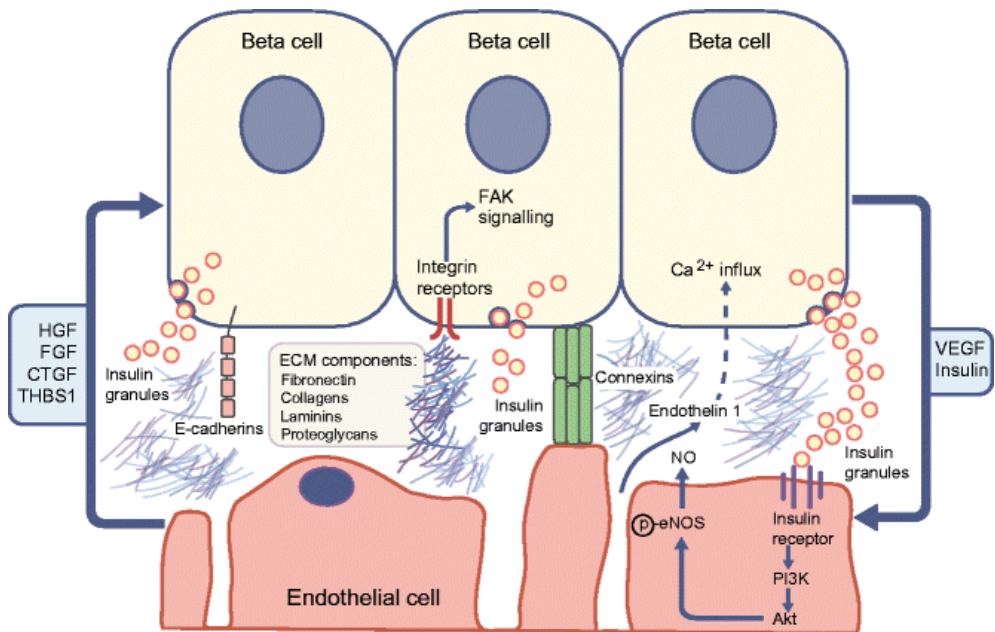
Figure 5: The main factors regulating the islet beta cell-endothelial cell axis. Adapted from[72].

Thus, signals produced by the beta cell impinge on the islet endothelial cell, contributing to overall islet health. EC-derived products have been shown to improve β-cell function enhancing glucose-stimulated insulin secretion, insulin content and glucose oxidation rate[72,73]. Furthermore, it is thought that β-cells rely on adjacent ECs to form a basement membrane[77], consisting mostly of laminins, collagen IV, and fibronectin, which promote β-

cell function and survival [72]. β-cell secreted VEGF-A generates a permeable endothelium allowing insulin to be secreted rapidly into the bloodstream and is also responsible for the large number of ECs within the islets[53]. There is also evidence to suggest that vascular supporting cells, such as pericytes play an important role in β-cell homeostasis[39].

Current treatments for type 1 diabetes

For most patients with T1DM, the therapy of choice is that of daily subcutaneous insulin injections. The discovery of insulin in the 1920's (Banting and Best) has meant that patients with T1DM are able to lead a near normal lifestyle, with reasonable blood glucose control. However subcutaneous insulin injections cannot provide the fine-tuning of blood glucose control that occurs under normal physiological conditions and thus fluctuations in blood glucose concentration mean that insulin therapy does not eliminate the risk of chronic secondary complications that can occur with T1DM, despite reasonable glycaemic control in some patients[78–80]. In particular, these complications include neuropathy, nephropathy, retinopathy, limb amputations and cardiovascular disease, which account for most of the morbidity and mortality in T1DM[81] .Alternative strategies to insulin have been studied to optimize blood glucose control. The development of insulin pumps, which provides a continuous infusion of insulin into the subcutaneous tissue and has now become the primary therapy for basal insulin replacement. Moreover, insulin pumps offer potential future benefits of a closed-loop system in which the insulin pump would be linked to a glucose sensor, thereby acting as an artificial pancreas[81].

Although it is clear that intensive insulin therapy has improved the treatment of T1DM in terms of patient quality of life, metabolic control, and risk of

long-term complications, it can be associated with an increased risk of hypoglycemia, which is potentially dangerous or life-threatening. Transplantations appeared as the most efficient way to replace pancreatic ß-cell mass in order to restore glucose homeostasis and metabolic control. The first whole organ pancreas transplantation was performed more than fifty years ago[81], with the majority of pancreas transplants today being performed as simultaneous pancreas-kidney transplants. Until more recently, pancreas transplantation was associated with a higher success rate (in terms of maintained insulin independence) than allogeneic islet transplantation, but there is no evidence to suggest that the two strategies can result in comparable glycaemic control in patients[82,83], emphasizing the vast improvements that have already occurred within the islet transplantation field.

Islet cell transplantation has been shown to normalize blood sugar levels but issues with intrahepatic islet cell transplantation such as immediate blood-mediated inflammatory reactions, deleterious effects of chronic immunosuppressive drugs, lack of sustained insulin independence in some islet cell recipients, and lack of sufficient number of islet cell donors are all barriers to this as a viable treatment for the majority of people with type 1 diabetes[84]. Islet transplantation can eliminate severe hypoglycemia in patients with type 1 diabetes[85]. Islet transplantation is associated with lower morbidity, a reduced likelihood of surgical complications[85]. Direct comparison of these β-cell replacement strategies is however difficult, and the choice of islet or pancreas transplantation is complex, requiring an important consideration of the patient's metabolic complications, pre-existence of diabetic complications and psychological situation of the patient and family[85].

Islet transplantation

Successful islet transplantations were initially performed in humans in 1990. However, the overall success rate in terms of insulin independence was low. With the establishment of the Edmonton protocol, islet transplantation became a viable treatment for T1DM[86,87]. The Edmonton protocol (Ep) became a landmark on islet transplantation; it is based on multiple infusions of large quantities of fresh islets equivalents (ieq) – over 9000 ieq/Kg of patient body weight) and a specific glucocorticoid-free immunosuppressive regimen[86]. Despite the improvement brought by the Ep, in terms of the early stage rate of insulin independence, the long-term outcomes were still very poor. The graft failure and the return to exogenous insulin therapy were the final results for the majority of patients, only 10 percent of patients were insulin independent after 5 years[88,89]. Even though the decline in islet graft function, partial graft function means that only small doses of exogenous insulin are required, islet transplantation has been shown to confer stabilization of diabetic complications, including diabetic retinopathy and nephropathy[90]. Nowadays some centers reported insulin independence with only one donor transplantation, if reproducible the routine achievement of single-donor islet transplantation success is essential for increasing the number of patients who can be given allogeneic islet transplants, but also for increasing the acceptability of allogeneic islet transplantation within the transplant community, given that whole organ pancreas transplantation requires only a single donor[91–93].

Challenges in islet transplantation
Substantial improvements have already been made within the islet transplantation field. However, significant challenges to the islet transplantation which contributes to the decline in graft function and loss of insulin independence,

1. A large number of islet needed in a single infusion when compared with the low availability of islet, the necessity of multiple infusions of islets to guaranty insulin independence,

2. Autoimmunity: T1D is an autoimmune disease characterized by T cell-mediated destruction of β-cells, in which CD4+ T helper cells play a pivotal role. It can thus be anticipated that success of β-cell replacement requires not only suppression of allograft rejection, but also prevention of a recurrent T-cell mediated autoimmune process

3. Alloimmunity: Most islet allograft recipients develop anti-donor antibodies; the presence of specific anti-donor alloantibodies should exclude patients from receiving islets from donors expressing the recognized HLA allodeterminants because they predict graft failure[94,95]

4. Poor revascularization: see section "revascularization of the islet-graft."

5. Blood-mediated inflammatory reaction (IBMIR): Islets express tissue factor (TF)—a 47 kDa transmembrane glycoprotein that initiates the extrinsic coagulation system and is pivotal for activation of the intrinsic pathway. Vascular injury exposes TF to soluble coagulation proteins and triggers clotting[96]; TF binds to factor VIIa and thereby activates a number of intracellular signals that culminate in cell a nonspecific inflammatory and coagulation pathway, that is detrimental to islet survival[97–101].

6. Lifetime immunosuppressive therapy, which is associated with adverse side effects that deteriorate the quality of life for the patient, which in many cases means that the costs of this outweigh the benefits of the islet transplant. In particular, side effects include painful mouth ulcers, peripheral edema, and poor wound healing[78,81,102].

Recent strategies to improve recipient immunosuppression are focused on T-cell depletion therapies using an anti-CD52 antibody[103] and T-cell depletion with co-stimulation blockade, using belatacept to block co-stimulation signaling through the CD80-CD86 pathway[92]. Other strategies to prevent allogeneic graft rejection include immunoisolation of islets through various encapsulation technologies, such as nanoencapsulation[104–106]. Additional novel approaches to protect the transplanted islets from immune attack included cellular-based strategies, including a coating of islets with regulatory T-cells[107] or Mesenchymal Stem Cells (MSCs)[108–111].

Successful transplantation outcome depends not only on replacing the lost β-cells, with islets but also with insulin-producing cells[112–114], the first-in-human stem cell and extrahepatic transplant site trials into clinical investigation has positioned b-cell replacement to become the mainstay treatment for all T1DM patients in the near future[115]. Moreover, it is recognized preventing re-current autoimmunity[112–114,116], is critical for T1DM treatment. For example, antigen-specific strategies to restore self tolerance, relying on tolerogenic potential of endothelial cells[117,118]; or systemic delivery of coated nanoparticles, to promote the differentiation of disease-primed autoreactive T cells into TR1-like cells, which in turn suppress autoantigen-loaded antigen-presenting cells and drive the differentiation of cognate B cells into disease-suppressing regulatory B cells[119,120]; or even targeting Liver receptor homologue-1 (LRH-1to suppress the immune-dependent inflammation of pancreas in T1DM[121]. An extensive review of the current strategies to improve recipient immunosuppression or impairment of damaging autoimmunity is beyond the scope of this thesis, which is focused primarily on improving transplantation outcome through enhanced vascular engraftment.

Engraftment of islet-grafts

Islet-graft engraftment is critical for achieving and maintenance of insulin independence. Engraftment is the adaption of the transplanted islets to their implantation site with regards to revascularisation, reinnervation, and reorganization of other stromal components[122] and is essential for the long-term survival and function of transplanted islets.

Despite the implantation site, islet-grafts are subjected to challenges, which induces apoptotic or necrotic cell death [123–125] to nearly 60% of islets. Islet-grafts also undergo severe changes in gene expression, meaning that a significant proportion of the remaining islets do not function optimally[126]. Severe functional impairments include reduced glucose oxidation, and glucose-stimulated insulin secretion and (pro) insulin biosynthesis, as well as reduced mRNA expression of genes essential for β-cell function[127,128]. Therefore, islet graft survival and function are dependent on the reestablishment of new vessels within the grafts to derive blood flow from the host vascular system[51,122,129–131].

Revascularization of the islet-grafts

Angiogenesis is the predominant mechanism in avascular regions of any tissue [71] and is the predominant mechanism of blood vessel formation in the adult[132]. The revascularisation process is highly complex, involving the digestion of the vascular wall by proteases and the migration, proliferation, and differentiation of ECs [115]. Following isolation, islets are severed from their native vascular network[123] by collagenase digestion. This means that they are avascular during the immediate posttransplantation period [125,133]. One of the leading clinical problems in pancreatic islet transplantation is

deficient graft revascularization, which is responsible for scarce oxygen and nutrient delivery and impairing hormone and secretagogue modulation[134–136]. Altogether, these contribute toward the primary failure of transplanted islets[122,137]. Thus, the rate at which islets revascularize is essential to prevent excessive hypoxia-related cell death[123–125], several studies show that islet graft revascularisation is suboptimal irrespective of the transplantation site used [135,138–140]. The transplantation site also has an essential influence on islet revascularization as it dictates the distribution of ECs. Islets transplanted beneath the renal capsule, or in the anterior chamber of the eye typically fuse to form an aggregated mass of endocrine tissue, which therefore increases the distance over which host ECs must migrate to the center of the endocrine tissue. It is noteworthy that there are differences regarding the reorganization of stromal components, between islets transplanted intrapancreatically to their native microenvironment and that transplanted heterotypically (to the liver, spleen or beneath the renal capsule); with a higher percentage of richly vascularised connective tissue present in the grafts of islets transplanted to heterotypic sites[135,138,141,142].

Barriers to improving islet-graft revascularization

Strategies to ameliorate the survival and function of islet-grafts by modulating the "angiogenic switch" and improving revascularization. These strategies aim to increase the number of patients who can be treated with the limited human islet material available for clinical islet transplantation encompass.

The 'angiogenic switch' for improving revascularization

One of the most studies approaches to improve revascularization is the modulation of the 'angiogenic switch' by administering angiogenic factors,

or inhibiting angiostatic factors in the graft recipient, or directly in the islet-grafts, thereby driving the balance towards a proangiogenic microenvironment and enhancing the proliferation, migration, and maturation of ECs into functional vessels[143] .

The most studied angiogenic factor is VEGFA. Several studies reported the delivery or overexpression of VEGFA in islet-graft[144–149], in order to induce angiogenesis. This approach has shown some success at early stages of revascularization through the manipulation of gene expression[55,147–152] , although at long-term, islets resulted hypervascularized, compromising islet architecture and inducing the loss of ß-cell mass and the consequent loss of islet function[144–146] (Figure 6). Whilst many of the transgenic studies have been valuable for emphasizing the positive correlation between islet graft vascular density and function, it is unlikely that this will be translated in a clinical setting due to safety concerns. Other solutions to modulate the angiogenic switch are required!
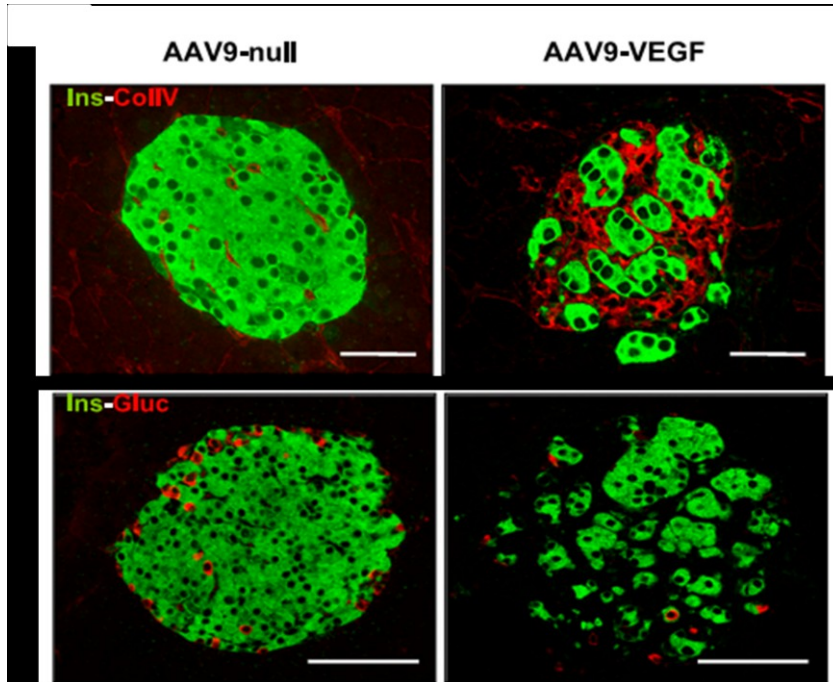
Figure 6: AAV-mediated VEGF overexpression in β-cells increased islet vascularization. Two-month-old wild-type (WT) mice were injected with VEGF-expressing (AAV9-VEGF) or nonexpressing (null) AAV9 vectors: Ten days after AAV injection vasculature structure was revealed by immunostaining for collagen IV (red) and insulin (green). Insulin (green) and glucagon (red) expression showed islet disorganization (bottom).

SodiumTungstate

Sodium tungstate historical perspective

Tungstate is the periodic table element 74, it has the highest melting point of all metals and has been found to be the most substantial element to be used by living organisms; its carbide also displays a hardness approaching that of the diamond. It cannot be formed by nuclear fusion processes in stars, as is the case for those elements with a lower atomic number, but originates only by neutron or proton absorption of already existing more prominent nuclei.

 The name Wolfram is closely related to today's important tungsten mineral *wolframite*. In the Middle Ages (16th century) tin miners in the Saxony-Bohemian Erzgebirge in Germany reported about a mineral which often accompanied tin ore (tinstone). "It tears away the tin and devours it like a wolf devours a sheep", a contemporary wrote in the symbolic language of those times. The miners gave this annoying ore German nicknames like "wolffram", "wolform", "wolfrumb" and "wolffshar". The name Tungsten came from the other important tungsten ore, which is now called *scheelite*. In 1750, The first person who mentioned the mineral was Axel Frederik Cronstedt in 1757, who called it Tungsten {composed of the two Swedish words *tung*(heavy) and *sten* (stone)}, the outstanding Swedish chemist Carl Wilhelm Scheele published the results of his experiments on the mineral tungsten in Kongl. Vetenskaps- Academiens Nya Handlingar, with the title: "The Constituents of Tungsten"[153–155]. In 1781/1782, the Spanish nobleman, Juan José de D´Elhuyar analyzed a wolfram species, and showed it to be an iron and manganese salt of a new acid. He also concluded that wolfram contained the same acid as Scheele had gained from tungsten. His discovery, jointly with his brother Fausto Jermin, was published in 1783 by the Royal Society of Friends of the Country in the City

of Victoria ("Analysis quimico del volfram, y examen de un Nuevo metal, que entra en su composition por D Juan Joséf y Don Fausto de Luyart de la Real Sociedad Bascongada"). The new metal was named VOLFRAM after the mineral used for analysis[154]..
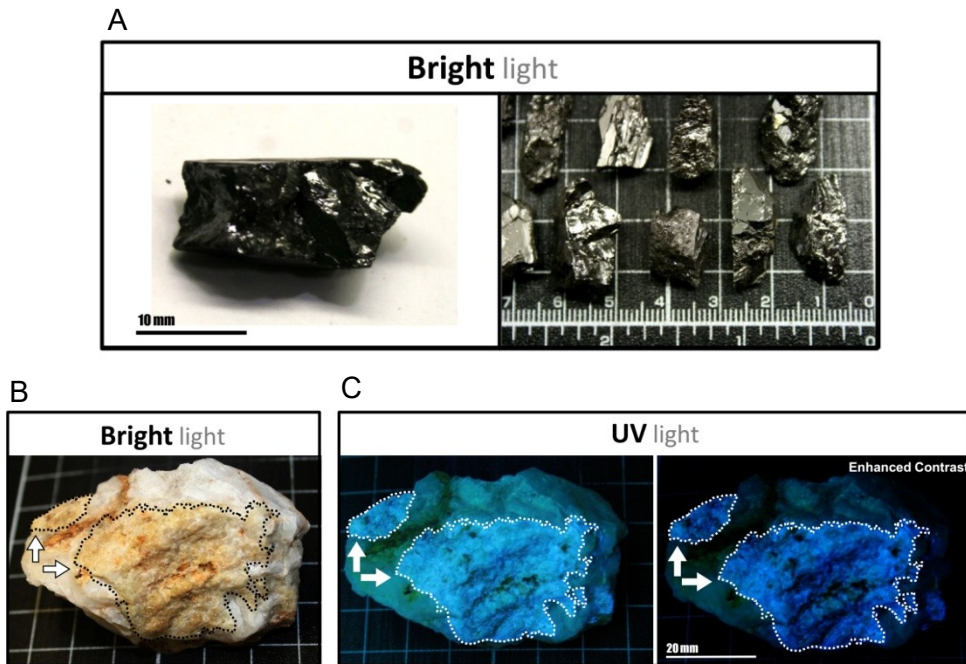
Figure 7: Wolframium (A) and Scheelite (B and C). A. Wolfram mineral, $(Fe2+)WO4$ to $(Mn2+)WO4$, color: sub-metallic, greyish-black; B and C. Scheelite mineral. Formula: $Ca(WO4)$; Color: golden-yellow, tan; Fluorescence in UV light: bright blue-white

In 1847, a patent was granted to the engineer Robert Oxland. This included the preparation of sodium tungstate, formation of tungstic acid, and the reduction to the metallic form by oil, tar or charcoal. The work constituted an important step in modern tungsten chemistry, and opened the way to industrialisation. Although the use of tungsten for high strength steels was well known at the beginning of the 20th century, it was considered early as a strategic material (majority of tungsten belonged to Germany and Austria), and large amounts of tungsten were used for the

ordnance industry. It was used for tool steels, armour plates, cannons, shells and - in large amounts - for gun barrels in the World War I[154,155].

Sodium tungstate as an anti-diabetic drug

The sodium tungstate (formula $Na_2WO_4 \cdot 2H_2O$) is an inorganic compound and the salt of tungstate. Tungstate presents a tetrahedral structure, and as a transition metal, it can be found in different oxidation states (from +2 to +6), a property that confers its ability to replace other endogenous metals. Tungstate's chemical and physical properties are very similar to other metals, such as vanadate and molybdenum[156]. These metal have biological relevance, as they integrate the catalytic pores of enzymes or compete directly with phosphate[157,158]. Tungsten can replace molybdenum in Mo.containing enzymes such as xanthine oxidase, and sulfite oxidase in kidneys and intestine.

For all metals that can mimics phosphate and compete with it for the catalytic domain in proteins, sodium tungstate appears to have the lowest toxicity[157,159]; the acute oral toxicity varies depending on the tungsten compound: The LD50 values are 240 mg sodium tungstate/kg body weight (mouse), > 2000 mg tungsten carbide/kg body weight (rat) and >20000mg tungsten metal/kg body weight (rabbit and dog). Sodium tungstate concentrations that are active in vitro are similar to the plasma levels determined in treated animals[160], and no apparent toxicity has been reported in several studies[161–165]. Regarding bioavailability studies with sodium, tungstate was carried in rodents (rat and mice) and beagle dog[160,166,167], where sodium tungstate bioavailability was almost 92%in rats and 62%, in dogs. When analyzed the tissue distribution, sodium tungstate, present increasing tungsten levels in all organs with an increased dose of exposure, with the highest concentration found in the bones and the lowest

concentration found in brain tissue. Gender differences were noticed only in the spleen (higher concentration of tungsten in female animals). Moreover, the primary route of elimination of tungstate is through urine [168]. Based on these studies Leggett (1997) developed a kinetic model for the calculation of the distribution and retention of sodium tungstate in humans[169].Leggett suggests that 85% of all consumed sodium tungstate should be eliminated by 24h, and 97% by 1 month. In this model, it was predicted that the majority of the tungstate would be retained in bone, primarily by mechanisms of replacement of phosphate in bone[169].

Table 2: Acute toxicity data of tungsten and its compounds. Adapted from[168]

Substance	Animal species	Administration route	LD_{50} [mg/kg body weight]	References
Tungsten metal				
	rat	i.p.	5000	Fredrick and Bradley 1946
Sodium tungstate				
	rat	oral	1190	Nadeenko 1966
	mouse	oral	240	Venugopal and Luckey 1978
	rabbit	oral	875	Nadeenko 1966
	guinea pig	oral	1152	Nadeenko 1966
	rat	i.p.	185	Caujolle *et al.* 1959, Pham-Huu-Chanh 1965
	mouse	i.p.	135	Caujolle *et al.* 1959, Pham-Huu-Chanh 1965
	rat	s.c.	223–255	Kinard and van de Erve 1940
	rat	i.m.	140–160	Kinard and van de Erve 1940
	rabbit	i.m.	105	Lusky *et al.* 1949
Tungsten carbide				
	rat	oral	>2000	HCST 2001
	rat	dermal	>2000	HCST 2001

Sodium Tungstate is widely known as a non-toxic anti-diabetic agent that inhibits several phosphatases[158,170].Studies in animal models of diabetes have shown that tungstate, being administrated orally, can reverse hyperglycemia[163,164,171,172] and to restore the number and function of immune cells as well as the immunoglobulin level in STZ diabetic models[173]. Tungstate treatment has been shown to normalize liver glucose metabolism in streptozotocin (STZ) and Zucker Diabetic Fatty rats[163,164,171], and triglycerides levels[174,175]. Tungstate also stimulates weight loss[175] and promote pancreatic beta cell function by restoring glucose-induced insulin secretion, enhancing insulin production, and increasing beta-cell survival and proliferation[172,176–178]. Despite the evidence described above strongly suggest that sodium tungstate exerts beneficial effects at the physiological level, the mechanism of action is more elusive

Sodium Tungstate is an inhibitor of phosphatases

Phosphorylation of tyrosine residues of intracellular or membrane proteins is critical as the balance of activation of PTP-1B regulates critical phosphotyrosine levels in the signal transduction pathways necessary for intracellular signaling, cell growth, differentiation, metabolism or gene transcription[179]. Inorganic phosphate (IP) is the hydrolytic product of the PTP reaction. IP is a competitive inhibitor of PTP-1B with a K_i value of 17 mM. Other oxyanions with structural similarities to the phosphate group inhibit PTPs with different affinities: molybdate, arsenate, tungstate, and vanadate: K_i (IC_{50}) values of 1.5 µM (vanadate), 210 µM (tungstate), 200 µM (arsenate), and 54 mM (nitrate) were measured[180]. Vanadate has a propensity to form a covalent intermediate analogous to the phospho-intermediate in contrast to the other anions, which form Michaelis-like

complexes, and geometric factors, such as in the case of nitrate, which has a planar geometry[158,180,181].
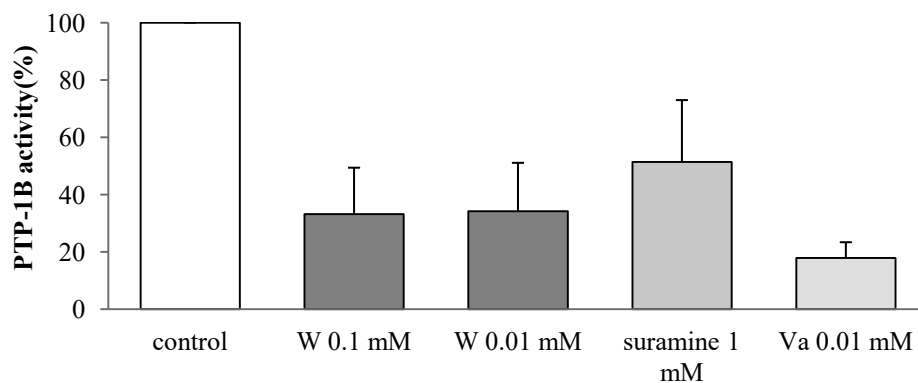
Figure 8: PTP-1B inhibition by sodium tungstate (W) 0.1 and 0.01mM, suramin 1mM and Vanadate 0.01mM. Data are kindly given by Dr. Belen Nadal .

Effects of sodium tungstate in tissue

The following sections will describe some of the general effects of the sodium tungstate treatment in liver, pancreas, muscle, adipose tissue and brain, from rodent models. A compilation of the most critical effect can be found in Figure 9.

Enhances glucose uptake and protein synthesis Improvement of contractile deficits. Decrease of ROS production.

Promotes β-cell survival through induction of proliferation and inhibition of apoptosis. Enhances insulin production.

Induces neuronal plasticity and remodeling of hypothalamic nuclei. Modulates feeding behavior.

Stimulates hepatic glycogen synthesis and inhibits hepatic endogenous glucose production.

Reduces the amount of glucose absorption in diabetic rats. Anti-oxidant mechanisms of intestinal mucosa.

Reduces weight gain and food intake. Increases thermogenesis in obese animal models.

Figure 9: Multiple organ effects of the sodium tungstate treatment in rodent models

Effects of sodium tungstate in Liver

Oral administration of sodium tungstate to streptozotocin (STZ) –diabetic rats and Zucker diabetic fatty rats (ZDF) stimulates hepatic glucose metabolism and increase glycogen levels[161,163,164,171,182].

Sodium tungstate does not directly activate IR, or other tyrosine kinase receptors, such as EGF or IGF receptors in hepatocytes[183]. Instead, it activates Gαi2 and Gβγ subunits of GPCR, to stimulate the activity of the small GTPase[183], initiating the signaling transduction through sequential phosphorylation of Raf-1, MEK1/2, and ERK1/2, which in turn phosphorylates GSK3β and p90rsk[164,165]. Phosphorylated GSK3β is inactive and alleviates the inhibitory phosphorylation over GS, favoring activation of glycogen synthesis[184]. Although it has not been demonstrated for sodium tungstate action, p90rsk is known to be involved in GSK3β inactivation, PP1 activation and negative feedback upstream in the pathway through inactivation of SOS[185]. PP1 is the main phosphatase activity participating in GS dephosphorylation and stimulation of glycogen synthesis, but the actual participation of sodium tungstate in PP1 activation remains to be established[186]. In parallel, sodium tungstate -mediated ERK1/2 activation stimulates c-fos and c-jun and inhibits PGC-1 transcriptional expression through yet unknown mechanisms[187,188]. Since PGC-1 is a positive modulator, whereas c-fos and c-jun are negative regulators of the transactivation of gluconeogenic genes, sodium tungstate action finally induces down-regulation of gluconeogenic enzymes and, hence, the gluconeogenic pathway[188–192]. In IRS2 KO mice, sodium tungstate was unable to exert consistent effects on glycogen synthesis and gluconeogenesis, highlighting the importance of IRS2 in sodium tungstate signaling pathway in hepatocytes[170].

Effects of sodium tungstate in muscle

Muscle is the primary site of insulin-dependent glucose uptake, and its ability to remove blood glucose is significantly impaired in the diabetic condition[186]. Sodium tungstate induced-ERK1/2 activation led to

phosphorylation and inhibition of TSC2, relieving inhibition on MTOR[200–205].Activated mTOR phosphorylates and activates S6K1, which inhibits eIF4E-BP1, alleviating eIF4E inhibition, and promoting protein translation. Moreover, ERK1/2 phosphorylates FOXO3 and Mef2 transcription factors[178,187–194]. Phosphorylated FOXO3 is inactive and cannot translocate into the nucleus to transactivate MurF1 and ATROGIN1 genes, down-regulating the expression of these critical ubiquitin ligases and reducing the activity of the ubiquitin-proteasome pathway of protein degradation. Besides, sodium tungstate induces a decline in auto-phagosome formation through the down-regulation of Bnip3[187–192,194,195].On the other hand, phosphorylated Mef 2 is active and can enter the nucleus to promote Glut4 gene expression, which together with above-mentioned eIF4E stimulation led to enhanced protein synthesis of the GLUT4 transporter. Finally, sodium tungstate-induced ERK1/2 activation stimulates fusion of GLUT4-containing vesicles with the plasma membrane, maybe through direct activation of PLD, enhancing GLUT4 activity and glucose uptake[178,187–194].

Effects of sodium tungstate in the pancreas

In the pancreas, ß-cell produces and secrete insulin and other hormones in order to maintain glucose homeostasis. Treating a diabetic STZ model of rats with sodium tungstate one week before diabetes induction, prevented STZ-induced mass, preserving islet volume and density, increased pancreas antioxidant power and decreased lipid peroxidation[196,197], and induces a dose-dependent stimulation of insulin secretion by a mechanism dependent on ß-cell glucose metabolism and stimulation of exocytosis, as the insulinotropic effect of Sodium tungstate is abolished by diazoxide, somatostatin, and amylin[177]. A transcriptomic analysis of pancreas from STZ-diabetic rats has revealed that the majority of genes whose expression

is altered during diabetes are restored to different degrees by sodium tungstate treatment[198].

In neonatally STZ (nSTZ)-induced diabetic rats, a model of T2D, treatment with sodium tungstate partial recovery of insulin content and pre-proinsulin mRNA levels was detected, together with the restoration of β-cell response to an increase in glucose concentration[199]. In isolated islets from treated rats, it was observed p38 and PDX-1 phosphorylation. P38 together with PI3K, mediates high glucose-induced phosphorylation, nuclear translocation and activation of the pancreatic and duodenal homeobox 1 (PDX-1) transcription factor. Phosphorylation of PDX-1is involved in pancreas development, insulin expression and β-cell functionality, in fact, sodium tungstate treatment augments the number of insulin and PDX-1 positive cells in pancreas from sodium tungstate treated STZ-diabetic rats [172,200].

In IRS-2 knockout diabetic mice, sodium tungstate treatment has a significant effect. It decreased β-cell apoptosis and inflammatory response, and also increased β-cell replication, explaining total increase in β-cell mass, in a model that starts losing β-cell mass due to apoptosis at 8 weeks of age[178,198], sodium tungstate primarily targets β-cell death mechanisms through activation of endogenous kinases. When incubating INS1E cells with incubated with serum from sodium tungstate-treated diabetic rats, the rate of proliferation was significantly enhanced, suggesting that the proliferative effect on the pancreatic β-cell is through indirect mechanisms[198]. Furthermore, Raf kinase inhibitory protein (Rkip) gene expression was found upregulated in the diabetic pancreas and normalized by sodium tungstate treatment, according with an anti-proliferative function of Rkip in ß-cell, as ERK1/2 has been shown to be upregulated in proliferation of INS-1E cells induced by the treatment; in the IRS-2 knockout mice, treatment restore phosphorylation. Given that Rkip inhibits Raf-1 kinase, which phosphorylates MEK, which in turn phosphorylates ERK1/2,

sodium tungstate-induced normalization of Rkip expression leads to an increase in the MAPK pathway activity, favoring proliferation. And finally, sodium tungstate treatment was found to suppress upregulated proapoptotic and inflammatory genes in IRS-2 knockout mice, through the activation of the MAPK pathway[172,178].

Effect of sodium tungstate in adipose tissue and brain

Sodium tungstate is a potent anti-obesity agent, reducing weight gain and food intake, and increasing oxygen consumption and thermogenesis in obese animal models in a leptin-dependent fashion. ERK1/2, but not PKB/Akt activation, is necessary at least to explain treatment-mediated inhibition of triglyceride accumulation and decreased adipogenesis.

Sodium tungstate treatment acts on adipocyte metabolism in an IR-independent manner[198], it induces up-regulation of GLUT4 mRNA expression, and increased glucose transport and consumption[198]. The treatment with sodium tungstate decrease triglyceride accumulation, as it reduces the expression of lipoprotein lipase (LPL), adipocyte protein 2 (aP2), acetyl-CoA carboxylase (ACC1) and fatty acid synthase (FAS), as well the transcriptor factors involved in adipocyte differentiation, with a decreased expression of CCAAT/ enhancer-binding protein (C/EBP)-α and PPARγ2 and increased expression of C/EBP-β in a dependent on ERK1/2 manner[201,202]. Treating high-fat-diet-induced obese rats with sodium tungstate decreased body weight gain and adiposity, by decreasing white adipose tissue mass through apoptosis and reduction of adipocytes size without modifying caloric intake, intestinal fat absorption, or growth rate[175]. Moreover, it is observed the upregulation of UCP-2 in white adipose tissue and UCP-1 in brown adipose tissue via the upregulation of PGC1α, LPL, aP2, and mCPT-1[175,203,204]. Finally, like in other tissues, sodium tungstate

induced the up-regulation of proteins involved in signal transduction, especially Raf-1 kinase, which in turn activates the ERK pathway[205].

Sodium tungstate can act as a leptin-mimetic compound in vivo, correcting feeding behavior. Moreover, it crosses the blood-brain barrier and induces neuronal plasticity and remodeling of hypothalamic nuclei. The anti-obesity effects of sodium tungstate are dependent on leptin signaling pathway since treatment of obese leptin receptor-deficient (fa/fa) Zucker rats or obese leptin-deficient (ob/ob) mice did not result in reduced body weight gain and food intake, or increased energy expenditure[204].In the arcuate nucleus of the hypothalamus, leptin binds to its receptor, inhibiting neurons that express orexigenic neuropeptide Y (NPY) and agouti-related peptide (AgRP) and activating neurons that express anorexigenic proopiomelanocortin (POMC) and cocaine- and amphetamine-related transcript (CART)[206]; sodium tungstate treatment downregulates NPY/AGRP, and increased CART gene expression[204], and 24 hours after injection of sodium tungstate directly in the third cerebroventricular cavity, it is observed the same effect produced by leptin injection[207]. Moreover, in the arcuate nucleus, treatment with sodium tungstate activates MAPK pathway, and increases c-fos positive cells and of GFAP-positive astroglia[174,207]. Furthermore, it reduces f β tubulin and syntaxin 1 (HPC-1) and increases neurogenic differentiation (NeuroD)-1 transcription factor and synaptosomal-associated protein (SNAP)-25 expression[174].

Protein tyrosine phosphatase 1B

Protein tyrosine phosphorylation is a dynamic regulatory system of many many cellular processes through the fine-tuning of critical phosphotyrosine levels in the signal transduction pathways necessary for intracellular signaling. Dysregulation of this process can have broad implications for cancer, metabolism, inflammation and cardiac function. The process of tyrosine phosphorylation is orchestrated by two seemingly opposing enzymes. Initially thought of as strictly being the counterbalance to the action of tyrosine kinases, recent evidence has established the roles of protein tyrosine phosphatases (PTPs) as both initiators and terminators of cellular signals[208,209]

The human genome contains 107 PTPs divided into several subgroups[210]. The cysteine-based PTPs constitute the most significant group which includes the classical non-transmembrane PTPs is PTP-1B (PTPN1 gene), only have an affinity for phosphotyrosine residues, possesses a catalytic N-terminal domain, a regulatory region, and a membrane-localization domain that tethers the enzyme to the cytosolic side of the endoplasmic reticulum (ER)[211]. PTP-1B dephosphorylates several substrates including the insulin, leptin receptors enf EGF receptors. As a result, it as an essential role in metabolism and angiogenesis.

PTP-1B catalytic domain and inhibition by tungstate

The catalytic domain of PTP-1B is characterized by 280 residues, and it is where the phospho-tyrosine substrates engage in the enzymatic mechanism of dephosphorylation of phosphorylated substrates. Once engaged, a conformational change of the conserved sequence, WPD loop,

occurs, moving the loop closer to the phospho-tyrosine allows the side chain of Asp181 to act as a general acid/base. The side chain of Arg221 changes orientation and assists the closure of the WPD loop. Interactions between the re-positioned Arg221, which stabilizes the phosphate group, and the Trp179 and Pro180 residues stabilize the WDP loop in the closed conformation. The sulfhydryl group of Cys215 is the catalytic residue; it performs a nucleophilic attack on the phosphate group of the phospho-tyrosine substrate while Asp181 transfers a proton to the tyrosine oxygen group of the substrate. The phospho-cysteine intermediate is hydrolyzed; the Gln262 aligns a water molecule for the nucleophilic attack on the phospho-cysteine intermediate while Asp181 now functions as a general base accepting a proton. The removal of the phosphate from the catalytic cysteine leads to the re-opening of the WPD loop, terminating the catalytic cycle[208,209,212–214].

Tungstate behaves like other phosphate mimetics, namely closing the WPD loop[215]. In contrast to vanadate, tungstate does not form a covalent intermediate. Briefly, the mechanism by which tungstate inhibits PTP-1B comprises the formation of hydrogen bonds between two oxygens of tungstate with the amine groups of Ser216, Ile219 and Gly220. Tungstate binding to the catalytic site of PTP-1B causes conformational changes in the enzymes, changing the WPD loop to a closed conformation, inhibiting this way the access of other phospho-substrates to the catalytic domain[209,212]

PTP-1B in insulin signaling

Insulin secreted by pancreatic ß-cell acts as the significant regulator of glucose homeostasis by acting through the insulin receptor. PTP-1B is an established regulator of insulin signaling (Figure10) as evidenced by biochemical, genetic and inhibitor studies[216]. As insulin binds to IR, it induces its autophosphorylation on tyrosines (Tyr1158, 1162, 1163), leading to the recruitment of insulin receptor substrates[208,216], which in turn are phosphorylated by the IR activating several downstream pathways including phosphatidylinositol 3-kinase (PI3K)-Akt and MAPK pathways[217,218]. PTP-1B as a regulator of insulin signaling *in vivo*, the mouse model of Whole-body PTP-1B knockout (PTP-1B KO) is characterized by increased systemic insulin sensitivity and glucose tolerance[219]. Moreover, PTP-1B KO mice show enhanced insulin-induced IR phosphorylation in liver and muscle establishing. When fed high-fat diet, PTP-1B KO mice exhibit resistance to weight gain and develop insulin resistance[219].
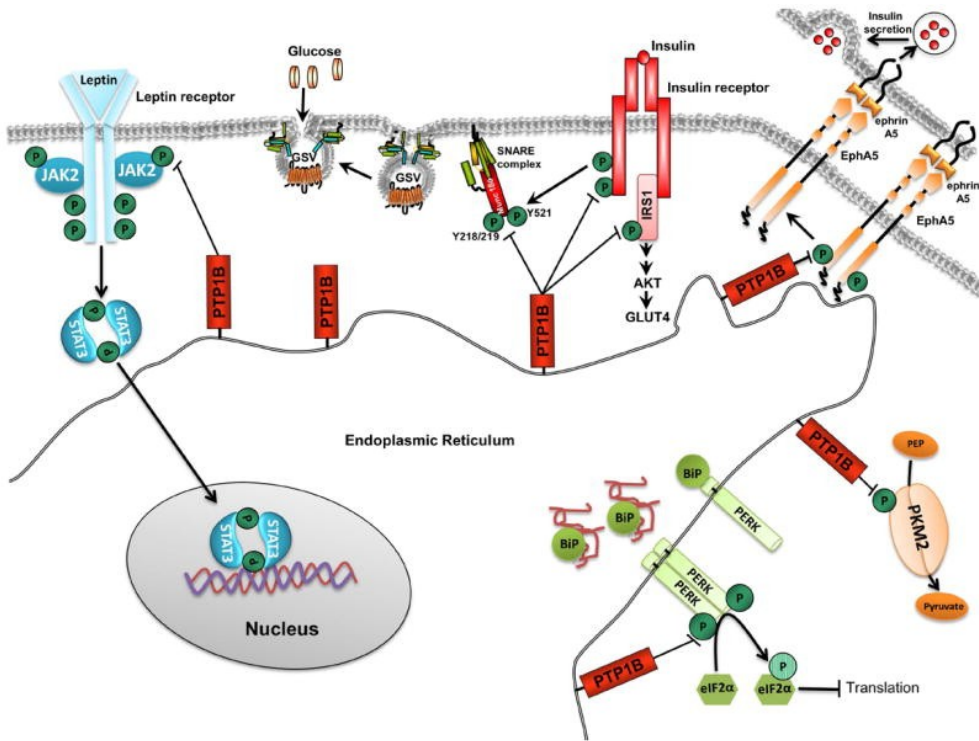
Figure 10: PTP-1B-substrate interaction and metabolic regulation. Adapt from[216].

Furthermore, muscle-specific PTP-1B deficiency has equivalent body weight to control mice but exhibit improved systemic insulin sensitivity similarly, to mice with liver-specific PTP-1B[220–222]. Mice with myeloid cell-specific PTP-1B deficiency exhibit improved glucose tolerance and protection against lipopolysaccharide-induced hyperinsulinemia[223]. Furthermore, and in contrast, overexpression or re-expression of PTP-1B in liver attenuates hepatic IR phosphorylation at Tyr1162/1163 by PTP-1B, where PTP-1B over-expression in muscle impairs insulin-stimulated IR activation and decreases muscle glucose uptake[224,225].

Endoplasmic reticulum stress response

The ER plays an essential role in protein folding and accumulation of unfolded proteins within the ER lumen causes ER stress. As a response to ER stress, cell utilizes ER transmembrane sensor to attenuate stress and maintain homeostasis, one of this sensor is PERK, which is regulated by tyrosine phosphorylation at Tyr615[226–228]. PTP1B and PERK was established and PERK Tyr615 identified as a mediator of the association: mice with liver-specific PTP-1B deficiency are protected against high fat diet-induced ER stress and exhibit attenuation of PERK and eIF2α phosphorylation; similarly PTP-1B deficiency in adipose tissue and adipocytes leads to upregulation of PERK-eIF2α phosphorylation and sensitizes adipocytes to chemical-induced ER stress; and PTP-1B deficiency in pancreatic β-cell lines leads to increased chemical-induced PERK/eIF2α signaling[229–232].

Cell-cell communication

PTP1B likely regulates cell-cell communication by engaging numerous substrates at regions of cell-cell contact, being crucial for metabolic regulation and maintaining homeostasis. Eph RTKs and their PM-bound ephrin ligands exhibit a unique feature of bidirectional signaling and are essential for regulating cell-cell communication. Eph RTK pharmacological inhibition enhances glucose-stimulated insulin secretion (GSIS) from mouse and human pancreatic islets[233]. PTP-1B engages PM substrates at regions of cell-cell contact and can regulate cell-cell communication. PTP-1B regulates EphA3 function and trafficking and EphA2 tyrosine phosphorylation specifically at regions of cell-cell contact[233,234].

Leptin signaling and energy balance

Leptin is an adipocyte-derived hormone that regulates feeding and energy homeostasis[235,236]. Leptin acts by binding to LepRb, JAK2 is activated, autophosphorylates and subsequently phosphorylates tyrosine residues along the intracellular tail of LepRb enabling the recruitment of downstream effectors such as signal transducer and activator of transcription 3 (STAT3)[237]. Mice with combined leptin and PTP-1B deficiency display decreased weight gain, reduced adiposity and increased resting metabolic rates[238–240].

Energy balance is an essential component in metabolic homeostasis, where AMP-activated protein kinase (AMPK) is a fuel-sensing enzyme complex and a regulator of adipose function [121]. PTP1B-deficient brown adipose tissue [122] and brown adipocytes [81] exhibit increased AMPK activity. In addition recent evidence for PTP-1B negatively regulate pyruvate kinase M2 (PKM2)[241], which is a rate-limiting glycolytic enzyme that catalyzes the generation of pyruvate and ATP from phosphoenolpyruvate (PEP) and ADP; further, decreased PKM2 Tyr105 phosphorylation in adipose tissue correlates with glucose intolerance and insulin resistance in rodents, non-human primates and humans[241,242].

PTP-1B in pancreatic islet

Pancreatic β-cells are equipped to sense ambient glycemia rapidly. In order for the cells to respond appropriately with insulin secretion, glucose must be metabolized within the β-cells [243]. Vanadate and tungstate inhibit most PTPs and has been shown to exert direct glucose-dependent insulinotropic effects in isolated rodent islets by mechanisms involving phosphoinositide

hydrolysis and Ca^{2+} handling[243]. In isolated islets from sodium tungstate treated rats, it was observed augments the number of insulin and PDX-1 positive cells in pancreas from sodium tungstate treated STZ-diabetic rats [172,200]. The whole-body PTP-1B KO mice present increased β-cell proliferation *in vivo*. Morphometric analysis of pancreatic islets showed a higher β-cell area, concomitantly with higher β-cell proliferation and a lower β-cell apoptosis when compared to islets from their respective wild-type cognates[244]. Moreover, at a functional level, isolated islets from PTP-1B KO mice exhibited enhanced glucose-stimulated insulin secretion[244]. These mice are also able to partially reverse streptozotocin-induced β-cell loss, all indicating that inhibition of PTP-1B activity in islet cells may be a therapeutic avenue to promote islet function[244].

To investigate the metabolic role of pancreatic PTP-1B, a mouse model with specific pancreatic deletion of PTP-1B (panc-PTP-1B KO) was generated[245]. Results showed that aged panc-PTP-1B KO exhibited mild glucose intolerance[245]; high-fat feeding promoted earlier impairment of glucose tolerance and attenuated glucose-stimulated insulin secretion in panc-PTP-1B KO mice[245]. At the molecular level, PTP-1B deficiency in vivo enhanced basal and glucose-stimulated tyrosyl phosphorylation of EphA5 in islets[245]. The intra-islets inhibition of PTP-1B in rat fed with a high-fat diet, achieved by infection with recombinant adenoviruses containing siPTP1B in isolated islets from high-fat diet rats, results in an improved glucose-stimulated insulin secretion[245]. In contrast, other studies revealed that overexpression of protein tyrosine phosphatase 1B impairs glucose-stimulated insulin secretion, down-regulated the expression of glucokinase (42%) and glucose transporter-2 (48%), in INS-1 cells[245].

PTP-1B and angiogenesis

In endothelial cells (ECs), tyrosine phosphorylation of the VEGF type 2 receptor (VEGFR2) and the adhesion molecule VE-cadherin constitute important initial signaling events by which VEGF stimulates angiogenesis, which leads to activation of different critical angiogenic enzymes involved in ECs proliferation, migration[246] and loss of cell-cell contacts[247] (Figure 11). Thus, tyrosine phosphorylation of VEGFR2 and VE-cadherin are essential initial signaling events by which VEGF stimulates angiogenesis in ECs. VEGFR2 is a Receptor Tyrosine Kinase (RTK) predominantly expressed in endothelial cells (ECs) and their embryonic precursors[248–250], although its expression can be detected in neuronal cells and hematopoietic stem cells ; Deletion of VEGFR2 or its principal ligand VEGFA leads to early embryonic lethality in mice (E8.5/9.5 and E9.5/10.5) due to severe impairment of vascular development and hematopoietic cell maturation[248–250].

Binding of VEGFA to VEGFR2 induces receptor dimerization and autophosphorylation at multiple tyrosine sites including Y1054/1059, Y1175, Y951, and Y1214 and others less characterized[251]. Each site is thought to promote different downstream signaling pathways, which are linked to different cellular responses such as proliferation, migration, survival and permeability[252,253]. Both receptor and non-receptor protein phosphatases can regulate VEGFR2 signaling and will be discussed in turn.
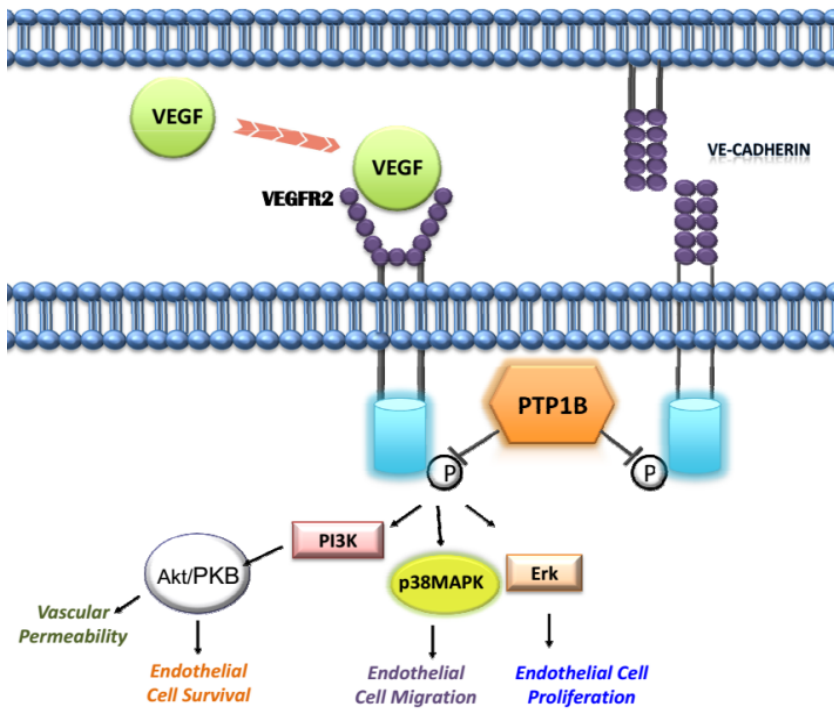
Figure 11: PTP-1B substrates interaction in ECs and angiogenesis regulation. Adapt from[243]

PTP1B substrates include the insulin receptor VEGFR2 and β-catenin[243]. PTP1B dephosphorylates immunoprecipitated VEGFR2 and silencing of PTP1B in HUVEC leads to increased VEGFA-induced VEGFR2 phosphorylation (tested Y1175 only) and proliferation[243] [81]. Similar findings show that primary mouse EC isolated from PTP1B null mice display increased VEGFA-induced VEGFR2 phosphorylation and augmented proliferation and migration in response to VEGFA[243]. General PTP inhibitors have been shown to promote VEGFR2 activation and accelerate neovascularization in rat ischemia hindlimb models[254], suggesting PTPs as potential therapeutic targets to promote neovascularization. However, little is known about the role of endogenous PTPs in VEGF signaling in ECs. Tonks et al. identified protein tyrosine

phosphatase 1B (PTP1B) as among the significant PTPs whose expression is dramatically induced during angiogenesis in a mouse ischemic hindlimb model[255].Nakamura et al. provided evidence that PTP1B negatively regulates VEGF-induced phosphorylation of VEGFR2 in ECs via binding to the receptor, as well as stabilizes cell-cell adhesions through reducing tyrosine phosphorylation of VE-cadherin[256]. These results are consistent with previous reports that PTP1B inhibition of platelet-derived growth factor (PEGF) induced proliferation of cultured vascular smooth muscle, whereas PTP1B expression is increased in vascular injury model[257,258]. These studies suggest that ischemia-induced upregulation of PTP1B may represent an essential compensatory mechanism that blunts overactivation of angiogenic signaling *in vivo*, at least in part, by inhibiting tyrosine phosphorylation of VEGFR2 and VE-cadherin.

Hypothesis and Objectives

It is hypothesized that oral administration of tungstate could improve islet-graft revascularization and transplantation outcome, by a mechanism dependent on PTP-1B. Therefore targeting PTP-1B on islets improves islet-graft's revascularization and survival, constituting a proof-of-concept for future therapy in islet transplantation.

Objective 1: To investigate the effect of tungstate on graft revascularization and survival:

> ***1.1.*** To investigate the effect of tungstate on graft revascularization and survival;

> ***1.2.*** To investigate if the action of tungstate in the revascularization of islet-grafts is mediated by PTP-1B;

Objective 2: To investigate if PTPB1 is a critical target for improving the function, survival, and revascularization of engrafted islets.

> **2.1.** To evaluate the effect of tungstate treatment *in vitro* on islets isolated from PTP-1B$^{-/-}$ mice;

> **2.2.** To evaluate the effect of tungstate treatment *in vivo* on diabetic mice transplanted with islets isolated from PTP-1B$^{-/-}$ mice;

> **2.4.** To investigate whether iECs are critical players in PTP-1B$^{-/-}$ graft revascularization.

Objective 3: To investigate the molecular pathways activated/potentiated by the inhibition of PTP-1B on pancreatic islets that modulate islet survival as well as the capacity of vessels formation;

> **3.1** To investigate the expression of VEGFA on PTP-1B$^{-/-}$ islet-graft and isolated islets;

3.2 To investigate if the expression of VEGFA in the absence of PTP-1B, is dependent on HIF activation, or PGC1-α/ERR-α pathway activation

Objective 4: to investigate if the PTP-1B-dependent islet-graft revascularization is conserved in human islets

4.1 To Silencing PTPN1 gene in human islets;

4.2 To investigate if the signaling events previously studied are conserved in human islet;

4.3 To investigate human islet-graft revascularization after silencing PTP-1B.

Material and Methods

Animal models

Animals were housed on standard light/dark cycle; food and water were provided *ad libitum*. All animal handling and care procedures fulfilled the requisites of the Animal Science Associations (FELASA)-trained scientists, the local ethical commit, the Spanish royal decree 214/1997 and the European Directive 2010/63/EU. Six weeks old male BALB/c mice, and 6 weeks old male Wistar rats were acquired to former Harlan Laboratories, now Envigo Laboratories (Huntingdon, United Kingdom), and the experiments were performed at the age of eight weeks. The experiments were performed in 7 week old mice and 7 weeks old Wistar rats.

PTP-1B transgenic mice (wild-type, PTP-1B$^{+/+}$; and deficient, PTP-1B$^{-/-}$) were obtained from Abbot Laboratories (Abbott Park, IL)[259]. The experiments were performed with 8 and 9 weeks old male mice littermates, maintaining the genetic background of 129/SvJxC57Bl6/J. Genotyping for all mice was performed by polymerase chain reaction (PCR) on tail deoxyribonucleic acid (DNA) using the following primers (5'-3'): GCGAGCTGTGGAAAAAAAGG (PTP-1B telomere repeat binding factors, *Trf2*), CGATCTCCTGCAATCCCTTC (PTP-1B endogenous right #3, Erp3), CAGTCTTGGTCTACAGAGTG (PTP-1B endogenous Left) and CCGCCTTTTCGCTAGCTGAC (PTP-1B neo). The PCR was carried out using HotStarTaq DNA Polymerase (Qiagen, Hilden, Germany). The reaction was performed by denaturation at 95 °C for 15 min and 35 cycles of amplification (94 °C for 45 s, 53°C for 60 s, and 72 °C for 60 s), finishing with 5 min at 72 °C. Male BALB/c mice were acquired to Charles River Laboratories (London, England) at the age of 6 weeks and experiments were performed at the age of 8 weeks. For each DNA sample the following reaction mix used:

Table 3: **Reaction mix for PTP-1B genotyping**

Reactive	Volume (µL)
H2O	13.6
PCR Buffer 10x	2.5
Q buffer 5x	5
MgCl2 50mM	0.75
Primer 5' 100µM*	0.2*
Primer 3' 100µM*	0.2*
dNTP mix 10 mM	0.5
TAQ 5U/µL	0.25
DNA sample	2

*For each primer

STZ-diabetes induction

Diabetes was induced in BALB/c mice, by a single-intraperitoneal injection of streptozotocin (STZ, Sigma-Aldrich, STL, USA) 160mg/Kg, at the age of 7 weeks[260,261]. STZ is a glucose analog (D-glucopyranose), and a diabetogenic agent which causes pancreatic ß-cell destruction[262,263]. It is an alkylating agent, that directly methylates DNA[264], producing profound modification and aberrations leading to cell death[265,266]. In mice, STZ is known to entre ß-cell through the low-affinity glucose transporter GLUT2, located at the plasma membrane[267,268].In this sense, previously to STZ injection, mice were fasted at least 4 hours, to reduce the competition between glucose and STZ for the transporter. Fasting conditions were maintained 30 minutes after STZ administration.

 STZ was reconstituted in a hood, under a sterile condition, due to its volatility. As STZ only maintain a biological half-life, in cell culture, of approximately 19 minutes, and its stability for 30 minutes in solution, we reconstitute STZ immediately before the injection. STZ was reconstituted in cold 0.1M citrate buffer pH 4-5, to a concentration of 30mg/mL. Body weight and blood glucose levels (collecting a drop of blood through the tail vein) were monitored daily, for seven days, and mice were considered diabetic when presented a sustained blood glucose level above 250 mg/dL for three consecutive days.

.

Pancreatic islets Isolation from mouse

Islets were isolated by intraductal injection of the common bile duct (Figure 12) with ice-cold collagenase P (Roche Diagnostics GmbH, MHG, Germany). Collagenase P was reconstituted 0.7mg/mL (1.7U/mg of specific activity) in cold Hank's balanced salt solution (Hbss; from Sigma-Aldrich). All steps of this procedure were performed with the help of a stereoscopic microscope.

Figure 12: Schematic and photographic images of mouse anatomic localization of the common bile duct and major duodenal papilla.
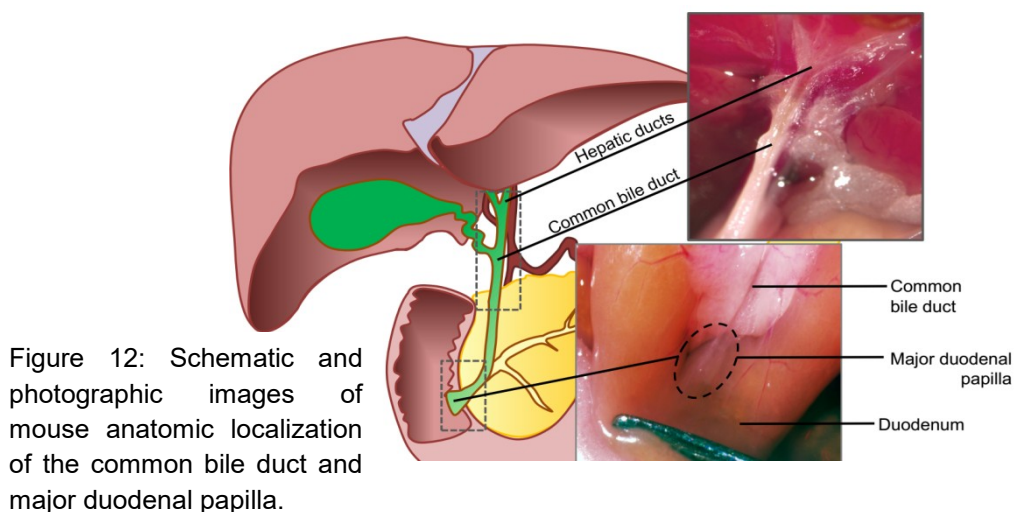
The procedure consists in collapse the distal outlet (or major duodenal papilla) of the mice's common bile duct (Figure 13), with the help of two dissecting forceps (one curved, one straight) and a Hartman curve hemostat (F.S.T., Heidelberg, Germany).
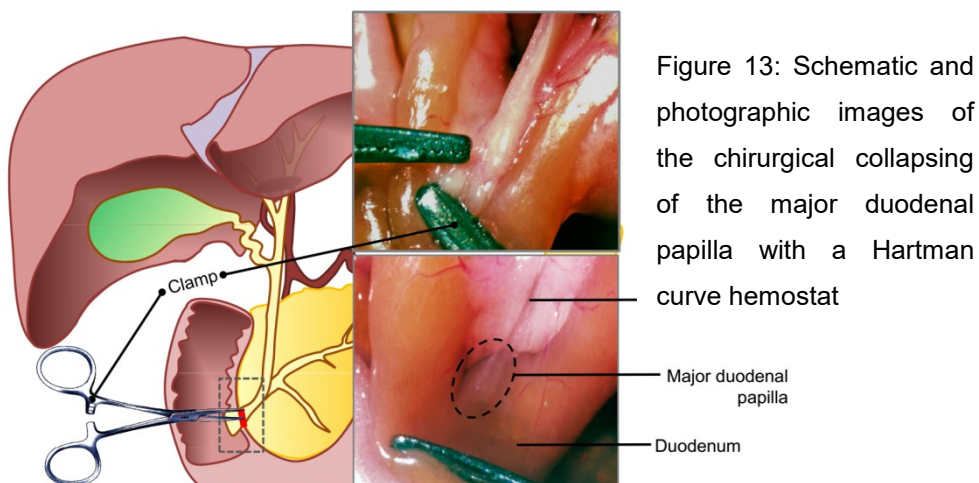
Figure 13: Schematic and photographic images of the chirurgical collapsing of the major duodenal papilla with a Hartman curve hemostat

Two milliliters of the reconstituted collagenase was injected in the proximity of the duct's cystic and hepatic ducts with a 30Gauge needle attached to a 2mL syringe loaded with the cold collagenase solution (Figure 14). The pancreas was distended, and a pancreatectomy was performed with the
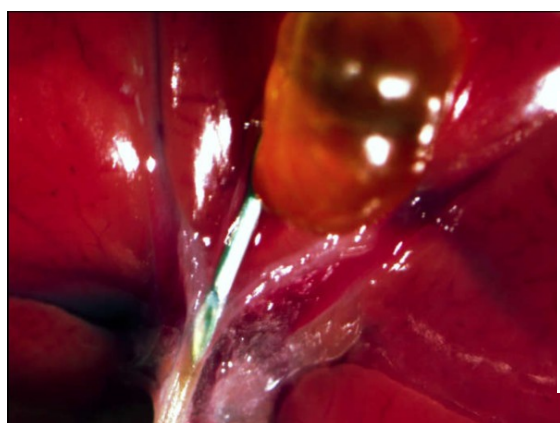
Figure 14: Photographic representation of a 30gauge needle introduced in the proximity of the mouse cystic. and hepatic ducts

help of a dissecting forceps and a fine dissection scissors. The pancreas was transferred into 37°C bath and digested with continuous and gentle

agitation (80rpm). The pancreata were transferred into a sterile environment using horizontal laminar flow hood, where the digestion was stopped by adding sterile ice-cold Hbss complemented with 0.1% bovine serum albumin (BSA). Islets fraction was purified by a gradient centrifugation at 800Gs with Histopaque 1119g/mL, 1:1 mix of Histopaque 1119g/mL and 1077g/mL (Sigma-Aldrich), and Hbss+0.1%. All solutions must be added carefully, to avoid mixing the phases. The Islets were handpicked, at room temperature, from the interface between Histopaque and Hbss, washed and cultured for posterior experimentation.
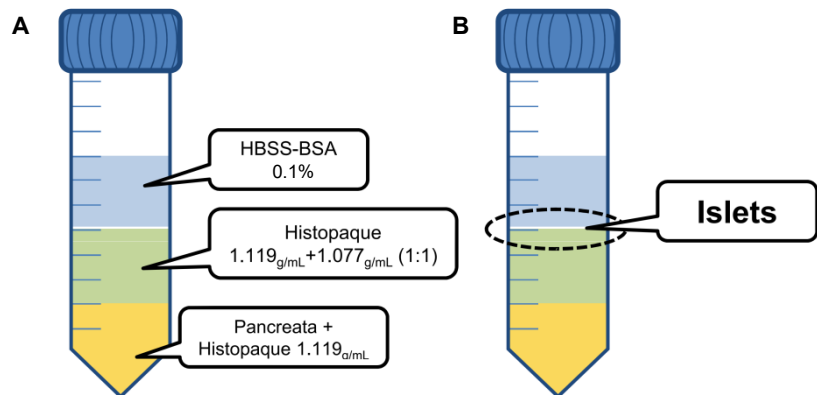
Figure 15: Representation of the gradient-purification of islets. A. Gradient setup with pancreata located at the bottom, followed by the Histopaque 1119g/mL, the 1:1 mix of Histopaque 1119g/mL and 1077g/mL and finally Hbss+BSA 0.1%. B. Interface where purified islets will be located, after centrifugation of 800g.

Pancreatic islets Isolation from rat

Islets were isolated by intraductal injection of the common bile duct with ice-cold collagenase P. Collagenase P was reconstituted 1mg/mL (1.7U/mg of specific activity) in cold Hank's balanced salt solution (Hbss; from Sigma-Aldrich). This procedure was performed at naked eye. After

being fully anesthetized in a chamber saturated with isoflurane, the rats were decapitated; the abdominal cavity was open allowing the exposure of the pancreas and common bile duct. The common bile duct was then collapsed at the distal outlet (or major duodenal papilla) with a Hartman curve hemostat. The pancreas was then perfused with 15mL of 1mg/mL cold collagenase P solution (Sigma-Aldrich) by through the proximity of the duct's cystic and hepatic ducts; the distended pancreas was isolated and incubated at 37ºC for 18 minutes with gentle shaking. After digestion, islets were separated from exocrine tissue by mechanical disgregation (using a plastic Pasteur pipette first and second by a 14G needle) and by density gradient with Histopaque (Sigma-Aldrich, St. Louis, MO, USA)): bottom layer, 1.119g/mL with pancreata resuspended; second layer: 1.077g/mL, top layer Hbss. The density separation was performed by a 20minute centrifugation of 1000G at 11ºC. The purified fraction of the islets was picked from the interf¡phase between the second and the top layer of the gradient. Then, islets were rinsed into a Petri dish and isolated from any contaminating exocrine material by handpicking.

Pancreatic islet culture

Standard culture

Following isolation the mouse or rat islets were cultured in RPMI 1640 medium (Sigma-Aldrich) containing 11mM of glucose, 0.3g/L L-glutamine, 2g/L $NaHCO_3$, 10% heat-inactivated fetal bovine serum (Hyclone, Logan, UT), HyClone™ Penicillin-Streptomycin (100 units/ml penicillin, 100 pg/ml streptomycin) (GE Healthcare Life Sciences, PGH, USA). The islets were cultured at 37°C under a 5% CO_2 and 95% air-humidified atmosphere. Standard culture for islet transplantation involves a 48h culture before transplantation, where the first 24h were for islet recovery from isolation (consult "islets labeling and transplantation section).

Elimination of mouse intraislet endothelial cells

It is known that iECs are lost, in culture, over time[269]. To eliminate iECs, PTP-1B^{-/-} and PTP-1B^{+/+} isolated islets were cultured for 7 days from isolation, under 37°C, 5% CO_2 and 95% air-humidified atmosphere, for 48h, in RPMI 1640 with 11mM of glucose, 3g/L L-glutamine, 2g/L $NaHCO_3$, 10% heat-inactivated fetal bovine serum 100 units/ml penicillin, 100 pg/ml streptomycin. The culture medium was renewed every two days. By the end of the seven days of culture, islets either were transplanted or collected for in vitro characterization.

Nutrient deprivation protocol

To investigate the effect of PTP-1B on the VEGF-A expression we culture PTP-1B^{-/-} and PTP-1B^{+/+} islets under nutrient deprivation. Nutrient deprivation conditions[66] involved culturing islets, under 37°C, 5% CO_2 and 95% air-humidified atmosphere, for 48h, since their isolation, in Hbss with 2g/L of glucose, 100 units/ml penicillin, and 100 pg/ml streptomycin. After 48h, islets were collected and processed for analysis.

Islets labeling and transplantation

Diabetic BALB/c mice (8 weeks of age) were used for allo and syngeneic transplantation. These mice were transplanted with 200 islets (suboptimal transplantation), in the anterior chamber of the eye (ACE). These mice were followed for 25 or 28 days. The anterior chamber of the eye is a privileged transplantation site. It enables non-invasive in vivo imaging[258,270], fast islet engraftment by blood vessels of the host iris (a highly vascular site)[271–273], and reduced graft early rejection sustained by an ocular immune privilege that suppresses immune cell proliferation and purge of

the immune cells that enters the eye[274]. In xenotransplantations, 9-15 week old male and female Nod Scid gamma (NSG, The Jackson Laboratory, ME, USA) mice were used as recipients for human islets. The NSG mice combine an immune deficiency mutation (scid) and an IL2 receptor gamma chain deficiency which disables cytokine signaling, resulting in the lack mature T cells, B cells, functional NK cells, and in a deficient cytokine signaling. This severe immunodeficiency allows the mice to be humanized by the engraftment of human islets.150 human islets, with PTP-1B knocked-out by a shPTPN1 Lentivirus, were transplanted into the anterior chamber of the eye, and transplanted mice were maintained for 8 days.

Islets labeling

The day previous to transplantation islets were labeled with carboxyfluorescein diacetate, succinimidyl ester (CFDA SE; Invitrogen, OR, USA) that, allows not only the evaluation of the viability of islet-graft cells but also the localization of islet-grafts during *in vivo* microscopy[275,276]. CFDA SE passively diffuses through the membrane of viable cells. CFDA emits fluorescence after intracellular esterases cleaved its acetate groups. The resulting carboxyfluorescein-succinimidyl ester groups react with intracellular amines, forming fluorescent conjugates that are well-retained[277]. For the labeling with CFDA SE, cultured islets were washed with Dulbecco's phosphate buffer saline (PBS; Sigma-Aldrich) with 0.1% BSA. Next, they were incubated at 37°C, in a 5% CO_2 and 95% air-humidified atmosphere for 15 min in a 10µM CFDA SE- PBS/BSA dilution to load cells with the probe. Loaded islets were then incubated in standard culture medium for 30 min at 37°C, to allow CFDA SE acetate hydrolysis by intracellular esterases. Labeled islets were finally placed in culture with fresh medium, for 24h, before being transplanted.

Human islets were not labeled with CFDA; these islets possessed GFP, transduced after the infection with the Lentivirus, that will be used to trace the grafts (please consult the "short hairpin Lentivirus infection" section, for more information)

Islet transplantation

Previously to transplant handcrafted blunted cannulas were prepared according to the following protocol:

1. Detach a 30gauge injection needle shaft (Becton, Dickinson and Company, Franklin Lakes, NJ, USA) from its hub, with the help of heat;

2. Blunt the needle bevel with the help of sandpaper and a stereoscopic microscope,

3. Prepare a fine bore polythene tubing: 0.40 mm i.d., 0.80 mm o.d. (Smiths Medical, Kent, UK; ref. 800/100/140) with 400mm of length;

4. Heat one extremity of the tube and seal it against the blunted shaft.

5. Clean the cannula with ethanol 70%, and place the cannula under ultraviolet light for at least 15 minutes, for sterilization.
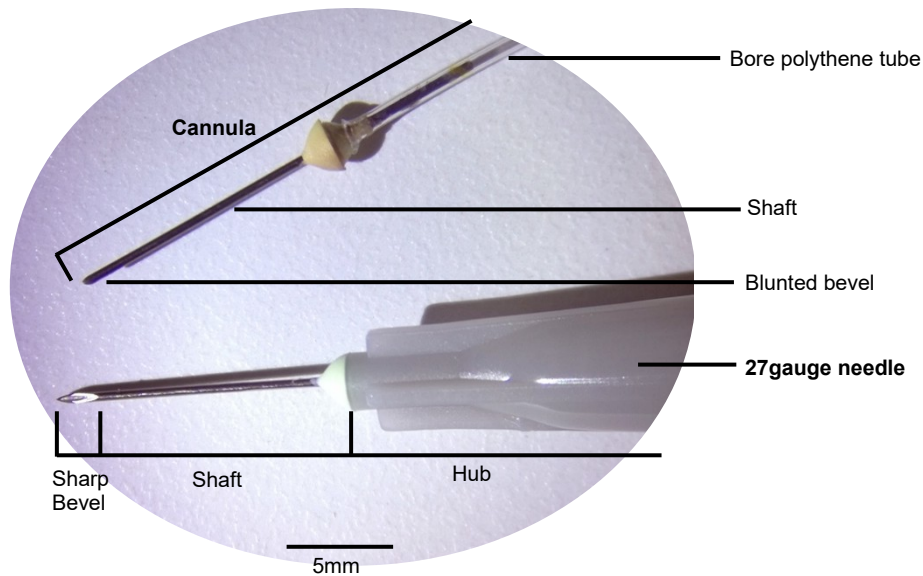
Figure 16: Representation of a cannula for transplantation, prepared from a 27gauge injection needle.

Immediately previous to transplantation, handcrafted blunted cannulas were loaded with 200 islets and maintained at 37°C. Transplantation protocol was followed accordingly to the recommendations of a well-recognized protocol[270,278].

Anesthesia and analgesia: mice were anesthetized intraperitoneally with a mix of ketamine-xylazine (100mg/Kg and 7.5mg/Kg) and received a subcutaneous injection of the analgesic, buprenorphine (0.05mg/Kg) to alleviate postoperative pain. Intraperitoneal injection was given in the lower right quadrant of the mice abdomen to prevent puncturing the sleep, located on the left side. The mouse head should be tipped downward while the mouse is held upside down to prevent puncturing the intestines. The injection was performed using a 30-25 gauge needle at a 45º angle.

<u>Transplantation:</u> Mice were placed over a heat blanket and under a stereoscopic microscope, in a sterile environment. The skin around the eye was retracted to facilitate access. An incision was made in the cornea near the corneoscleral junction with a 25 or 27gaude needle. After cleaning the l aqueous humor that leaked out of the ACE, the loaded cannula, connected to a 500μL syringe, was introduced into the incision, without damaging the iris, and the islets were gently injected. Finally, after the withdrawal of the cannula, a drop of carboxymethylcellulose sodium (Allergan, Ireland) was administrated to the operated eye, and the animals were placed under supervision in a warm environment until full recovery. BALB/c mice were followed for 25 days (for the study of sodium tungstate treatment), or 28 days for the study of the PTP-1B effect on isle-graft revascularization; NSG mice were maintained for 8 days. All mice were housed in standard light/dark cycle; food and water were provided *ad libitum.*

Physiological study: weight, glycemia and glucose tolerance test

During the experiment, weigh, and non-fasting blood glucose levels were measured within the same schedule at the indicated days. Blood glucose levels were measured by collecting blood from the tail vein directly to the glucometer strap. Glucose tolerance test was performed after a 6h fast. Mice were injected intraperitoneally with 1.5g/Kg D-glucose. Blood glucose levels were measured at 0, 15, 30, 60, 90 and 120 minutes after the glucose-bolus; in parallel blood was collected from the tail vein into a capillary blood collection system (Microvette, Sarstedt, Nümbrecht, Germany) to analyze serum insulin level. Insulin levels were measured by a highly specific ELISA kit (Mercodia, Uppsala, Sweden).

In vivo revascularization and cell death Imaging

Functional graft revascularization and cell death were assessed *in vivo*, by two-photon laser scanning microscopy (TPLSM; Leica SP5 TPLSM, Leica Microsystems, Wetzlar, Germany)[279]. The TPLSM presents as a principal advantage the use of a pulsed infrared laser for fluorescent dye excitation. This feature allows deeper tissue imaging of biological tissues in living animals with a micrometric spatial resolution and a lower phototoxicity[280,281] than the conventional microscopy techniques. Briefly, the electron of the fluorescent dyes will absorb energy from an excitatory infrared laser (composed of two photons), until reach excitation state. The return to their ground state is based on the emission of radiation that is detected and multiplied by photodetectors. The photodetector produces an electronic signal that is translated by the computer into numerical values and subsequently in colors.

The dextran is a naturally synthesized polysaccharide with excellent water solubility and low toxicity. Dextran is biologically inert due to the α-1,6-poly-glucose linkages that offer resistance to cleavage making it a useful water-soluble carrier for dyes, like rhodamines, to study the tracing of circulating cells or compounds or hydrodynamic properties of microcirculation[282–285]. Moreover, dextran can be produced with different molecular weights that will facilitate or reduce its permeability through vessels, this way we choose rhodamine B isothiocyanate-dextran of 70kDa. Dextran molecules larger than 70 kDa are retained in the blood for hours under homeostatic conditions, indicating the existence of a permeability resistance in vessels for molecules around 70-kDa, Matching with the permeability of physiological molecules like albumin (66kDa), or transferring (80kDa)[286]. Propidium iodide (PI, Invitrogen) is a small fluorescent molecule that can only enter cells that have compromised membranes where it binds

stoichiometrically to nucleic acids. Therefore fluorescence is proportional to the DNA and RNA content of a cell[287].

Protocol: Briefly, BALB/c mice were anesthetized intraperitoneally with a mix of ketamine-xylazine (100mg/Kg and 7.5mg/Kg). Following this, the mice received an intravenous injection with a mix of rhodamine B isothiocyanate-dextran 100mg/Kg (RITC-dextran, λem595nm; MW: 70kDa; Sigma-Aldrich), propidium iodide 250µg/Kg (PI; Invitrogen) and Hoechst 12mg/Kg (Invitrogen). NSG mice were BALB/c mice were anesthetized intraperitoneally with a mix of ketamine-xylazine (75mg/Kg and 5mg/Kg). Following this, the mice received an intravenous injection with rhodamine B isothiocyanate-dextran 100mg/Kg,

Anesthetized animals were transferred to the microscope stage with the operated eye positioned in a cover glass with a drop of carboxymethylcellulose sodium, in the direction of the objective (40x water immersion objective, Leica). A microscope incubator chamber maintained the adequate temperature. Islet-graft were traced using CFDA (mouse islets) or GFP (human islet). Fluorescence Images of the grafts were acquired at with 0.23µm between each in a length of 50µm, using a two-photon laser at 780nm, an external detector, and a 25x water-objective; an automatic motion artifact correction was used to minimize breathing and heart rate involuntary movements. Images were collected for later analysis with ImageJ software v1.50d (Wayne Rasband, NIH, USA). By the end of the experiment, animals were placed under supervision in a warm environment until full recovery or euthanized to perform enucleation the eye for posterior immunohistochemistry analysis.

Immunohistochemistry-immunofluorescence in paraffinized eye sections

The eyes were obtained by enucleation, after euthanizing mice by cervical dislocation. E enucleation is the most reliable technique to obtain the eye globe without damaging its tissues[288].

Enucleation protocol:

1. Use a curved serrated tip forceps (0.5 x 0.4 mm), gently press on the top of the canthus with the forceps until the eyeball dislocates from the eye-socket out;

2. Press and hold the optic nerve, located behind the eye with the forceps, to lift the globe from the eye-socket and clamp the optic nerve;

3. Performing circular movements holding the forceps in the direction with the least resistance;

4. Constrict the optic nerve and detach de eyeball by gradually increasing the speed of the circular movements;

5. Quickly wash the detached eyeball in cold PBS, and perform two equidistant punctures in the sclera with a 27gauge needle to improve access of fixative agents to the anterior chamber of the eye;

Tissue dehydration, paraffin embedding, and assemblage of the eyes sections

Following enucleation, the eyeball was embedded in paraffin. For this protocol the eye was, previously, kept O/N, at 4ºC, in paraformaldehyde

2%; then incubate for at least 48h in a sucrose solution of 2.1M; and finally dehydrated in a sequential process in which the eyes are incubated in 50% ethanol (EtOH) for 30minutes, twice in 70% EtOH for 30minutes, twice in 96% EtOH for 30minutes, twice in absolute EtOH for 30minutes, followed by an incubation in xylol, 45minutes twice and in paraffin for 60minutes also twice. For paraffin embedding, the dehydrated eyes were transferred onto a metal holder, and then covered with liquid paraffin, and finally placed over a cold surface, until paraffin solidify.

Paraffin sections: Transplanted islet will be engrafted within the anterior chamber of the eye or on the surface of iris[258,278,279]. The Ace has approximately 300µm of depth and the iris a 200µm of thickness[289–291]. In this sense, the eye paraffin blocks were cut with a microtome. Consecutive sections were cut with a 3µm thickness, (on a total of 350µm), and were placed over a polylysine-treated slide and kept at room temperature until proceeding the standard immunohistochemistry-immunofluorescence (IHC-IF) protocol.

IHC-IF protocol

To perform IHC-IF, first, the slides with the paraffin-embedded eyes sections were rehydrated.

1. *Rehydration:*
   1. Incubate slides in xylol for 5minutes;
   2. Transfer slides to absolute EtOH for 3minutes;
   3. Transfer slides to 96% EtOH for 3minutes;
   4. Transfer slides to 70% EtOH for 3minutes;
   5. Transfer slides to 50% EtOH for 3minutes;
   6. Transfer slides to d deionized water for 3minutes;

2. _Antigen retrieval:_

   Place slides in citrate buffer pre-heated to 100ºC, for 10 minutes, in a pressure cooker, and cold-down for 30 minutes;

3. Wash slides twice in phosphate buffer solution (PBS), for 5minutes;

4. _Permeabilization:_

   Place slides in Triton-x100 1%(Sigma-Aldrich, diluted in PBS), for 20minutes;

5. Wash slides in PBS twice for 5minutes;

6. _Blocking nonspecific biding:_

   Slides were blocked with serum against the species in which the secondary antibody was grown for 60minutes, or blocked with 5% BSA in PBS for 60minutes;

7. Wash slides in PBS three times, for 5minutes;

8. _Primary antibody incubation:_

   Incubate slides O/N, at 4ºC in with the primary antibody diluted in antibody diluent (Dako, Glostrup, Denmark);

9. Wash slides in PBS twice for 5minutes;

10. _Secondary antibody incubation:_

    Incubate slides 2h, at room temperature, with the secondary antibody diluent in antibody diluents (Dako);

11. Wash slides in PBS twice for 5minutes;

12. _Nuclei staining:_ Incubate slides with Hoechst 1:500 in PBS;

13. Wash slides in PBS once for 5minutes;

14. Mount slides with mounting media.

Images were acquired in a Leica DMR HC epifluorescence microscope (Leica Microsystems) and analyzed using ImageJ software v1.50d (Wayne Rasband, NIH, USA).

Immunohistochemistry-immunofluorescence in paraffinized pancreas sections

The pancreas was obtained by a pancreatectomy from mice, after drying, it was weighted and transfer into histological cassettes, for further processing. Pancreases were fixed with formalin 10%, O/N at 4ºC, and further processing steps, dehydration, paraffin embedding, cut, and IHC-IF staining were performed as described in the previous section.

Immunohistochemistry-immunofluorescence in whole islets

IHC-IF studies in whole cultured islet offer several advantages over traditional methods such as constructing a three-dimensional mapping of iECs networks by optically sectioning islets with a confocal microscope[292]. The method used for IHC-IF in the whole islet is described below.

Solutions:

- Wash solution 1: PBS;
- Wash solution 2: Triton-x100 0.05%(Sigma-Aldrich) in PBS;
- Fixative solution: paraformaldehyde (PFA; Sigma-Aldrich) 4% in water;
- Permeabilization solution: Triton-x100 0.3% in PBS (4ºC);
- Blocking solution: Bovine serum albumin 1% (Sigma-Aldrich), Triton-x100 0.1% in PBS;
- Antibody dilution solution: Triton-x100 0.1% in PBS;
- Mounting medium: ProLongGold Dapi anti-fade reagent with Dapi (Thermo Fisher Scientific, MA, USA);

Protocol:

1. Transfer islets to a plate with wash solution 1;
2. Repeat step 1 two times;

3. Incubate cells with the Fixative solution at room temperature (RT) for 20 minutes;

4. Wash three times with washing solution 2;

5. Incubate cells with the Permeabilization solution at RT for 15 minutes;

6. Wash three times with washing solution 2;

7. Incubate cells with the Blocking solution at RT for 1h;

8. Prepare primary antibody in the desired dilution with cold Antibody dilution solution;

9. Incubate cells with primary antibody at 4ºC, overnight (O/N);

10. Wash three times with washing solution 2;

11. Incubate with the secondary antibody at RT, 1h (protected from light);

12. Wash three times with washing solution 2;

13. Transfer islets into a μ-slide flat bottom chamber for use in microscopy (IDIBI, Martinsried, Germany) with 250μL of mounting medium in each well

14. Incubate islet for 18-24h at RT (protected from light)

15. Acquire images by confocal microscopy.

IF in whole islets fluorescence was assessed in a confocal microscope (LEICA TCS SPE, Leica Microsystems) for each islet, optical section images were acquired since the peripheral cell layers with 5μm (in the case of PECAM-1 labelling) or 10μm apart, in a total of 60μm/islet, using a 40x oil immersion objective. The 405, 488 and 532 lasers were used, and settings (laser intensity, pinhole, gain, offset, phase and zoom), were maintained unaltered between islets and conditions during the entire experiment.

Antibodies used for IHC-IF detection

For IHC-IF in paraffinized sections and whole islet, the primary and secondary antibodies are listed in Table 4 and Table 5.

Table 4: **List of the primary antibodies used for IHC-IF**

Antibody	Dilution Paraffinized section	Dilution Whole islet	Company
Guinea-pig anti-**INSULIN IgG**	1:1000	1:250	Dako, Glostrup, Denmark
Mouse anti-**GLUCAGON IgG**	1:500	1:100	
Rabbit anti- **PECAM-1** IgG	1:20	1:20	Abcam Cambridge, UK
Rabbit anti-**VEGF-A** IgG	1:100	1:100	
Rabbit anti- Cleaved **CASPASE3** IgG	1:400	1:100	Cell Signaling MA, USA
Mouse anti-**Ki-67** IgG	1:20	n.a.	BD Biosciences NJ, USA
Goat anti-**PTP-1B IgG**	n.a.	1:50	Santa Cruz Biotechnologies Tx, USA

n.a. – not applicable

Table 5: **List of secondary antibodies used for IHC-IF**

Antibody	Dilution Paraffinized section	Dilution Whole islet	Company
Alexa Fluor 555 anti-guinea pig	1:500	1:250	
Alexa Fluor 488 anti-guinea pig	1:500	1:250	
Alexa Fluor 555 anti-rabbit (1:500)	1:500	1:250	Thermo Fisher Scientific, MA, USA
Alexa Fluor 488 anti-rabbit (1:250)	1:250	1:250	
Alexa Fluor 488 anti-mouse	1:100	1:100	
Alexa Fluor 555 anti-goat (1:500)	1:500	1:250	

RNA extraction and analysis

RNA extraction, quantification, and retrotranscription

Total RNA was prepared from isolated islets using the RNeasy Mini Kit (Qiagen, Hilden, Germany). The concentration of RNA in the different samples was determined by absorbance spectroscopy, measured at 260 nm using a Nanodrop 1000 spectrophotometer (Thermo Scientific Wilmington, MA).

RNA was retrotranscribed using the High Capacity cDNA Reverse Transcription Kit (AB Applied Biosystems, USA). For each 10µL of RNA a total of 10µL of reverse transcription master mix (Table 6).

Table 6: Retrotranscription master mix

Component	Volume (µL
10x Reverse transcriptase buffer	2.0
25x dNTP mix (100mM)	0.8
10x Reverse transcriptase Radom Primers	2.0
MultiScribe™ Reverse Transcriptase	1.0
RNase inhibitor	0.5
Nuclease-free water	3.7

Retrotranscription was performed according to the thermal cycling conditions in Table 7.

Table 7: Retrotranscription thermal cycling program

	Step1	Step 2	Step 3	Step 4
Temperature (ºC)	25	37	85	4
Time (min)	10	120	5	∞

Quantitative reverse transcription real-time PCR

Quantitative real-time PCR (qRT-PCR) was performed in a LightCycler 480 System (Roche) using Mesa Green qPCR Master Mix (Mesa Green, Eurogentec, Belgium). All reactions were performed in a 96-well optical plate. For each 2,5µL of cDNA, a total of 7.5 µL of amplification mixes were added (Table 8).

Table 8: **qRT-PCR** amplification **mix**

Component	Volume (µL
Mesa Green qPCR Master Mix	5.0
Nuclease-free water	2.0
Primer 5'	0.25
Primer 3'	0.25
cDNA	2.5

The expression of mouse genes in isolated pancreatic islets was measured, using the gene TATA box binding protein (*Tbp) gene* as the endogenous control (housekeeping gene) for quantification, for human islets the beta-actin *(ACTB)* gene was used.

The qRT-PCR technique is based on the detection of a fluorescent signal from a fluorescent dye (Mesa Green dye) that is being broken down during the amplification of the target sequence in a PCR cycle. The cycle number where the fluorescent signal overcomes the threshold signal of the background noise is called the C_T. The data from the qRT-PCR is expressed in C_T values. For analysis, each CT value was referred to the housekeeping C_T value. Results were expressed as the relative fold change respect to control levels: $2-\Delta\Delta C_T$. The $\Delta\Delta C_T$ value is calculated as the variation between ΔC_T of each sample (variation between the C_T of each gene for a sample and housekeeping C_T for the same sample) minus the ΔC_T of the control condition.

Primers

The mouse and human primers used in this study are listed in Table 9 and Table 10

Table 9: **Mouse primers used in the study**

Gene	Foward	Reverse
Caspase3	ATGGGAGCAGTCAG	GTCCACATCCGTACCA;
Caspase9	ATGCAGGGTGCGCCT	GGTCTCAAGGTCTGTG
Pecam1	GCCTCACCAAGAGAACGGAAG	GCTTTCGGTGGGGACAGGCTC
Kdr	CACTCTCCACCTTCAAACTCTC	*CTATTCCCCTTCCTCACTCTTC*
Cdh5	TTGCCCTGAAGAACG	ACTGCCCATACTTGAC
Vegfa	CACTTCCAGAAACACGACAAAC	TGGAACCGGCATCTTTATCTC
Hif1a	CCCATTCCTCATCCGTCAATTA	GGCTCATAACCCATCAACTCA
Ppargc1a	GCCGGAGCAATCTGAGTTAT	GATCACCAAACAGCCGTAGA
Esrra	AAGTCCTGGCCCATTTCTATG	CATCATGGCCTCAAGCATTTC

Table 10: **Human primers used in the study**

Gene	Foward	Reverse
PTPN1	GCTATGGTGAGGTGTGGATAAG	AGCTCGCTACTTCTCTAACA
HIF1A	*CCAGTTAGCTTCCTTCGATCAG*	GTAGTGGTGGCATTAGCAGTAG
VEGFA	CAGGACATTGCTGTGCTTTG	CTCAGAAGCAGGTGAGAGTAAG
PPARGC1A	CCTTAAGTGTGGAACTCTCTGG	CAGCTTTGGAGAAGCCTAA
ESRRA	TGCTGCTTAATCCTACC	GCCCAATGCAAATGAGAG
GAPDH	AGGTCGGTGTGAACGGATTTG	TGTAGACCATGTAGTTGAGGTCA

Protein analysis

Nuclear protein extraction

Nuclear protein extracts of1000 isolated islets cultured in complete medium and in Hbss were obtained, by bursting the islets cells with a hypotonic buffer (HEPES 10mM, KCl 10mM, EDTA 0.1mM, EGTA 0.1mM, pH8), with NP40 0.05%, and 2µL of sodium orthovanadate 200mM, and 20µL of dithiothreitol (DTT) 50mM for each 1mL of solution. After centrifuge the obtained nuclear pellet was incubated with a hypertonic buffer (HEPES 20mM, NaCl 400mM, EDTA 10mM, EGTA 10mM, Glycelro 20%) with 20µL of dithiothreitol (DTT) 50mM for each 1mL of the solution, to obtain nuclear protein extract. Extracts were kept at -80°C until quantification.

Protocol:

1. Wash islets twice with PBS;
2. Centrifuge 1200g, 2 minutes, 4ºC;
3. Resuspend pellet in 40µL of hypotonic buffer complemented with sodium orthovanadate DTT, and 1% of a protease and phosphatase inhibitors;
4. Incubate suspension in ice, for 15minutes;
5. Add 2µL NP40 1%;
6. Vortex suspension 10seconds;
7. Centrifuge at 11000g, for 30seconds;
8. Recover supernatant (cytosolic fraction);
9. Resuspend pellet with 40µL of cold hypertonic buffer supplemented with DTT, 1% of a protease and phosphatase inhibitors;
10. Incubate suspension in ice, for 15minutes, while vortexing each 2minutes.
11. Centrifuge at 11000g, 5minutes;
12. Recover supernatant (nuclear fraction).

Protein extraction

Protein extraction of isolated islets was obtained using RIPA lysis buffer (Tris 50 mmol/l, pH 7.5, EDTA 5 mmol/l, NaCl, 150 mmol/l, Triton X-100 1%, SDS 0.1%, sodium fluoride10 mmol/l, sodium deoxycholate1 %, or TDLB buffer (triple detergent lysis buffer: Tris 50mM pH 8, NaCl 150mM, SDS 0.1%, NP40-Igepal 1%, sodium deoxycholate 1 %). Each buffer supplemented with 10% phosphatase inhibitor cocktail (Roche) and 4% protease inhibitor cocktail (Roche). For the extraction, islet lysates were frozen and thawed twice in 3 consecutive cycles of 2 minutes: temperatures, -20ºC and 37ºC, followed by a pulse-mode ultrasonication with 3 short burst cycles of the 30s at 20kHz (20 000 cycles/s). Finally, samples were centrifugated at 4500g, for 15 min at 4°C. The supernatants were collected and transferred to a new microfuge tube.

Protein quantification

Protein quantification was determined with the Lowry protein assay kit (Bio-rad, Hercules, CA, USA), using following manufacturer's instructions. Proteins were diluted to a proper concentration, in order to load a total of 20µg of extract. All extracts were stored at -80°C until required.

Western blotting

The protein extracts were separated by molecular weight using sodium dodecyl polyacrylamide gel electrophoresis using a precast gradient gel 4%-15% (Bio-rad). After loading the gel-containing tray with the electrophoresis running buffer 1x, the extracts (20µg), the Laemmli loading buffer 2x (), and molecular markers (GE, healthcare) were loaded.

Electrophoresis running buffer 10x:

- Tris(hydroxymethyl) aminomethane 25mM;

- Glycine 192mM;
- SDS 1%;
- miliQWater up to1L
- pH8.3

Laemmli loading buffer 2x:

- Tris(hydroxymethyl) aminomethane-HCl 0.5M;
- Glycerol 40%;
- SDS 10%;
- 2ß-mercaptoethanol 10%
- miliQWater 2mL
- 2 drops of bromophenol blue

The electrophoresis was performed at a constant voltage 120V for 1-2 hours. Then, the proteins were electrotransferred onto a PVDF membrane (Perkin Elmer, USA):. Before being mounted, the PVDF membrane was activated in methanol, 1minute, and wash in transfer buffer 1x. All components were placed in the tray together with an ice block. The transfer was performed at 200mA, for approximately 1h45minutes to 2hours.

Transfer buffer 1X:

- Electrophoresis running buffer 10x, 100mL;
- Methanol 200mL
- miliQWater, up to 1L

TBS 1x (tris buffered saline):

- Tris(hydroxymethyl) aminomethanel 20mM
- NaCl 150mM
- miliQWater
- pH7.4

TBST 0.05% (tris buffered saline – tween20):

- Tris(hydroxymethyl) aminomethanel 20mM
- NaCl 150mM
- Tween-20 0.05%
- miliQWater
- pH7.4

The membranes were blocked for 1 h with blocking solution: 0.05% Tween-20 and 5% NFDM or 5% BSA (dependent on the manufacturer's recommendation), to avoid non-specific biddings of the membrane with the antibody.

Protein immunoblotting and immunodetection

1. Wash the membrane with TBST twice, for 5minutes;
2. Incubate the membrane, O/N, at 4ºC with the primary antibody diluted in blocking solution;
3. Wash the membrane with TBST twice, for 10minutes;
4. Incubate the membrane, 2h, at room temperature with the secondary antibody diluted in the blocking solution;
5. Wash the membrane with TBST twice, for 10minutes;
6. Incubate the membrane with ECL (Thermo Fisher Scientific) to the membrane , for 1 minute at room temperature;
7. Acquire the blot- image, exposing the membrane in the ImageQuant LAS4000 (Leica), adjusting the time of exposure for an optical signal.
8. Revealed membranes were analyzed using Image J software v1.50a.

9. *For multiple antibody analysis, proceed to antibody removal:*
   1. Wash the membrane with TBST twice, for 10minutes;
   2. Incubate membrane with stripping buffer at room temperature;

3. Wash the membrane with TBST twice, for 5minutes;

4. Repeat the blocking and the immunoblotting /detection protocols.

Antibodies used for immunoblotting detection

The membranes were incubated overnight at 4 °C with the primary antibodies listed in Table 11

Table 11: List of the primary antibodies used for IHC-IF

Antibody	Dilution used	Detected band (kDa)	Company
Rabbit anti - **HIF-1-ALPHA** IgG	1:1000	120	Abcam Cambridge, UK
Rabbit anti - **PGC-1-ALPHA** IgG	1:1000	92(105)	
Rabbit anti – **ERR-ALPHA** IgG	1:1000	55	
Rabbit anti-**VEGF-A** IgG	1:1000	43	
rabbit anti- Cleaved **CASPASE3** IgG	1:1000	17;19	Cell Signaling MA, USA
Rabbit anti-**PTP-1B IgG**	1:500	50	Upstate biotechnologies NY, USA
Rabbit anti- LAMIN-B1	1:1000	68	Cell Signaling MA, USA
Mouse Anti ALPHA-TUBULIN	1:1000	50	Sigma-Aldrich, STL, USA

VEGFA secretion quantification

In vitro VEGF-A secretion was studied by culturing islets for 48h in complete medium without FBS supplementation or directly in nutrient deprivation conditions (Hbss). Islets and culture medium were collected.

The protein contents from culture mediums were concentrated by centrifugal ultrafiltration (3kDa, Merc-Millipore, MA, USA). VEGF-A secretion and islet's content were quantified by ELISA (Abcam) following the manufacturer's indications.

In vitro insulin secretion and pancreas content quantification

In vitro Insulin secretion was performed using separated batches of 8 isolated islets from 4-5 different mice from each group were first pre-incubated at 37°C in a 5.6 mM glucose Krebs-Ringer bicarbonate buffer solution (KRBH) for 30 min. The supernatant was discarded, and islets were incubated for 60 min at 37°C in KRBH containing 2.8 mM or 16.7 mM glucose, respectively. After incubation, supernatants were collected. To pancreatic insulin content, the pancreas was isolated, homogenized in acid alcohol, and extracted overnight at 4°C. The solution was centrifuged to remove tissue in suspension and neutralized. Insulin secreted, and islet-insulin content was measured by using a highly specific mouse- insulin ELISA kit (Mercodia, Uppsala, Sweden).

Human islets isolation and culture

Human islets were obtained from 5 deceased donors after circulatory death (Table 12). Human islets were isolated at the Laboratory for Diabetes Cell Therapy (Montpellier, France) according to a modified version of the automated method[293,294]. Briefly, the pancreas was perfused with cold Collagenase NB1 solution, using controlled pump perfusion. The pancreas was digested at 37°C in the digestion camera, and the islets were purified from the pancreata in a differential gradient using a COBE 2991 cell processor. After isolation, the islets were culture for recovery during 1-5

days in CMRL-1066 medium (Invitrogen) containing 1g/L glucose, 10% FBS, antibiotics, and glutamine. For the experiments on silencing PTP-1B, the islets were cultured on RPMI 1640 medium (Sigma-Aldrich) containing 11mM of glucose, 0.3g/L L-glutamine, 2g/L $NaHCO_3$, 10% heat-inactivated fetal bovine serum (Hyclone), 100 units/ml penicillin, 100 pg/ml streptomycin (GE Healthcare Life Sciences). The islets were cultured at 37°C under a 5% CO_2 and 95% air-humidified atmosphere.

Table 12: **Clinical characteristics of the donors**

Gender	Male (%)	60
	Female (%)	40
	Age (years)	60.8+-12.4
	BMI (Kg/m^2)	28.8+-2.48
Cause of deceased	Trauma (%)	40%
	Vascular injury (%)	60%

Human islets purity

In order to check batch purity, a random sample was stained with dithizone (DTZ). DTZ is a zinc chelating-dye, in pancreatic preparations; zinc is mainly present in the ß-cell secretory granules couple to insulin, forming a hexamer[295]. When chelated with zinc DTZ produced bright red/pink islets when viewed by white-light microscopy in a stereoscopic microscope. The average purity calculated for the 4 batches.

DTZ staining protocol:

1. Prepare Dithizone stock solution 5mg/mL, store at 4ºC, protected from light, up to 1month;

2. Prepare work solution by diluting stock solution 1:5 with HBSS-BSA;

3. Filter work solution with a 0.45µm pore-sized membrane filter;

4. Transfer 2mL of working solution into a 35mm Petri dish;

5. Transfer a random sample of your islet suspension into the previous Petri dish;

6. Incubate islets for 15 minutes at 37°C under a 5% CO_2 and 95% air-humidified atmosphere;

7. Observed and count islets using a stereoscopic microscope.

Human islet viability assessment

Islet viability assay is based on the evaluation of the islet cell membrane integrity using the fluorescent dyes carboxyfluorescein diacetate/propidium iodide (CFDA 1µL/mL. PI 2.5µg/mL).

Viability protocol:

1. Prepare CFDA work-solution, 1mL of CFDA 10mM per 1mL of Hbss-BSA 0.1%;

2. Wash islets with Hbss-BSA 0.1%;

3. Incubate islets with CFDA work-solution, at 37°C under a 5% CO_2 and 95% air-humidified atmospher;

4. Transfer islets into Hbss-BSA 0.1%, and incubate for 30minutes, at 37°C under a 5% CO_2 and 95% air-humidified atmosphere;

5. Prepare a PI 2.5µg/mL and Hoechs 50µg/mL work-solution from stocks solution of 1mg/mL and 10mg/mL, respectively.

6. Incubate islets in PI–Hoechst work-solution , for 20 minutes, at 37°C under a 5% CO_2 and 95% air-humidified atmosphere;

16. Transfer islets into a µ-slide flat bottom chamber for use in microscopy (IDIBI, Martinsried, Germany) with 250µL of PI–

Hoechst work-solution and Acquire images by confocal microscopy. CFDA (λexcitation:492nm; λemission:517); PI (λexcitation:535nm; λemission:617)

CFDA/PI-Hoechst fluorescence in islets was assessed in a confocal microscope. For each individual islet, optical section images were acquired from the peripheral cell layers with 10µm apart, in a total of 60µm/islet, using a 40x oil immersion objective. The 405, 488 and 532 lasers were used, and settings (laser intensity, pinhole, gain, offset, phase and zoom), were maintained unaltered between islets and conditions during the entire experiment. Dead cells (PI staining) were stained red and viable cells (CFDA) were stained green, and both were quantified using the using Image J software v1.50a.

Viability analysis: The islets were matched into categories: 0: few or no viable cells and the majority stained for PI (average viability=non-viable), 1: approximately 75% of the cells presented PI staining (average viability=25%); 2: approximately 50% of the cells with PI staining (average viability=50%); 3: approximately 25% of the cells were positive for PI (average viability=75%); 4: all cell viable (average viability=100%). To determine the total viability of the batch the following equation was used: Total viable=(0.25 (Σ of cat 1)+0.5 (Σ of cat 2)+0.75 (Σ of cat 3)+(Σ of cat 1)) 100 / total number of islets.

siRNA transfection assay

Islets are compact cellular structures; in order to increase the diffusion of siRNA through the islet, we pre-incubated islets in a dilute solution of trypsin (50mg/mL or 2.1µM; dilution optimized previously optimized) for 1.5 minutes at 37°C. Incubation with diluted trypsin is intended to increase the

distance between islet cells, without compromise islet structure, allowing siRNA to diffuse into the core of the islet. In order to evaluate the diffusion of siRNA throughout the islets, we incubate islets, for 72h, at 37°C, in a 5% CO_2 and 95% air-humidified atmosphere, with a non-targeting Accell siRNA with eGFP, and visualize siRNA diffusion (Dharmacon, CO, USA), without fixing the islet and using confocal microscopy (laser 488nm) and bright field. The autofluorescence of islets without being incubated with the non-targeting siRNA with eGFP was also visualized and set as a negative control, using the same excitation and emission settings for eGFP (517 nm). Optical sections were acquired with 10μm apart in a total of 80μm and analyzed using Image J software v1.50a. To silence PTP-1B in islets a PTPN1 SMART pool Accell siRNA technology was used (Dharmacon), following the manufacturer's instructions. This pool is composed of four oligonucleotides design to target specific sequences of the *PTPN1* gene. Following a 72h culture with siRNA, the islets were collected, and RNA was extracted as described previously. Gene expression was assessed by quantitative real-time PCR.

Short Hairpin Lentivirus infection

Short hairpin RNA lentiviral particles (shRNA LV) represents a more effective strategy for sustaining the downregulation of a gene in islets[296–298], without affecting islet function[296–298] when compared with siRNAs. Therefore, using this technology allows evaluating the effect of PTP-1B knock-out in the revascularization of human islet-grafts. A shRNA LV for human PTPN1 (shPTPN1 LV) with a pGFP vector (to monitor the transfection efficiency) was acquired by OriGene Technologies (MD, USA). The shPTPN1 LV (Figure 17) possesses three major functional elements within the 5`-LTR and 3`-LTR regions:

1. shPTPN1 expression cassette driven by a U6 promoter
2. Puromycin resistance marker is driven by an SV40 promoter
3. GFP is driven by a CMV promoter.
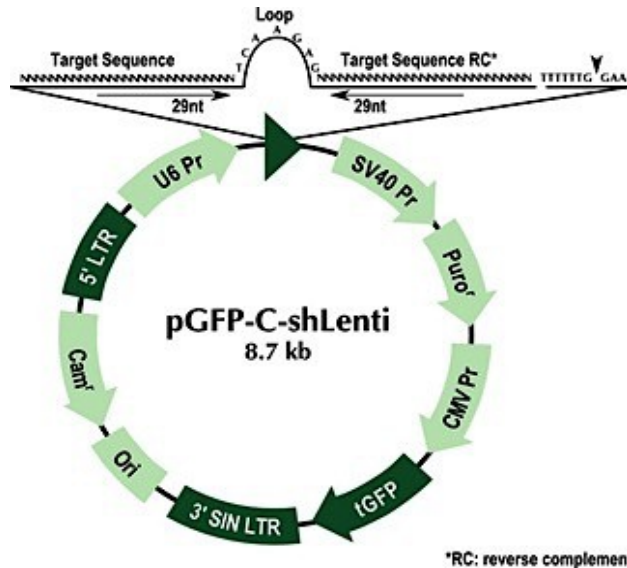
Figure 17: The pGFP-C-shRNA Lentivirus Vector. Start-End composition 835-1015 5`LTR; 2618-2624 EcoR1; 2693-2949 U6 promoter; 3033-3224 SV40 promoter; 3291-3890 Puromycin-N-acetyl transferase; 4265-4271 Xba1; 4282-4987 CMV promoter; 5030-5734 tGFP; 7066-7246 3`sinLTR; 7213-7832 pBR322 origin replication; 7892 8551 CAM[r] for Chloramphenicol resistance.

Four independent shPTPN1 expression vectors were used (Table 13), and a pGFP-C-shLenti vector containing a non-effective (scrambled) shRNA cassette was used as a specific negative control for gene down-regulation. To achieve a high efficient intra-islet transduction, the following, adapted protocol[296] was used:

1. Collect medium and islets from the plate in a 15ml falcon tube;

2. Centrifuge islets at 50 x g for 2 minutes and remove supernatant;

3. Incubate islets with 1000 µl of warm (37ºC) 0.5 X trypsin EDTA (250 (250mg/l trypsin; 0.48 mM EDTA) for 3 minutes in a cell culture incubator

(37ºC, 5% CO2). For trypsin- EDTA preparation: Aliquots of 0.5% Trypsin-EDTA 10 X (5000 mg/l; 9.6 mM EDTA) are diluted in Hanks Balanced Salt Solution (HBSS) 1 X to obtain a final concentration of 0.5 X trypsin- EDTA (250mg/l; 0,48 mM EDTA);

4. Pipette up and down 3 times slowly and carefully with a 1000 ul tip using a micropipette and subsequently add 1000 µl of complete RPMI (1g/L glucose, 10% FBS, pen-strep);

5. Centrifuge islets at 100 X g for 1 minute and remove supernatant;

6. Resuspend 150 islets in serum free RPMI. Place islets in a polystyrene Round-bottom tube (final volume does not exceed 100 µl);

7. Add lentiviruses at 20 Plaque Forming Units per cell (PFU/cell), assuming that a single islet has 1000 cells. Note that final volume must not exceed 300 µl and virus concentration must be in the range of 1.7x 10^4 PFU$^{/}$ µl. 5 µg/ml of polybrene was added;

8. Incubate islets over-night in cell culture incubator (37ºC, 5% CO2) for optimal lentiviral transduction;

9. Remove medium and add 500 µl of complete RPMI;

10. Transplant islets or incubate them in 12 well suspension plates (37ºC, 5% CO2) to assess the downregulation efficiency and VEGFA secretion.

Table 13: PTPN1 sequences for shPTPN1 LV

ACGAGGACCATGCACTGAGTTACTGGAAG
GCTTACCTCTGCTACAGGTTCCTGTTCAA
CCTTCTGTCTGGCTGATACCTGCCTCTTG
TGCGCTTCTCCTACCTGGCTGTGATCGAA

The transfection efficiency was monitored by fluorescent microscopy, by exciting and detecting the tranduced GFP. PTP-1B downregulation was assessed by Western blot, and VEGFA secretion was analyzed by ELISA. Islets were transplanted into the anterior chamber of the eye of NGS mice, and *in vivo* revascularization was assessed after 8 days.

Statistics

All data were plotted and analyzed using the software, GraphPad Prism (Prism version 6.00 for Windows, GraphPad Software, La Jolla California USA, www.graphpad.com). Data are depicted as Means ± SEM. unless otherwise specified. An unpaired Student's t-test was performed to analyze variances between two populations. Two-way ANOVA (Bonferroni's post hoc test) was used to compare multiple variables between multiple populations. Meanwhile, a one-way ANOVA was used to test one independent variable between multiple populations. A value of $p<0.05$ was considered significant, and data points were considered outliers if they presented a value equal or superior two standard deviations away from the mean.

Results

Chapter 1| Oral administration of sodium tungstate improves islet-graft revascularization and survival

Sodium tungstate treatment decreases glycemia of isotransplanted stz-induced diabetic mice.

To study the effect of sodium tungstate treatment on the engraftment of islets, we performed a suboptimal isotransplantation of islets isolated from BALB/c mice into the anterior chamber of the eye of STZ-induced diabetic BALB/c mice (Figure18A and B).
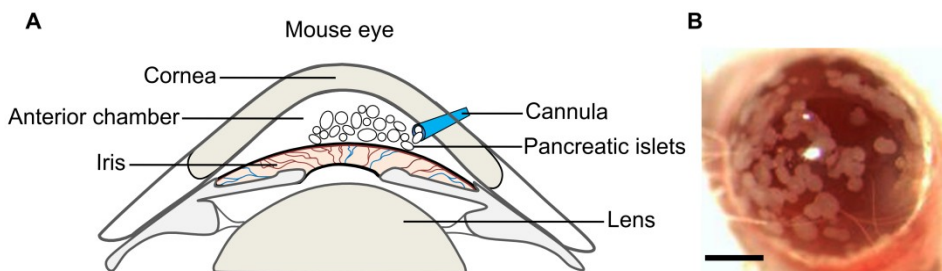
Figure 18: Schematic representation (A) and a representative image (B) of transplanted islets into the anterior chamber of the eye. Image scale bar 2mm

Mice were considered diabetic when presented with non-fasting blood glucose levels above 250mg/dL (diabetic threshold) for three consecutive days. Transplanted diabetic mice were randomly separated into two groups. One group was treated with sodium tungstate (Tx+Na_2WO_4), and another group non-treated served as control (Tx). Apart from these, other two groups of diabetic non-transplanted animals were constituted; one group was equally treated with sodium tungstate (non-

transplanted+Na$_2$WO$_4$) and the other not (non-transplanted). The four groups were monitored for 25 days.
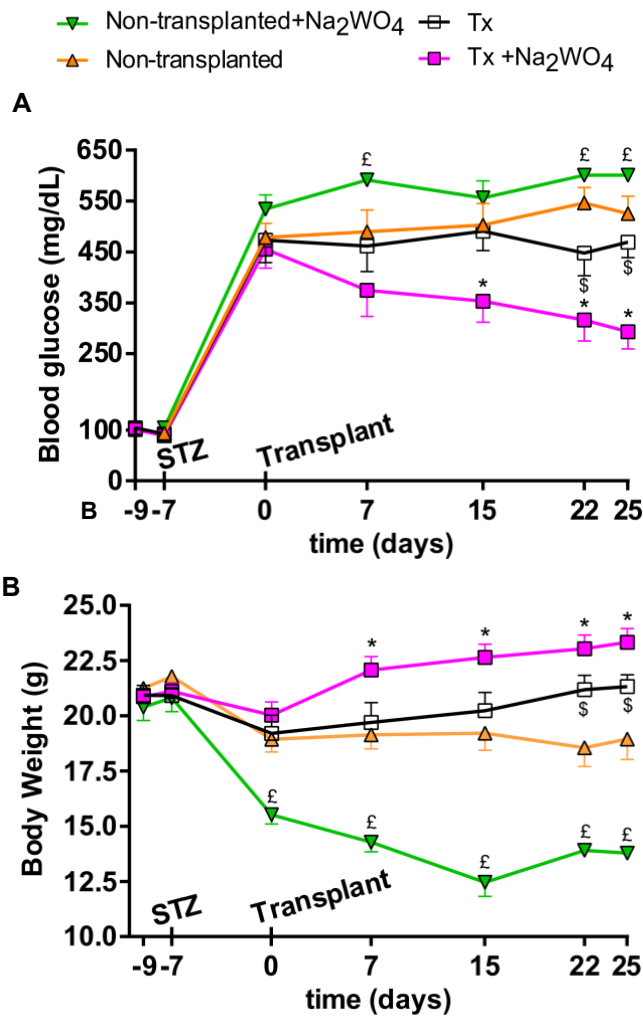
Figure 19: A. Blood glucose levels of the diabetic BALB/c mice during 25 days following transplantation: non-transplanted (n=9), non-transplanted and treated with sodium tungstate (non-transplanted+Na$_2$WO$_4$; n=12), isotransplanted (Tx, n=12) and isotransplanted and treated with tungstate (Tx+Na$_2$WO$_4$, n=9). Mice were considered diabetic after three consecutive blood glucose measures above threshold (250mg/dL). B. Body weight measurement of non-transplanted (n=9), non-transplanted+WO$_4$ (n=12), Tx (n=12) and Tx+WO$_4$ (n=9) mice for 25 days. Data presented as Mean ± SEM, *p<0.05, for Tx vs. Tx+Na$_2$WO$_4$; $p<0.05 for Tx

vs. non-transplanted and £p<0.05, for Tx vs. non-transplanted+Na_2WO_4, by two-way ANOVA.

During this period the Tx group display no improvement in their non-fasting blood glucose level (Figure 19A). The Tx+Na_2WO_4 mice exhibit a 35% reduction in the blood glucose levels, with regards to their initial values (Figure 19A). The non-transplanted and the non-transplanted+ Na_2WO_4 did not exhibit any decrease in their blood glucose. Regarding body weight, every STZ-induced diabetic mice presented a reduction as a counter-effect of STZ (Figure 19B). Following transplantation, Tx group registered a recovery in their body weight. However, Tx+Na_2WO_4 not only recovered their weight but continued improving until the end of the experiment (Figure 19B). The non-transplanted, and non-transplanted+Na_2WO_4 group registered a continuous decrease in their weight being this loss more pronounced in the later (Figure 19B).

Sodium tungstate treatment improves graft revascularization and survival.

As Tx+Na_2WO_4 demonstrate signs of improved engraftment, we assessed *in vivo* graft functional revascularization and survival by two-photon microscopy (Figure 20A) after the injection of RITC-dextran and propidium iodide. Regarding graft's functional revascularization we analyzed both vascularization area (as the graft's vessel area by total graft area) and vascular density (as the total number of vessels and newly formed branches by total graft area). We found that Tx+Na_2WO_4 grafts possessed 37% more vessel area (Figure 20B) and 83% more vessel density than Tx grafts (Figure 20C), demonstrating improved graft revascularization. Along with revascularization, graft's cell death was analyzed. Results revealed a

significant 86% decrease in positive propidium iodide nuclei staining in Tx+Na$_2$WO$_4$ grafts when compared with Tx grafts (Figure 20D).
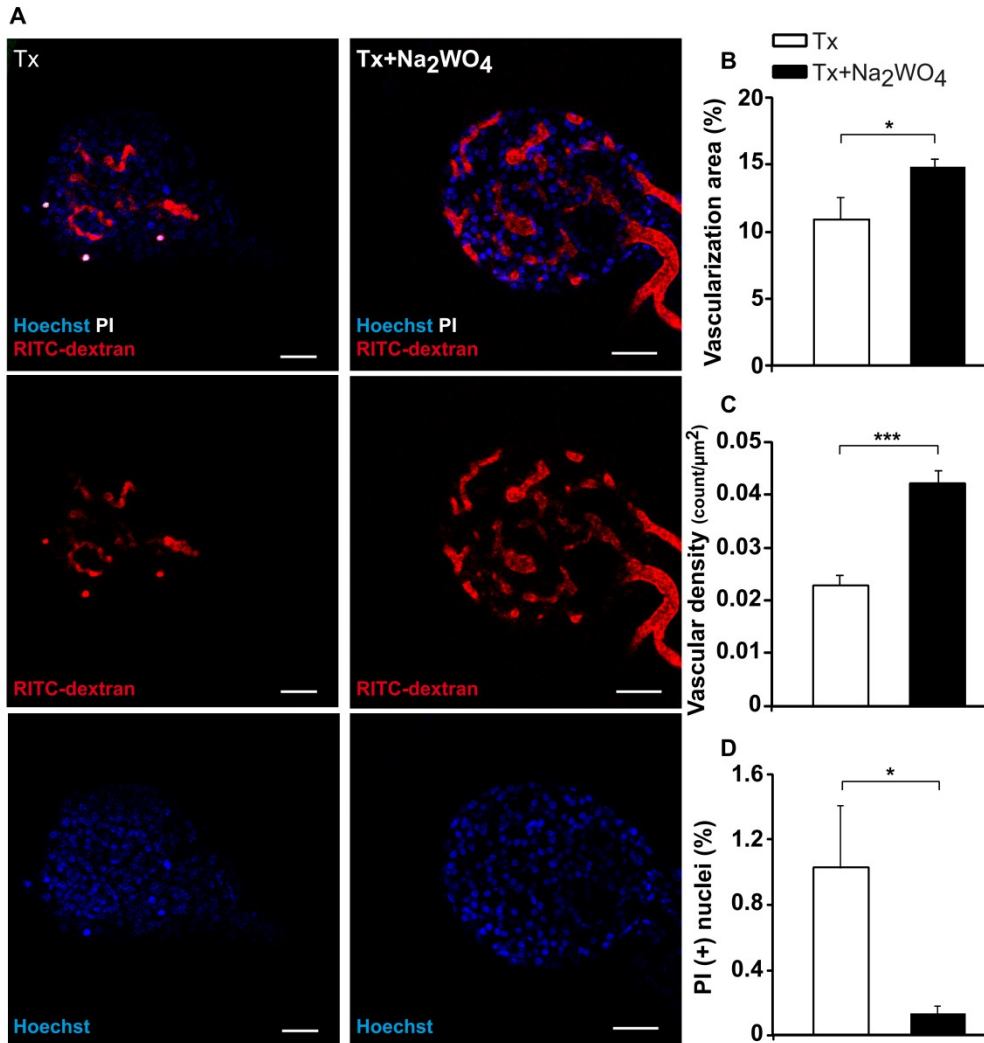
Figure 20: Sodium tungstate treatment improves graft revascularization and survival. A. Representative *in vivo* images of the functional vasculature (RITC-dextran labeling), and cell death (propidium iodide) in Tx and Tx+Na$_2$WO$_4$ (n=8 islets* 6 animals) acquired 25 days after transplantation using two-photon microscopy. B. Quantification of relative vascularization area by islet area, C, relative vascular density, and D, relative cell death (propidium iodide positively

stained nuclei) at day 25 (n=8 islets* 6 animals). Images scale bar 50µm. Data presented as Mean ± SEM; *p<0.05, ***p<0.001, by student's t-test.

Sodium tungstate treatment improves islet graft mass.

As sodium tungstate treatment improves graft revascularization, we study how graft's mass was affected by this increment of vessels. We analyzed the paraffinized sections of the engrafted eyes by staining INSULIN and GLUCAGON (Figure 21A). Results show that $Tx+Na_2WO_4$ grafts presented and graft area 4 fold higher than Tx grafts (Figure 21B). Moreover, the ß-cell area was 5 fold higher in $Tx+Na_2WO_4$ than in Tx (Figure 21C).
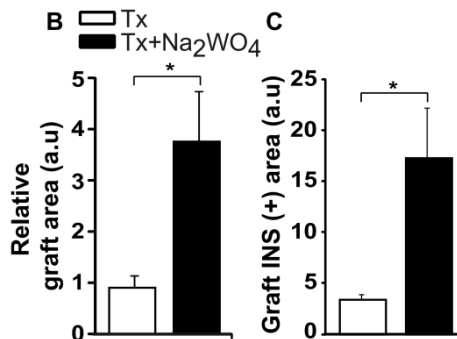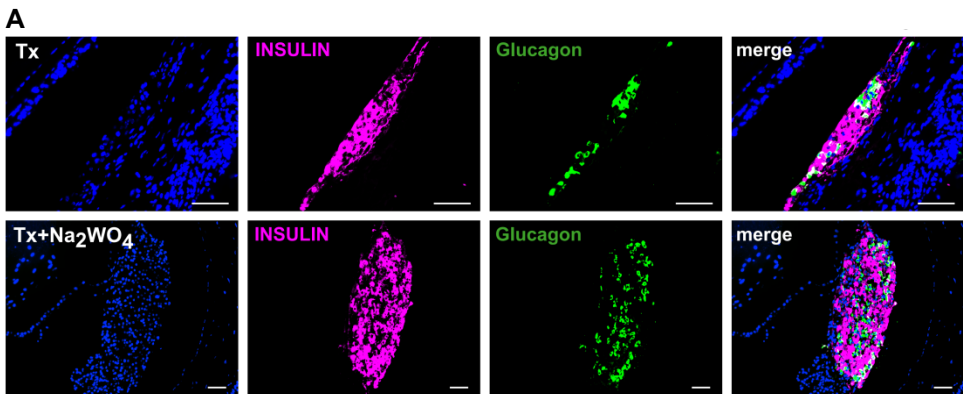
Figure 21: Sodium tungstate treatment improves islet graft mass. A. Representative immunofluorescence images of engrafted eyes from Tx and Tx+Na$_2$WO$_4$ (n=8 islets*6 animals), 25 days after transplantation: co-staining INSULIN with GLUCAGON analyzed the islet-graft area. Top panels represent Tx group and bottom panels Tx+Na$_2$WO$_4$ group. B. Relative islet graft Mean area (n=6 islets*6 animals). C. Graft relative insulin-positive area by total islet area (n=6 islets*6 animals). Images scale bars 50µm. Data presented as Mean ± SEM; *p<0.05, **p<0.01 by Student's t-test.

To elucidate if whether the increment in islet-graft areas was due to an effect of sodium tungstate in cells replication, we analyzed ß-cell co-localization with Ki67, a cell replication marker (Figure 22A). Results show no differences between groups (Figure 22B).

A

B
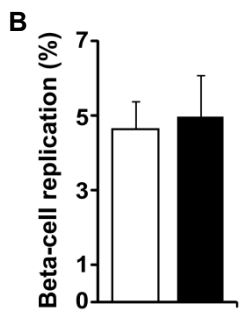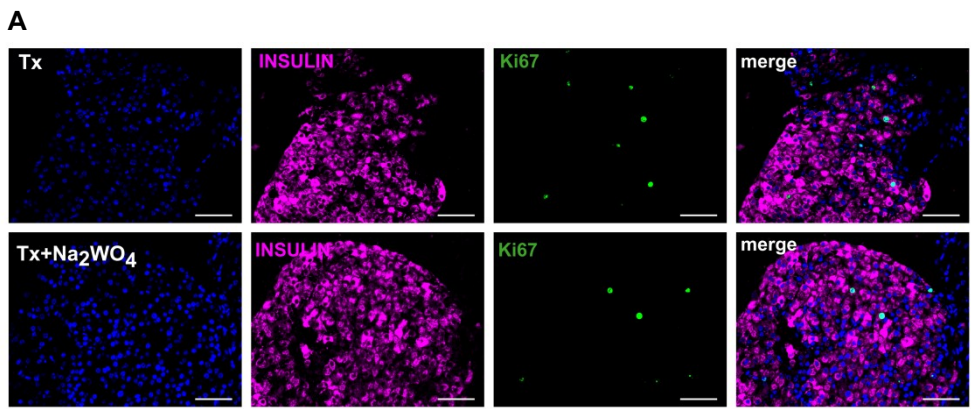
Figure 22: A. Representative immunofluorescence images of engrafted eyes from Tx and Tx+Na$_2$WO$_4$ (n=8 islets*6 animals), 25 days after transplantation: Cell replication, Ki67, co-stained with INSULIN. Top panels represent Tx group and bottom panels Tx+Na2WO4 group. B. Graft cell-replication by quantifying the co-localization of positive INSULIN-Ki67 cells (n=7 islets*6 animals). Images scale bars 50μm. Data presented as Mean ± SEM; *p<0.05, **p<0.01 by Student's t-test.

Furthermore, no effect in pancreas islets cell replication was observed among all four groups (Figure 23A, B, and C). This data indicates that sodium tungstate treatment improves relative graft's area by decreasing the graft's ß-cell apoptosis.
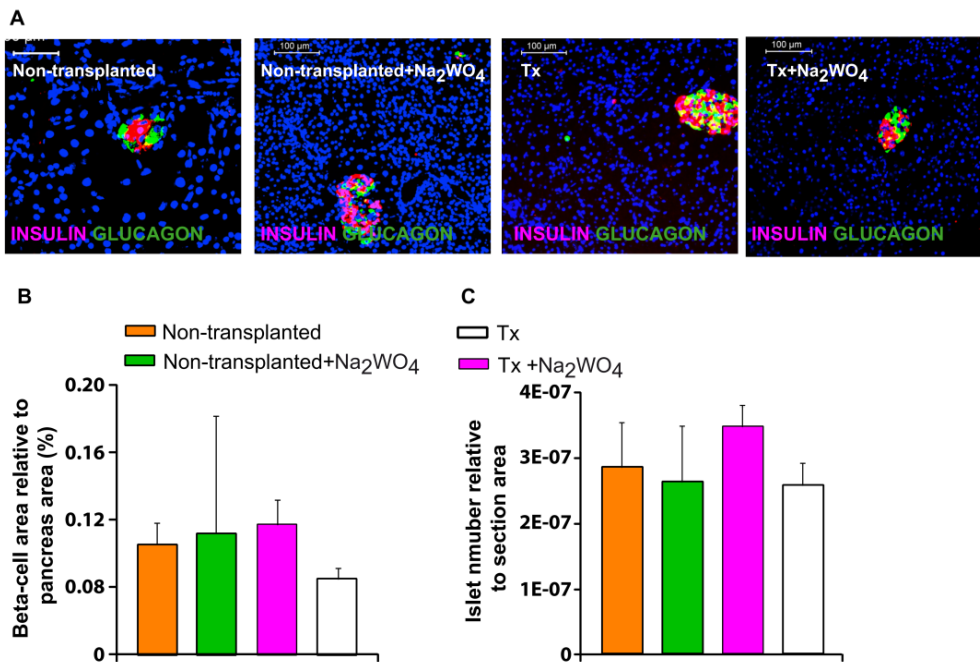
Figure 23: Sodium tungstate treatment does not induce ß-cell area recovery from STZ-induced diabetic mice. A. Representative immunofluorescence images of Pancreas slices from non-transplanted, non-transplanted+Na$_2$WO$_4$, Tx, and Tx+Na$_2$WO$_4$, 35 days following transplant. ß-cell area analyzed by co-staining of

INSULIN and GLUCAGON. B. The relative ß-cell area to pancreas area. C. Pancreatic islet number concerning by section slice. Images scale bar: 100μm.

PTP-1B mediates the improvement of revascularization of the post-transplantation treatment with sodium tungstate.

As tungstate strongly inhibits PTP-1B. Therefore we study if the observed increase in revascularization, after the treatment with sodium tungstate, was mediated by PTP-1B. In this sense, we performed a suboptimal allotransplantation PTP-1B$^{+/+}$ and PTP-1B$^{-/-}$ islets into the anterior chamber of the eye of diabetic mice. Four main groups of STZ-induced diabetic mice were constituted: the PTP-1B$^{+/+}$Tx group, transplanted with PTP-1B$^{+/+}$ islets; the PTP-1B$^{+/+}$ Tx+Na$_2$WO$_4$, transplanted with PTP-1B$^{+/+}$ islets and treated with sodium tungstate; the PTP-1B$^{-/-}$Tx group, transplanted with PTP-1B$^{-/-}$ islets and the PTP-1B$^{-/-}$ Tx+Na$_2$WO$_4$, transplanted with PTP-1B$^{-/-}$ islets and treated with sodium tungstate. Simultaneously other two groups of diabetic non-transplanted animals were used, with one being equally treated with sodium tungstate and the other not. All groups were monitored for 25 days.

Regarding non-fasting blood glucose, both non-transplanted groups did not exhibit any improvement while PTP-1B$^{+/+}$Tx showed a minor 10%decrease by the end of 25 days, regarding its initial value (Figure 24A). However, in contrast, the groups PTP-1B$^{+/+}$Tx+Na$_2$WO$_4$, PTP-1B$^{-/-}$Tx and PTP-1B$^{-/-}$ Tx+Na$_2$WO$_4$ exhibit a similar improvement by showing a decrease in their blood glucose levels between 30% and 45% (Figure 24A). Following the same pattern, the groups PTP-1B$^{+/+}$Tx+Na$_2$WO$_4$, PTP-1B$^{-/-}$Tx and PTP-1B$^{-/-}$ Tx+Na$_2$WO$_4$ showed not only a total recovery in their body weight but continued to improve it (Figure 24B), until the end of the experiment. The

PTP-1B$^{+/+}$Tx group did not present any change, and both non-transplanted groups presented a continuous decline in their body weight (Figure 24B).
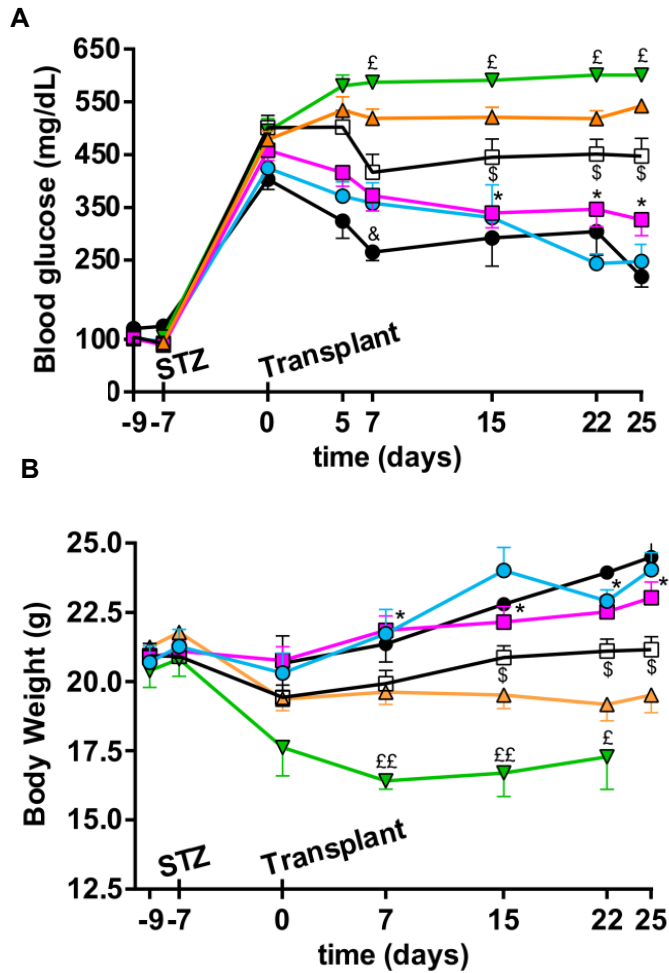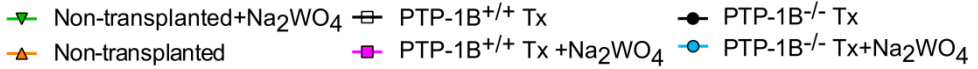
Figure 24: PTP-1B mediates the outcome of the post-islet transplantation treatment with sodium tungstate. **A.** Blood glucose levels and **B**.body weight of the diabetic BALB/c mice during 25 days following allotransplantation. Groups: non-

transplanted (n=12), non-transplanted and treated with tungstate (n=12), transplanted with PTP-1B$^{+/+}$ islets (PTP-1B$^{+/+}$Tx; n=9), transplanted with PTP-1B$^{+/+}$ islets and treated with tungstate (PTP-1B$^{+/+}$Tx+Na$_2$WO$_{44}$; n=9); transplanted with PTP-1B$^{-/+}$ islets (PTP-1B$^{-/}$Tx; n=6), transplanted with PTP-1B$^{-/-}$ islets and treated with tungstate (PTP-1B$^{-/}$Tx+Na$_2$WO$_4$; n=6). Images scale bar 50µm. Data presented as Mean ± SEM, *p<0.05, for PTP-1B$^{-/}$Tx+Na$_2$WO$_4$ vs. PTP-1B$^{+/+}$Tx; \$p<0.05 for PTP-1B$^{+/+}$Tx vs. non-transplanted; ££p<0.01, £p<0.05 , for PTP-1B$^{+/+}$Tx vs. non-transplanted+Na$_2$WO$_4$, &p<0.05 for PTP-1B$^{-/}$Tx vs PTP-1B$^{-/-}$Tx+Na$_2$WO$_4$, by two-way ANOVA.

As the phenotype of the transplanted groups indicates, PTP-1B might mediate the effects of the sodium tungstate treatment. In this sense, we assessed grafts *in vivo* revascularization and survival (Figure 25).
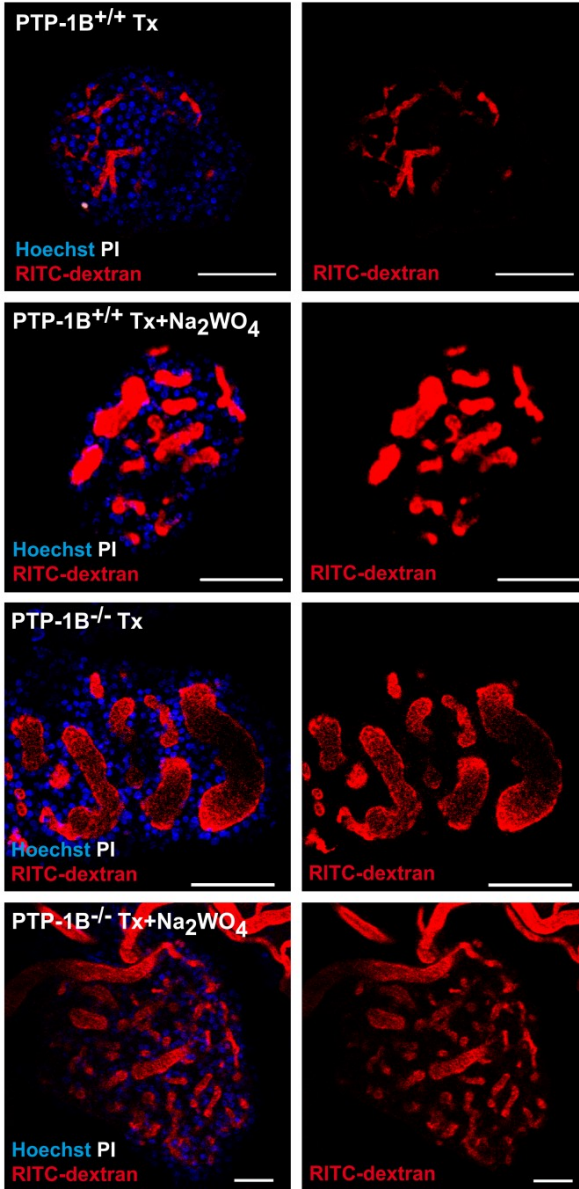
Figure 25:

Representative *in vivo* images of the functional vasculature, and cell death from PTP-1B$^{+/+}$Tx, PTP-1B$^{+/+}$Tx+Na$_2$WO$_4$, PTP-1B$^{-/-}$Tx, and PTP-1B$^{-/-}$Tx+Na$_2$WO$_4$ (n=6 islets* 6 animals) acquired 25 days after transplantation, using two-photon microscopy; nuclei were stained with Hoechst (blue); scale bars, 50µm.

As observed in Figure 25 the PTP-1B$^{+/+}$Tx+Na$_2$WO$_4$, PTP-1B$^{-/-}$Tx and PTP-1B$^{-/-}$Tx+Na$_2$WO$_4$ groups presented improved revascularization in relation to the PTP-1B$^{+/+}$Tx group. By quantifying vascular density and the vascularization area, it is observed a similar increment the PTP-

$1B^{+/+}Tx+Na_2WO_4$, PTP-1B$^{-/-}$Tx, and PTP-1B$^{-/-}$Tx+Na$_2$WO$_4$ groups concerning the PTP-1B$^{+/+}$Tx (Figure 26A and B).
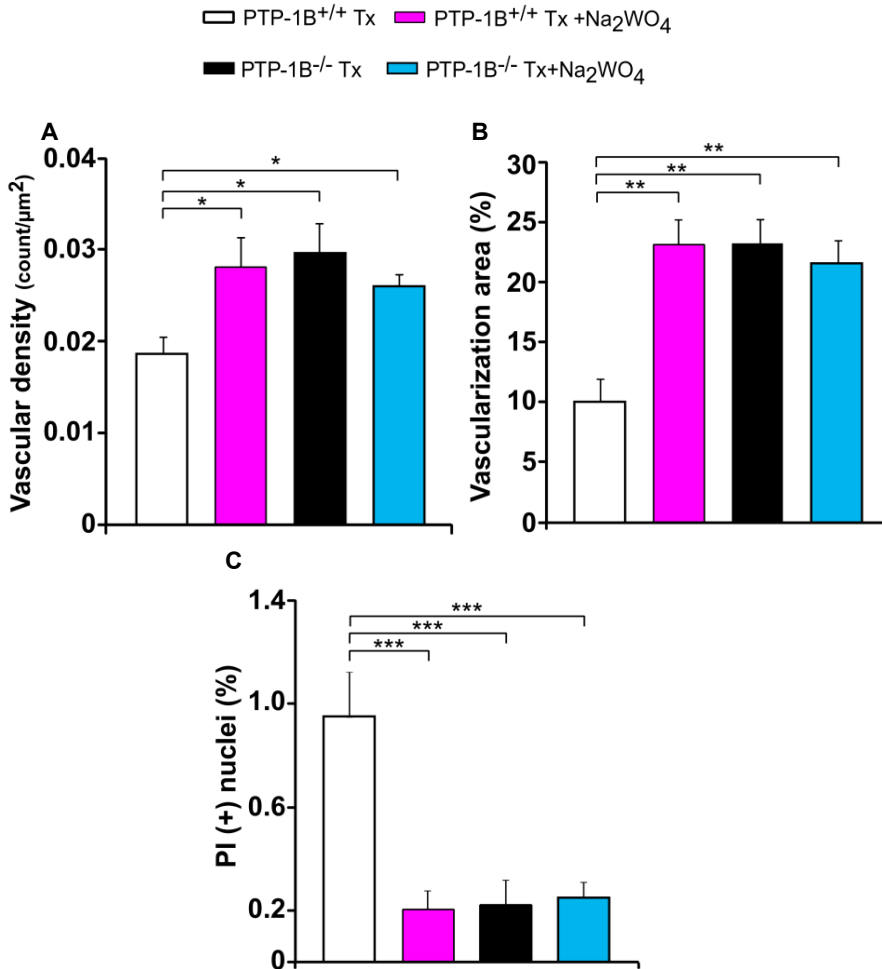
Figure 26: **A**. Quantification of relative vascular density; **B**, relative vascularization area by islet area; **C.** Quantification of relative cell death (propidium iodide positively stained nuclei) at day 25 (n=6 islets* 6 animals). Data presented as Mean ± SEM, *p<0.05, **p<0.01, ***p<0.001, by one-way ANOVA.

In respect to graft cell death, the analysis of positive-staining for propidium iodide showed an equal decrease in cell death for the PTP-1B$^{+/+}$Tx+Na$_2$WO$_4$, PTP-1B$^{-/-}$Tx and PTP-1B$^{-/-}$Tx+Na$_2$WO$_4$ groups in relation to the PTP-1B$^{+/+}$Tx group (Figure 26C). This data demonstrates that transplanting islets lacking PTP-1B can mimic the outcome as the sodium tungstate treatment, in terms of islet-graft revascularization and survival.

Chapter 2| Improving islet-graft revascularization by targeting islet's PTP-1B

The absence of PTP-1B in pancreatic islets does not affect apoptosis and decreases the rate of endothelial cell loss *in vitro*.

 To delineate the effect of the absence of PTP-1B in mouse islets, we performed an *in vitro* insulin secretion assay in response to glucose 2.8mM (low glucose) and 16.7mM (high glucose), using islets isolated from PTP-1B$^{-/-}$ and PTP-1B$^{+/+}$ mice, after 2 days of culture. Islets from both genotypes presented similar insulin secretion response (Figure 27A) and insulin content (Figure 27B). Normalization of insulin secretion by islet content did not diverge between genotypes (Figure C).
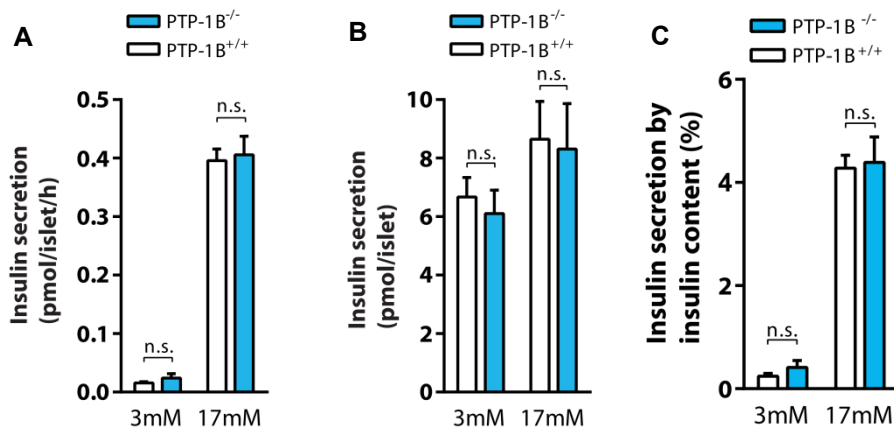
Figure 27: In vitro insulin secretion, in response to glucose 3mM and 17mM, of PTP-1B$^{+/+}$ (n=6) and PTP-1B$^{-/-}$ (n=6) islets. A. secreted insulin. B. insulin content per islet. C. Insulin secretion normalized by insulin content. data in mean ± s.d; n.s. not significant by Student's t-test.

PTP-1B has been described as a modulator of ER stress and apoptosis signaling in beta-cell lines and freshly isolated mouse islets[244,299]. However, we did not find any differences in gene expression of the apoptotic markers *Caspase3* and *Caspase9* between PTP-1B$^{-/-}$ and PTP-1B$^{+/+}$ islets (Figure 28).
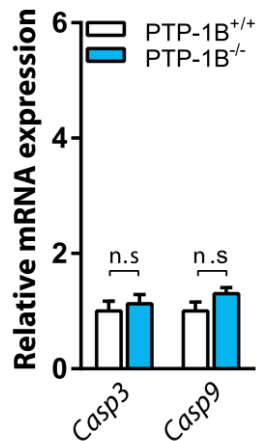
Figure 28: Expression of apoptotic markers *Casp3, Casp9,* analyzed by quantitative real-time PCR and compared between PTP-1B$^{+/+}$ (n=9) and PTP-1B$^{-/-}$ (n=12) islets. Data presented as Mean ± SEM. n.s. (not significant) by Student's t-test.

In addition, immunohistochemistry - immunofluorescence (IHC-IF) analysis of cleaved-CASPASE3 staining in whole islets cultured for 2 days (Figure 29A) revealed no discrepancy between PTP-1B$^{-/-}$ and PTP-1B$^{+/+}$ (Figure 29B).
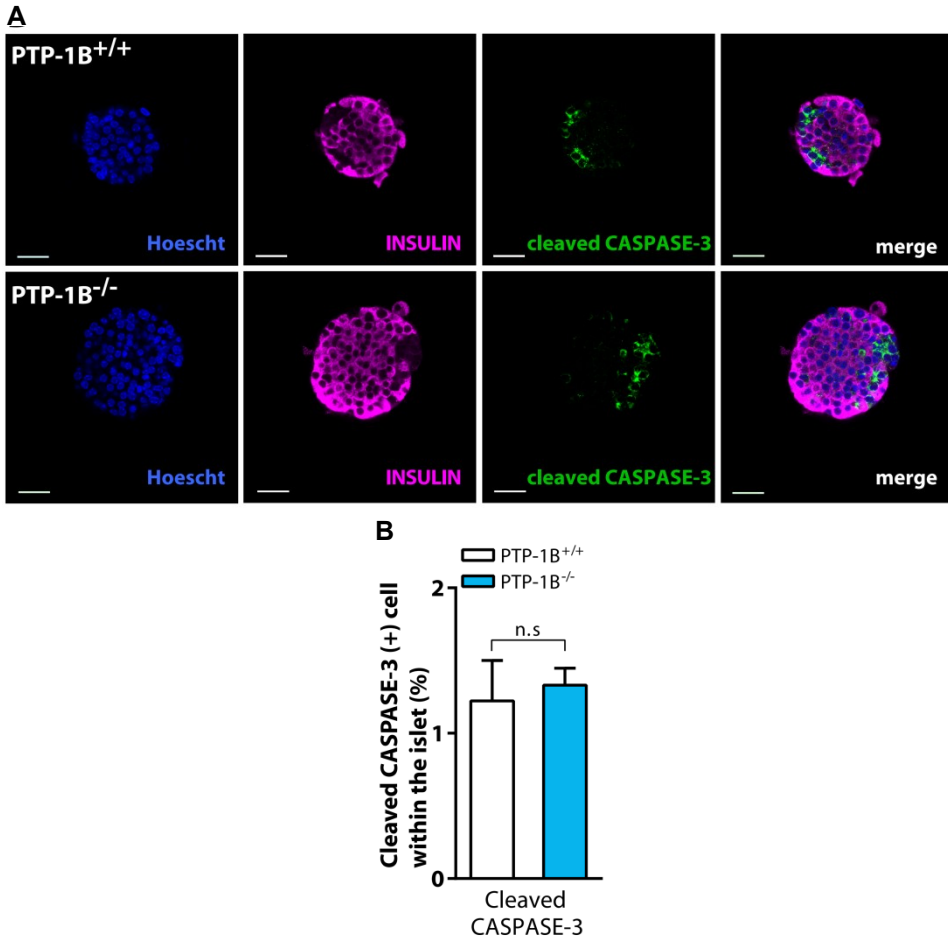
Figure 29: A. Representative images from the immunofluorescence staining of the apoptotic marker, cleaved CASPASE 3 in whole isolated islets. INSULIN was performed to study the existence of apoptotic ß-cells (merge, co-localization); nuclei stained using Hoescht: top panels are relative to PTP-1B$^{+/+}$ islets, bottom panels are relative to PTP-1B$^{-/-}$ islets; scale bars, 25µm. B. Percentage of immunofluorescence's positive cleaved CASPASE-3 cells in relation to total islet cells, in PTP-1B$^{+/+}$ (n=15) and PTP-1B$^{-/-}$ (n=15) islets; Mean ± SEM. n.s. (not significant) by Student's t-test.

We analyzed the differences in the expression of the endothelial markers: *Pecam1,* the cell adhesion protein characteristic of endothelial cells; *Kdr*, the receptor of VEGF-A, known to interact with PTP-1B directly and

modulate EC proliferation[300]; and *Cdh5,* the endothelial adhesion protein known to modulate endothelial cell migration[256]. Gene expression quantification revealed that PTP-1B$^{-/-}$ islets presented increased levels of the expression of these markers: 4.8-fold for Pecam1, 2.6-fold for Kdr and 1.7-fold for Cdh5 (Figure 30). Increased expression of Pecam1 in PTP-1B$^{-/-}$ suggests a higher prevalence of intra-islet EC (iEC). IECs have been shown to contribute toward early-stage graft revascularization rate and graft survival[301,302]. Along these lines, we studied the iEC population in fresh islets (0 days in culture) and islets cultured for 2 days, by performing IHC-IF analysis of PECAM-1 staining in whole islets (Figure 31A and B).
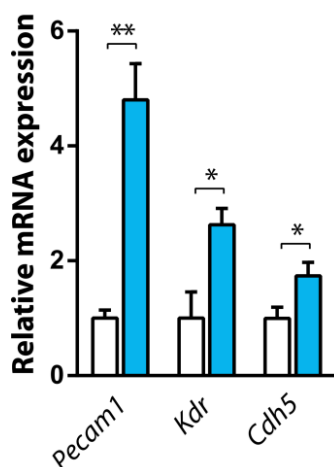
Figure 30: Expression of the vascular markers Pecam1, Kdr (or Vegfr2) and Cdh5 (or Ve-cadherin), analyzed by quantitative real-time PCR and compared between PTP-1B$^{+/+}$ (n=9) and PTP-1B$^{-/-}$ (n=12) islets. Data presented as Mean ± SEM. *<p0.05, by Student's t-test.

Although fresh islets maintained similar levels of the endothelial cell area, after two days of culture PTP-1B$^{-/-}$ islets presented an endothelial cell population, per islet area, that was 3 times higher than that on PTP-1B$^{+/+}$ islets, indicating a reduced endothelial cell loss in cultured PTP-1B$^{-/-}$ islets.

A

B
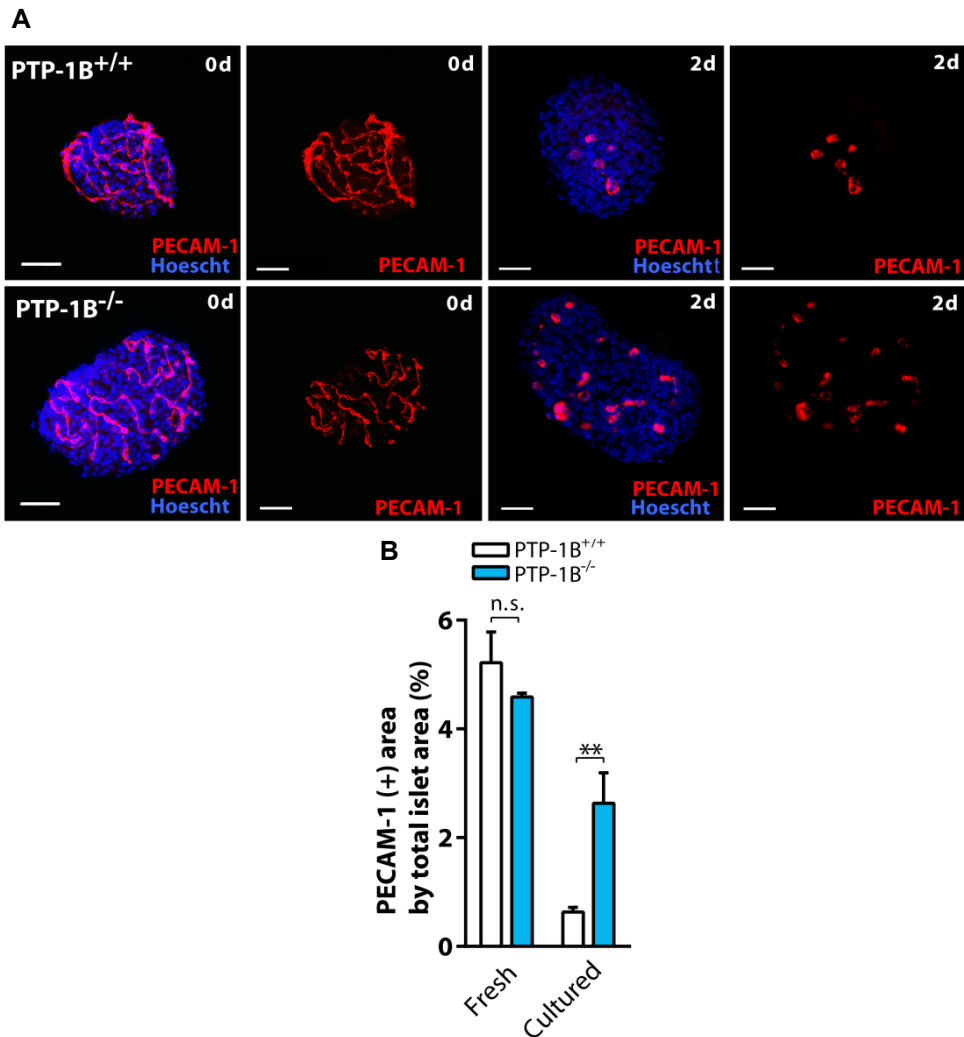
Figure 31: A. Representative maximum projections of image stacks from the immunofluorescence of PECAM-1 in whole islets (nuclei stained using Hoescht). Fresh islets (0 days of culture) were used as a comparison; top panels are relative to PTP-1B$^{+/+}$ islets, bottom panels relative to PTP-1B$^{-/-}$ islets; scale bars, 25µm. B. Percentage of the immunofluorescent positive PECAM-1 area in relation to total islet area, of fresh (0 days of culture) or cultured (2 days of culture) islets, from PTP-1B$^{+/+}$ (n=15) and PTP-1B-/- (n=16) mice. Data presented as Mean ± SEM. By one-way ANOVA for (g): n.s. not significant, **p<0.01.

Diabetic animals transplanted with PTP-1B$^{-/-}$ islets restore normoglycemia and insulin levels.

To study the effect of PTP-1B on the engraftment of islets, we performed a suboptimal allotransplantation of islets isolated from PTP-1B$^{-/-}$ or PTP-1B$^{+/+}$ into the anterior chamber of the eye in diabetic BALB/c mice. Single intraperitoneal injection of streptozotocin (STZ) induced diabetes in 70% of BALB/c mice (blood glucose levels above 250mg/dL in three consecutive days). 1 week after STZ administration, 85% of the mice presented an average blood glucose level of 340 mg/dL; no mice recovered spontaneously from STZ-induced diabetes. The STZ-treated mice were then randomly organized into 3 groups: the first group transplanted with PTP-1B-/- islets (PTP-1B$^{-/-}$tx$^{balb-stz}$ group), the second with PTP-1B$^{+/+}$ islets (PTP-1B$^{+/+}$tx$^{balb-stz}$ group), and the third and last without any transplant (non-transplanted group). The fourth group of not diabetic BALB/c mice was also monitored. Each transplanted mouse received 200 islets, previously isolated from PTP-1B$^{-/-}$ and PTP-1B$^{+/+}$ mice and cultured for two days (Figure 32).
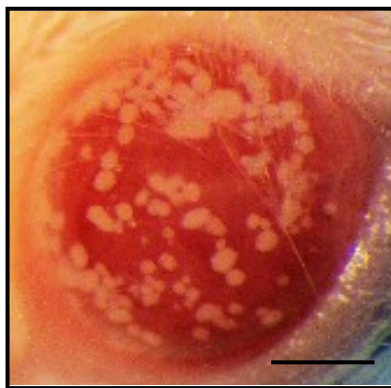
Figure 32: Representative image of transplanted islets in the anterior chamber of the eye of mice of STZ-induced diabetic BALB/c mice, image scale bar, 2mm.

All groups were monitored for 28 days. During this period, the PTP-1B$^{+/+}$tx$^{balb-stz}$ group exhibited no recovery in non-fasting glycemic levels (Figure 33A). Mice from PTP-1B$^{-/-}$tx$^{balb-stz}$ group improved their blood glucose levels and achieved normoglycemia by day 21, representing an improvement of 58.2% with regards to their initial blood glucose levels (Figure 33A). Normoglycemia threshold was obtained by following a group of non-diabetics mice (Figure 34A). Non-fasting glycemia of a diabetic non-transplanted group of mice was recorded for 28 days (Figure 34A). Data showed that non-transplanted mice did not exhibit any decrease in their blood glucose levels. In relation to body weight, all STZ-induced diabetic mice presented an initial decrease in body weight, due to the effects of STZ (Figure 33B).
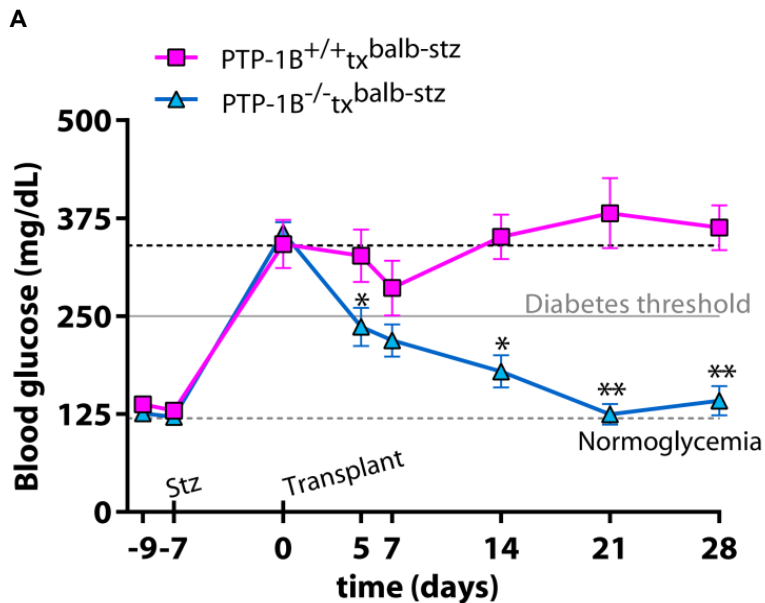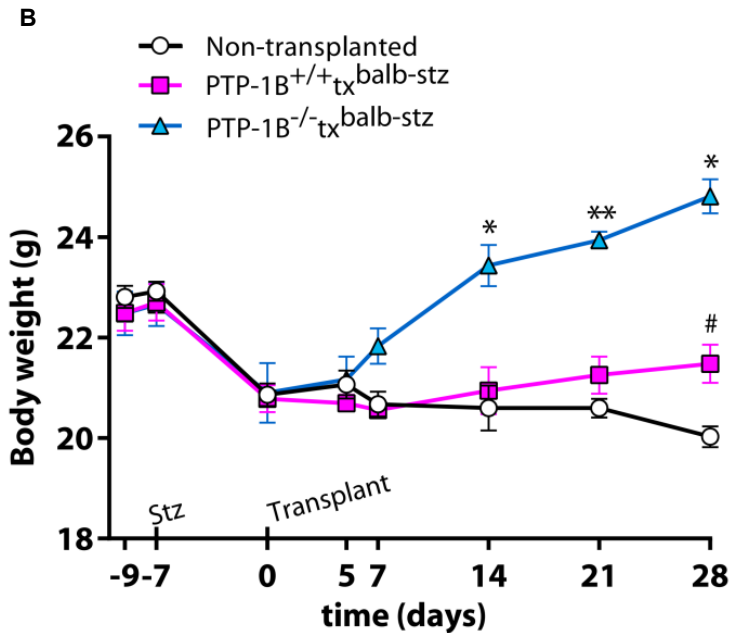
Figure 33: STZ-induced diabetic mice transplanted with PTP-1B$^{-/-}$ islets restore normoglycemia and insulin levels. A. Blood glucose levels of diabetic mice transplanted with PTP-1B$^{+/+}$ (PTP-1B$^{+/+}$tx$^{balb-stz}$, n=10) or PTP-1B$^{-/-}$ (PTP-1B$^{-/-}$tx$^{balb-stz}$, n=12) for 28 days; the median concentration of blood glucose at time 0 (moment of transplantation) is 340.0 mg/dL (n=24) and is represented with a black dashed line; the average concentration of blood glucose level of non-diabetic mice for 28 days is 119.7mg/dL (n=8) and is represented with a gray dashed line. Mice were considered diabetic after 3 consecutive blood glucose measures above threshold (250mg/dL). B. Body weigh measurement of PTP-1B$^{+/+}$tx$^{balb-stz}$ (n=10), PTP-1B$^{-/-}$tx$^{balb-stz}$ mice (n=12), and diabetic but non-transplanted mice (n=10) for 28 days. Data is presented as Mean ± SEM, *p<0.05, **p<0.01 for PTP-1B$^{+/+}$tx$^{balb-stz}$ vs PTP-1B$^{-/-}$tx$^{balb-stz}$; #p<0.05 for PTP-1B$^{+/+}$tx$^{balb-stz}$ vs not transplanted and n.s for PTP-1B$^{-/-}$tx$^{balb-stz}$ vs not diabetic mice, by two-way ANOVA.

Following transplantation, in the PTP-1B$^{-/-}$tx$^{balb-stz}$ group body weight not only recovered between day 7 and 14 but also continued improving until the end of the

experiment. Animals from the PTP-1B$^{+/+}$tx$^{balb-stz}$ and non-transplanted groups did not recover their initial body weight (Figure 33B).
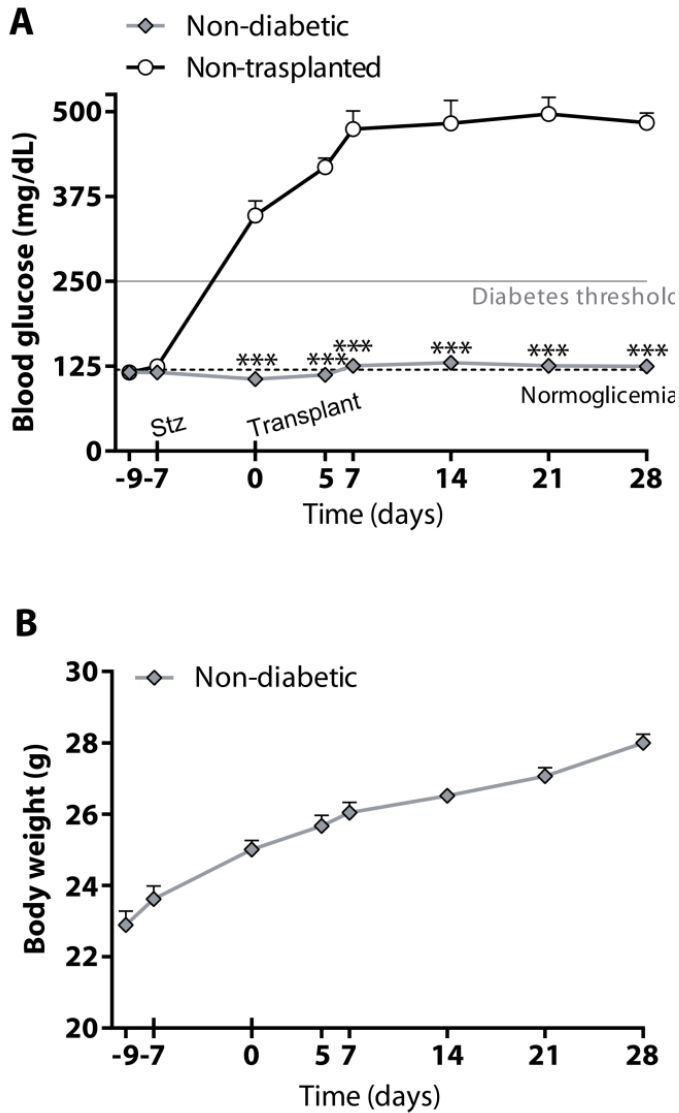
Figure 34: Blood glucose and body weight of non-diabetic and non-transplanted mice. a Blood glucose levels of non-diabetic (n=8) and diabetic non-transplanted mice (n=10) for 28 days. The average concentration of blood glucose level of non-diabetic mice for 28 days is 119.7mg/dL and is represented by a gray dashed line. Non-transplanted mice were considered diabetic after 3 consecutive blood glucose

measures above threshold (250mg/dL; gray line). b Body weighs measurement of non-diabetic mice (n=8) for 28 days. ***p<0.001, by two-way ANOVA

To assess graft function, we performed an ipGTT on day 28. Results showed that both PTP-1B$^{-/-}$tx$^{balb-stz}$ and non-diabetic groups presented a similar response to the glucose bolus, recovering basal levels of glycemia at the same time. On the other side, PTP-1B$^{+/+}$tx$^{balb-stz}$ and non-transplanted groups displayed increased basal blood glucose and severe glucose intolerance, being incapable of restoring blood glucose levels within 120 minutes (Figure 35A).
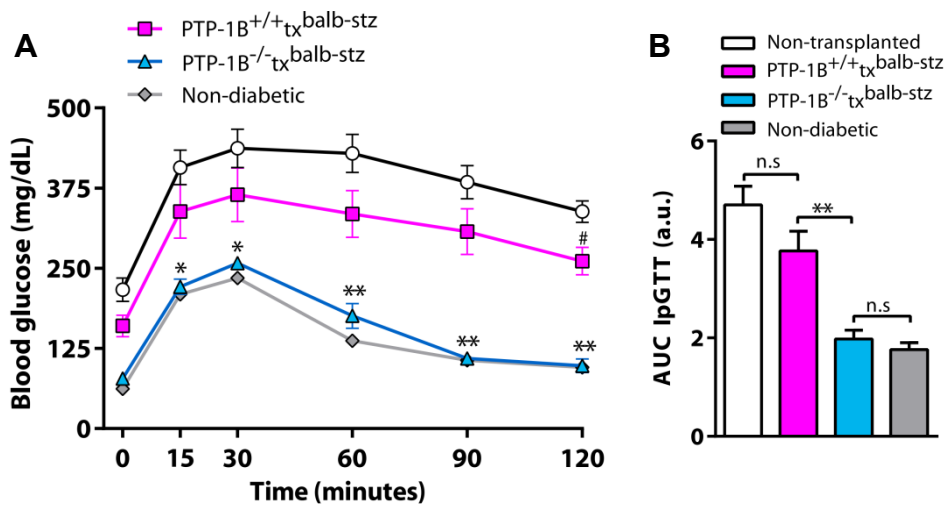
Figure 35 A. Intraperitoneal glucose tolerance test (IpGTT) PTP-1B$^{+/+}$tx$^{balb-stz}$ (n=10), PTP-1B$^{-/-}$txbalb^{-stz} (n=12), diabetic but non transplanted (n=10) and non-diabetic and non-transplanted mice (n=8), performed 28 days after transplantation. B. IpGTT quantification of the area under curve for the different groups. Data is presented as Mean ± SEM, *p<0.05, **p<0.01 for PTP-1B$^{+/+}$tx$^{balb-stz}$ vs PTP-1B$^{-/-}$tx$^{balb-stz}$, by two-way ANOVA.

These differences were also evident after calculating the area under the tolerance curve of each group, as PTP-1B$^{-/-}$tx$^{balb-stz}$ and non-diabetic groups presented similar areas and therefore similar glucose tolerance, whereas PTP-1B$^{+/+}$tx$^{balb-stz}$ and non-transplanted groups presented at least a 2-fold increase in the areas (Figure 35B). Following this, we determined the concentration of insulin in the plasma during the ipGTT. Results showed a similar fluctuation on plasma insulin between PTP-1B$^{-/-}$tx$^{balb-stz,}$ and non-diabetic groups, contrasting with, the PTP-1B$^{+/+}$tx$^{balb-stz}$ and non-transplanted groups that presented continuously low levels of plasma insulin, which correlates with their high glucose intolerance (Figure 36).
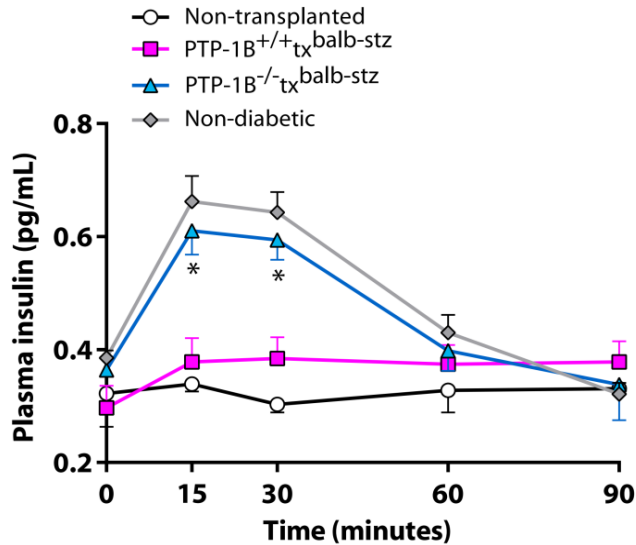
Figure 36: Plasma Insulin levels measured at each time point of the IpGTT. Data is presented as Mean ± SEM, *$p<0.05$, for PTP-1B$^{+/+}$tx$^{balb-stz}$ vs PTP-1B$^{-/-}$tx$^{balb-stz}$, by two-way ANOVA.

Finally, following these experiments, we collected the pancreas from all animals and analyzed insulin content. Results revealed that PTP-1B$^{-/-}$tx$^{balb-stz}$, PTP-1B$^{+/+}$tx$^{balb-stz,}$ and non-transplanted groups presented, as expected, an average a 10-15% remaining insulin content in relation to

mice from the non-diabetic group (Figure 37), that higher plasma insulin observed in PTP-1B$^{-/-}$tx^{balb}-stz mice during ipGTT originate from transplanted islets insulin secretion.
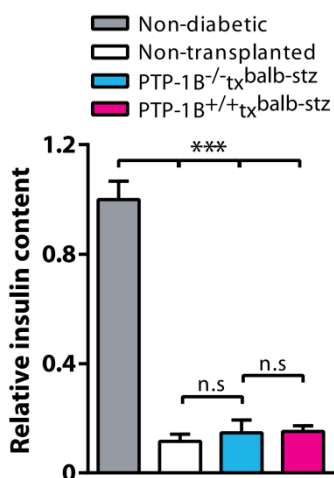
Figure 37: Pancreatic insulin content. Total pancreas insulin content was measured in not diabetic mice (gray, n=8), diabetic not transplanted (white, n=8), PTP-1B$^{-/-}$tx$^{balb-stz}$ (blue, n=12) and in PTP-1B$^{+/+}$tx$^{balb-stz}$ (magenta, n=10). The assay was performed at the end of 28 days following transplantation. ***$p<0.001$, by one-way ANOVA.

The absence of PTP-1B in transplanted islets improves graft revascularization and survival.

Since PTP-1B$^{-/-}$tx$^{balb-stz}$ presented improved glucose homeostasis, we investigated the differences in graft revascularization and survival in relation to PTP-1B$^{+/+}$tx$^{balb-stz}$, that might explain the previous observations. We assessed *in vivo* graft functional revascularization, 7, 15 and 28 days after transplantation, by two-photon microscopy after injection of RITC-dextran (Figure 38A and B). We analyzed and compared vascular density and the vascular area between both groups. We found that, at day 7, PTP-1B$^{-/-}$tx$^{balb-stz}$ graft, showed a 1.5-fold increase in vascular density than PTP-1B$^{+/+}$tx$^{balb-stz}$. At day 15, we observed that both groups presented an increase in graft vascular density with respect to day 7, although PTP-1B$^{-/-}$tx^{balb-}

^{stz} maintained a 1.5-fold increase over PTP-1B$^{+/+}$tx$^{balb-stz}$. At day 28, neither group displayed any difference in relation to day 15, whereas PTP-1B$^{-/-}$tx$^{balb-stz}$ maintained a 1.4-fold increase in relation to PTP-1B$^{+/+}$tx$^{balb-stz}$ (Figure 39A).
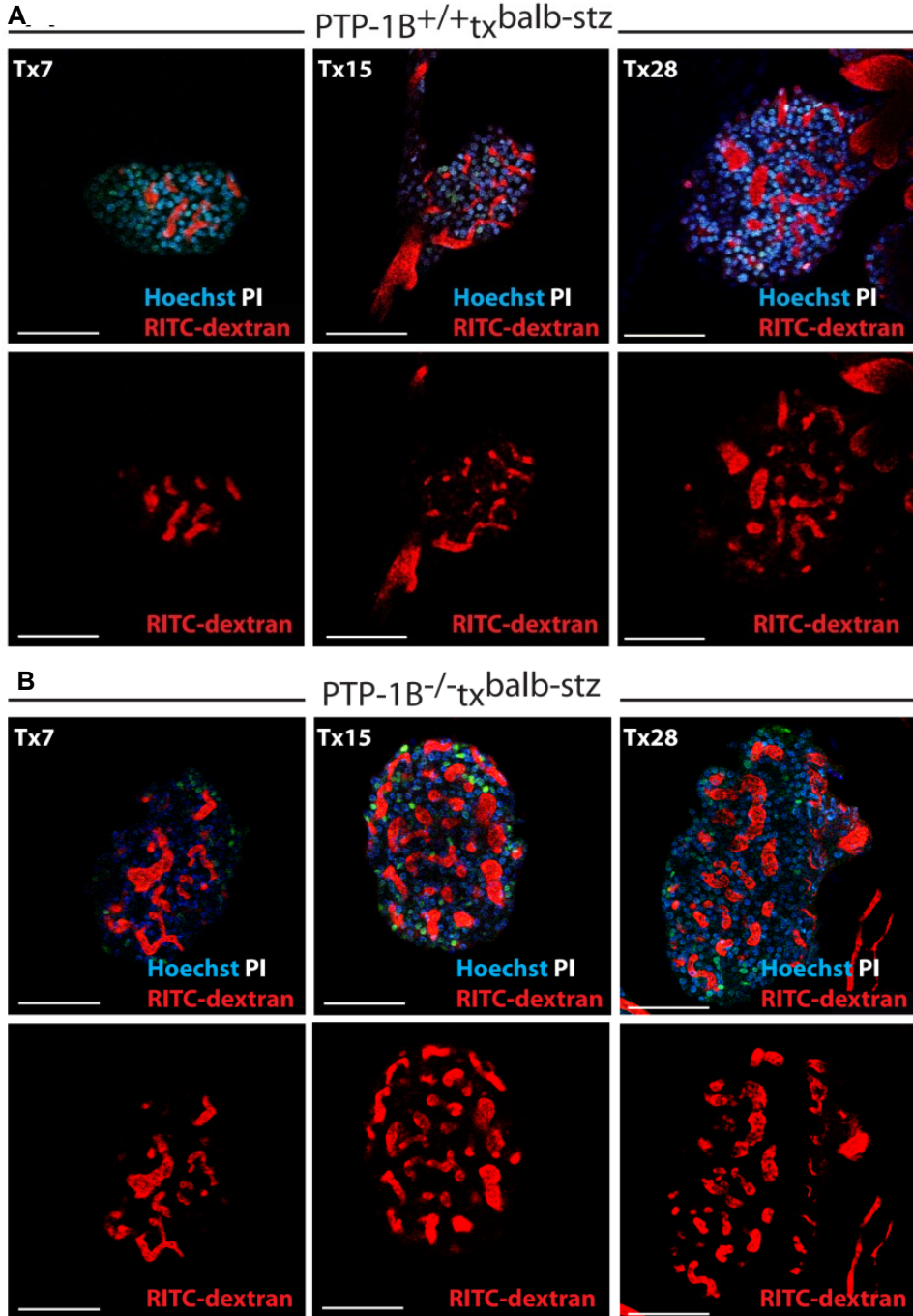
Figure 38: Absence of PTP-1B in transplanted islets improves graft revascularization and survival without the loss of ß-cell area. a Representative in vivo images of functional vessels (in red, RITC-dextran labeling), and cell death (white nuclei, propidium Iodide labeling) in A. PTP-1B^{+/+}tx[balb-stz] and B. PTP-1B^{-/-}tx[balb-stz] (right panels) grafts, acquired 7, 15 and 28 days after transplantation (Tx7, Tx15, and Tx28), using two-photon microscopy; nuclei were stained with Hoechst (blue); CFDA (green) stain islet cells; scale bars, 25µm.

These observations led us to infer that both groups presented maximum revascularization on day 15, as described in other studies[133,135]. Likewise, the analysis of vascular area demonstrated that the PTP-1B^{-/-}tx[balb-stz] graft at day 7, 15 and 28, had a 2-fold higher vascular area than PTP-1B^{+/+}tx[balb-stz] (Figure 39B).
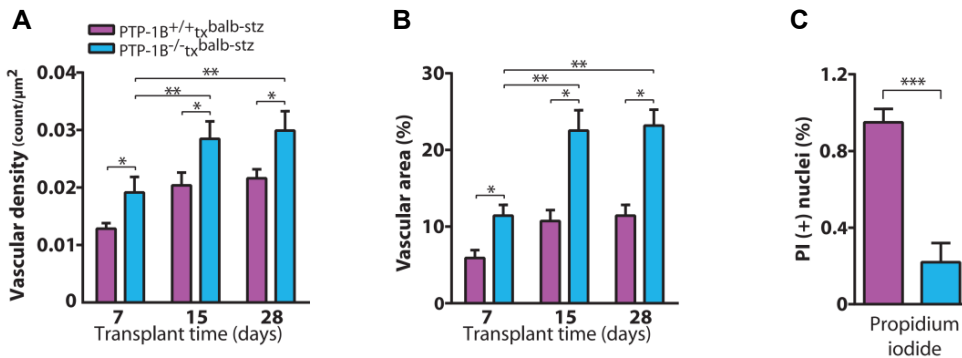
Figure 39: A. Quantification of relative vascular density; B. vascularization area by islet area and C. graft's cell death (this last at day 28) in . PTP-1B^{+/+}tx[balb-stz] and -1B[-/-]tx[balb-stz] grafts 7 (n=8 islets/animal, 7 animals), 15 (n=9 islets/animal, 7 animals) and 28 (n=8 islets/animal, 10 animals) days after transplantation. Data presented as Mean ± SEM; *p<0.05, **p<0.01, by two-way ANOVA in A and B; and ***p<0.001 by Student's t-test in C.

In parallel to graft revascularization, we assessed *in vivo* cell death after propidium iodide injection. Results revealed a significant decrease in the PTP-1B$^{-/-}$tx$^{balb-stz}$ graft when compared with PTP-1B$^{+/+}$tx$^{balb-stz}$ (Figure 38 and 39C). IHC-IF analysis of the paraffinized sections of the engrafted eyes supported *in vivo* cell death analysis findings, where a significant decrease in the cleaved-CASPASE3 staining was found in the PTP-1B$^{-/-}$tx$^{balb-stz}$ graft when compared with PTP-1B$^{+/+}$tx$^{balb-stz}$ (Figure 40 and 41A).

The absence of PTP-1B in transplanted islets induces graft expression of VEGF-A without compromising the graft ß-cell population.

In order to understand the increase in revascularization in the PTP-1B$^{-/-}$tx$^{balb-stz}$ graft, we investigated the expression of VEGF-A, a cytokine, produced by islet cells, that is known to be the principal inducer of angiogentesis[50,51]. IHC-IF analysis of the paraffinized section of the engrafted eyes demonstrated that 89% of total PTP-1B$^{-/-}$tx$^{balb-stz}$ graft cells expressed VEGF-A, against 18% in the PTP-1B$^{+/+}$tx$^{balb-stz}$ graft. Outstandingly, in both grafts, 90% of the cells expressing VEGF-A were ß-cells (Figure 40 and 41B). The direct overexpression of VEGF-A in islets is known to increase islet revascularization massively. However, this is followed by a destruction of ß-cell area[144–146]. In this sense, we assessed graft ß-cell population. Interestingly, insulin and glucagon staining of engrafted eye paraffinized sections revealed that, on average, 76% of PTP-1B$^{-/-}$tx$^{balb-stz}$ graft cells were ß-cells (Figure 40 and 41C), a value that did not correspond with the ß-cell loss. In parallel, a lower ß-cell area was found in the analysis of the PTP-1B$^{+/+}$tx$^{balb-stz}$ graft.
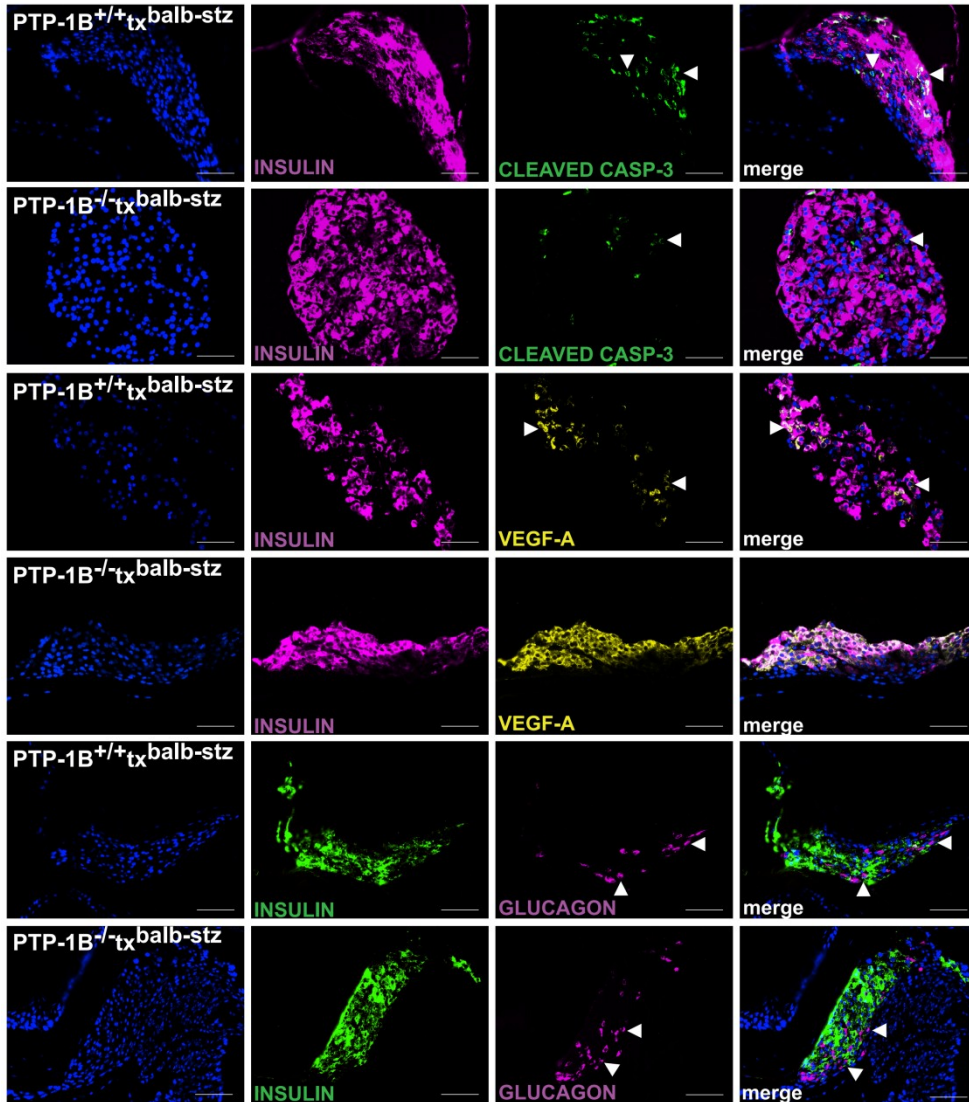
Figure 40 Representative immunofluorescence images from PTP-1B$^{+/+}$tx$^{balb-stz}$ and PTP-1B$^{-/-}$tx$^{balb-stz}$ graft's slices, 28 days after transplantation. Apoptotic marker, cleaved CASPASE-3, or pro-angiogenic cytokine VEGF-A were stained and analyzed against INSULIN; islet ß-cell area was analyzed by co-staining INSULIN and GLUCAGON. For each analysis, top panels represent PTP-1B$^{+/+}$tx$^{balb-stz}$ grafts and bottom panels, PTP-1B$^{-/-}$tx$^{balb-stz}$ grafts; scale bars, 25µm.
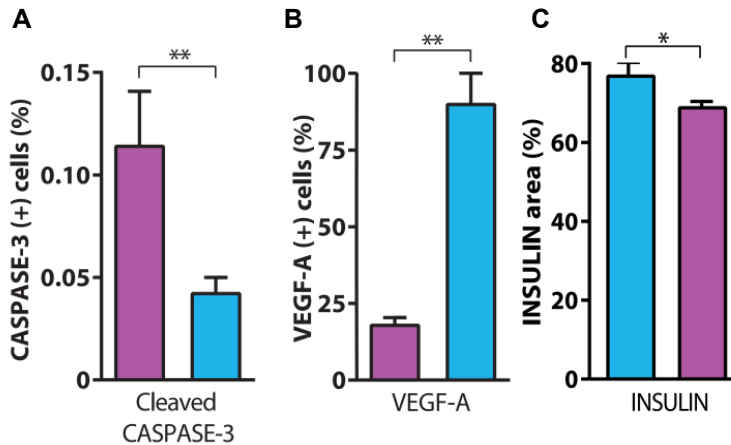
Figure 41: A. Quantification of relative immunofluorescent-positive cleaved CASPASE-3 cells by total islet in PTP-1B$^{+/+}$tx$^{balb-stz}$ (n=10 islets/animal, 7 animals) and PTP-1B$^{-/-}$tx$^{balb-stz}$ (n=10 islets/animal, 6 animals) grafts. B. Quantification of immunofluorescent co-locatization of positive VEGF-A/ß-cells in PTP-1B+/+txbalb-stz (n= 8 islets/animal, 9 animals) and PTP-1B-/-txbalb-stz (n=10 islets/animal, 7 animals) grafts; **p<0.01, by Student's t-test. C. Quantification of positive INSULIN area, by total islet area (INSULIN+GLUCAGON area); in PTP-1B$^{+/+}$tx$^{balb-stz}$ (n=5 islets/ animals, 6 animals) and PTP-1B$^{-/-}$tx$^{balb-stz}$ (n=5 islets/animals x 6 animals) grafts. Data presented as Mean ± SEM; *p<0.05, **p<0.01 by Student's t-test.

In vitro elimination of intra-islet endothelial cells does not compromise insulin secretion or islet survival.

The PTP-1B$^{-/-}$tx$^{balb-stz}$ graft showed an increased early and long-term graft revascularization, revealing a potential role of iECs in this process[269,301]. To assess the contribution of donor iECs toward graft revascularization, we eliminated iECs from islets before transplantation. Since the endothelial cell population within the islets is lost during culture time[302], we cultured PTP-1B$^{-/-}$ and PTP-1B$^{+/+}$ islets for 7 days and monitored endothelial cell

population using confocal microscopy and IHC-IF by performing PECAM-1 staining (Figure 42A). Results showed a continuous loss of positive PECAM-1 labelling in both cultures, although, as previously observed, PTP-1B$^{-/-}$ islets maintained a lower rate of endothelial cell loss than PTP-1B$^{+/+}$ islets: after 1 day of culture, PTP-1B$^{-/-}$ islets presented a 1.7-fold increase in iECs and, after 2 days of culture, a 2.8-fold increase in PTP-1B$^{+/+}$ islets. Nevertheless, after 7 days of culture, there was no PECAM-1 positive staining detected (Figure 42B). These results were validated by qRT-PCR analysis of *Pecam1* expression of islets cultured for 0, 2 and 7 days (Figure 42C); here we observed, as expected, a decrease in the expression of *Pecam1* over time in both genotypes. Islets cultured for 7 days were considered to be free of endothelial cells.
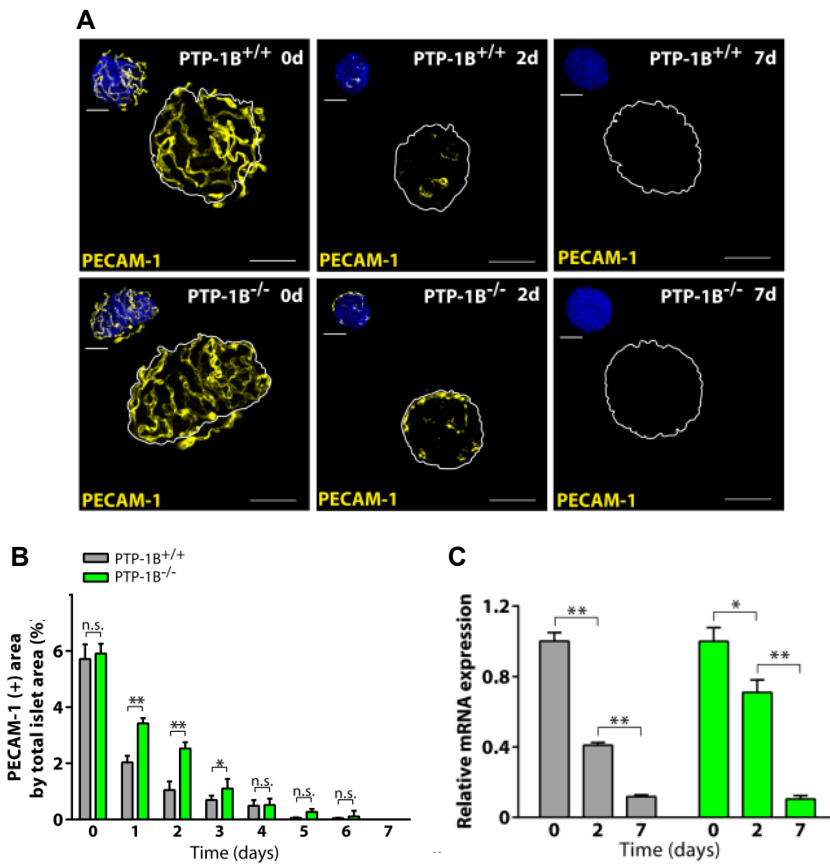
Figure 42: A Representative maximum projections of image stacks from the immunofluorescence staining of PECAM-1 (yellow) in PTP-1B+/+ a PTP-1B-/- islets after 0, 2 and 7 days of culture; a white line defines islet area; on the top left corner of each panel is represented the merger between PECAM-1 and nuclei (blue, Hoechst); scale bars 25µm. B,C Relative PECAM-1 area in relation to total islet area (B) and expression of Pecam1 (B) in PTP-1B+/+ (n=9) and PTP-1B-/- (n=12) islets, cultured over 7 days. Data presented as Mean ± SEM; n.s. not significant, *p<0.05,**p<0.01, by one-way ANOVA

To delineate the effect of the absence of iECs on islets, we performed an *in vitro* insulin secretion assay in response to glucose, from PTP-1B$^{-/-}$ and PTP-1B$^{+/+}$ islets, and cultured for 7 days. Islets from both genotypes presented similar insulin secretion (Figure 43A). Moreover, neither PTP-1B$^{-/-}$ nor PTP-1B$^{+/+}$ islets displayed any changes in the expression of apoptotic cell markers *Caspase3* and *Caspase 9* (Figure 43B). Finally, confirming the lack of endothelial cells, vestigial expression of the endothelial markers, *Pecam1*, *Kdr,* and *Cdh5*, was detected, but no differences were observed between genotypes (Figure 43C).
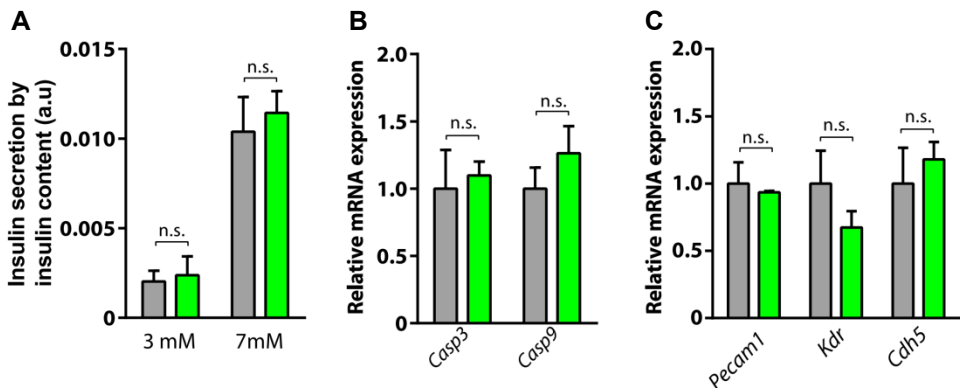
Figure 43: A In vitro insulin secretion, in response to glucose 3mM and 17mM; B,C Expression Casp3, Casp9 Pecam1, Kdr and Cdh5 in PTP-1B+/+ (n=5 and 7) and PTP-1B-/- (n=5 and 7) islets cultured 7 days. Data presented as Mean ± SEM; n.s. not significant, by Student's t-test.

The improved revascularization of PTP-1B$^{-/-}$ grafts is independent of intra-islet endothelial cells.

We assessed if iECs from PTP-1B$^{-/-}$ islets were responsible for the improvement in graft revascularization. *In vivo* studies were performed by transplanting a suboptimal amount of islets into the anterior chamber of the eye of STZ-induced diabetic BALB/c mice. Two groups of diabetic mice were constituted: PTP-1B$^{+/+}$EC$^{\varnothing}$tx$^{\text{balb-stz}}$ transplanted with PTP-1B$^{+/+}$ islets cultured for 7 days, and: PTP-1B$^{-/-}$EC$^{\varnothing}$tx$^{\text{balb-stz}}$, transplanted with PTP-1B$^{-/-}$ islets cultured for 7 days. These groups were monitored for 28 days.

B

Legend:
- Non-transplanted
- PTP-1B$^{+/+}$EC$^{\varnothing}$tx$^{balb\text{-}stz}$
- PTP-1B$^{+/+}$EC$^{\varnothing}$tx$^{balb\text{-}stz}$
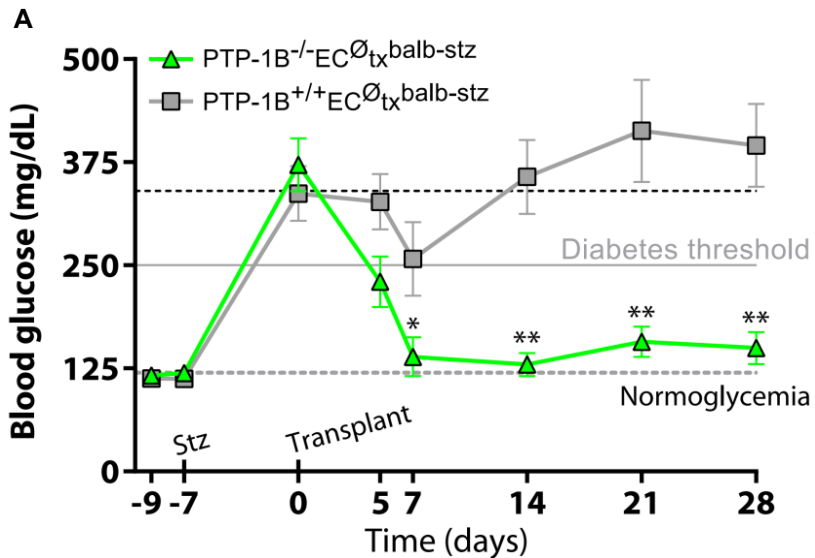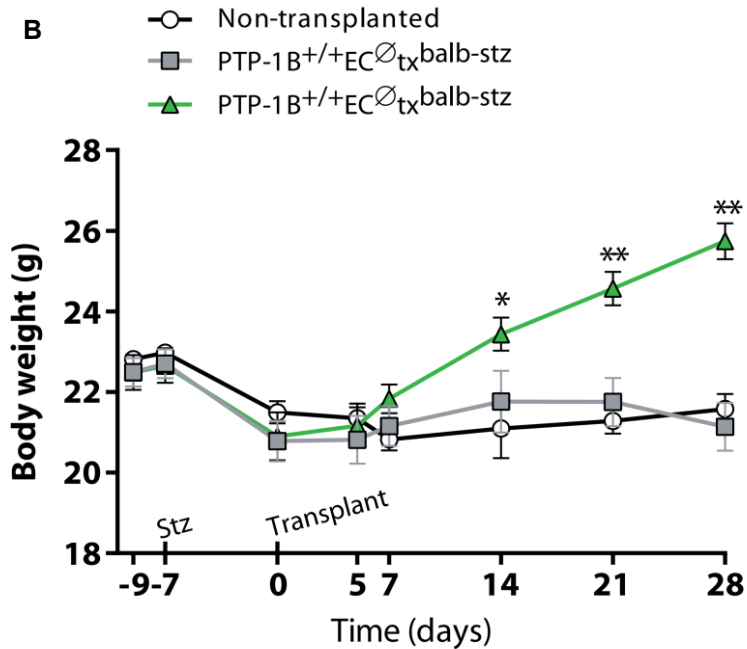
Figure 44: A. Blood glucose levels and body weight of diabetic mice transplanted with islets without ECs: PTP-1B$^{+/+}$EC$^{\varnothing}$tx$^{balb\text{-}stz}$ (n=7) and PTP-1B$^{-/-}$ EC$^{\varnothing}$tx$^{balb\text{-}stz}$ (n=7) over 28 days; median concentration of blood glucose levels at day 0: 346.8mg/dL (n=14, black dashed line); average concentration of blood glucose levels of non-diabetic mice over 28 days: 119.7mg/dL (n=8, gray dashed line); diabetes threshold: 250mg/dL. B. Body weight of diabetic animals transplanted with PTP-1B$^{-/-}$ and PTP-1B$^{+/+}$ without intraislet endothelial cells. Body weigh measurement of PTP-1B$^{+/+}$EC$^{\varnothing}$tx$^{balb\text{-}stz}$ (grey squares and line; n=7), PTP-1B$^{-/-}$ EC$^{\varnothing}$tx$^{balb\text{-}stz}$ mice (green triangles and line; n=7), and diabetic but non-ransplanted mice (black circle and line, n=7) for 28 days. Data are in mean ± s.d, *p<0.05, **p<0.01 for PTP-1B$^{+/+}$EC$^{\varnothing}$tx$^{balb\text{-}stz}$ vs PTP-1B$^{-/-}$ EC$^{\varnothing}$tx$^{balb\text{-}stz}$, by two-way ANOVA.

As for blood glucose levels (Figure 44A), the PTP-1B$^{+/+}$EC$^{\varnothing}$tx$^{balb\text{-}stz}$ group did not exhibit any improvement when comparing day 0 to day 28. PTP-1B$^{-/-}$EC$^{\varnothing}$tx$^{balb\text{-}stz}$ presented an improvement of 60%, achieving normoglycemia levels by day 7. Regarding body weight evolution, the PTP-1B$^{-/-}$EC$^{\varnothing}$tx$^{balb\text{-}stz}$ group recovered and continued gaining weight until day 28. The PTP-

A

1B$^{+/+}$EC$^{\varnothing}$tx$^{balb-stz}$ group did not present any significant variation in body weight (Figure 44B).

A

B

C
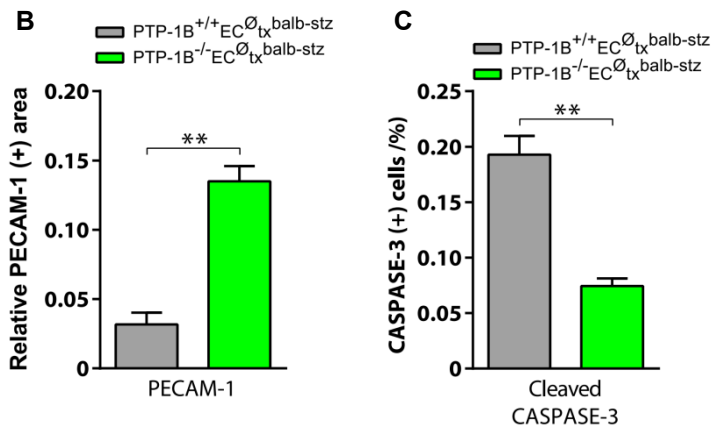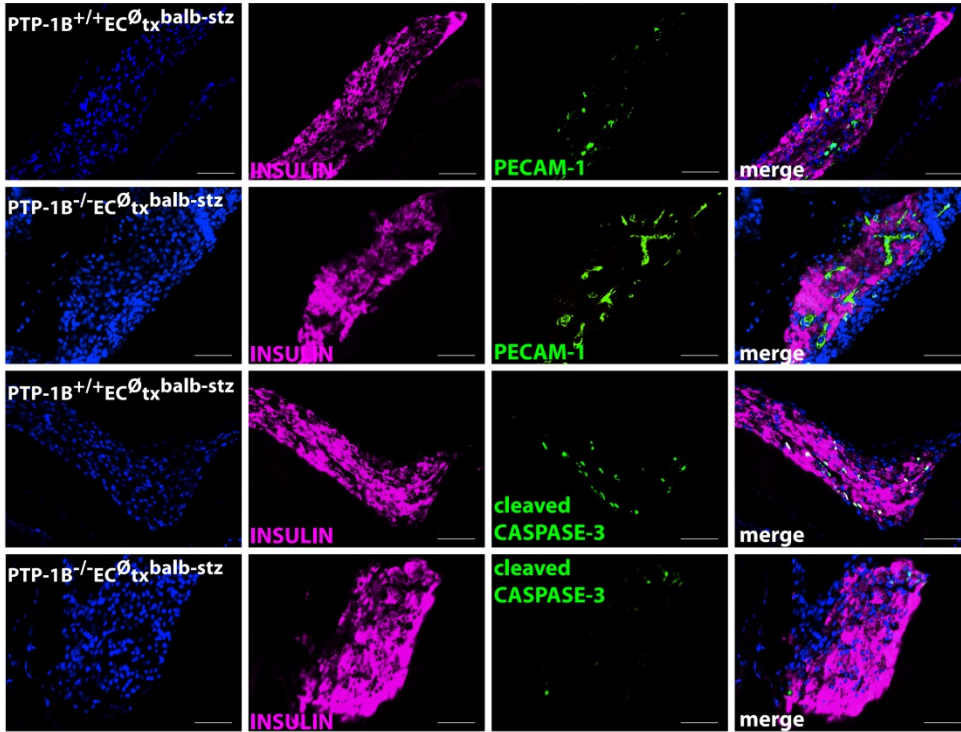
Figure 45: A. Representative immunofluorescence images from PTP-1B+/+EC$\varnothing$txbalb-stz and PTP-1B$^{-/-}$EC$^{\varnothing}$tx$^{balb-stz}$ graft paraffinized sections, 28 days

after transplantation. PECAM-1 (1st,2nd row: green), cleaved CASPASE-3 (3rd,4th rows: green) were co-stained with INSULIN (magenta); rows 1,3 represents PTP-1B$^{+/+}$EC$^{\varnothing}$tx$^{balb\text{-}stz}$ grafts and rows 2,4 PTP-1B$^{-/-}$EC$^{\varnothing}$tx$^{balb\text{-}stz}$ grafts; scale bars, 25µm. B,C. Relative immunofluorescence quantification of positive PECAM-1 (B) cleaved CASPASE-3 stained cells (C) in PTP-1B$^{+/+}$EC$^{\varnothing}$tx$^{balb\text{-}stz}$ (n=7-8 islets/animals, 5 animals) and in PTP-1B$^{-/-}$EC$^{\varnothing}$tx$^{balb\text{-}stz}$ (n=7-9 islets/animals, 5 animals) mice. Data presented as Mean ± SEM; **p<0.01 by Student's t-test.

IHC-IF analysis of paraffinized sections from the graft-containing eyes was performed by measuring PECAM-1 positive labeling to assess graft revascularization. We found a 4.2-fold increase in the percentage of endothelial cells within the PTP-1B$^{-/-}$EC$^{\varnothing}$tx$^{balb\text{-}stz}$ graft when compared with the PTP-1B$^{+/+}$EC$^{\varnothing}$tx$^{balb\text{-}stz}$ graft (Figure 45A and B). Furthermore, we investigated graft cell death by analyzing the apoptotic marker cleaved-CASPASE3. PTP-1B$^{-/-}$EC$^{\varnothing}$tx$^{balb\text{-}stz}$ grafts showed a 61% decrease in apoptotic cells when compared with PTP-1B$^{+/+}$EC$^{\varnothing}$tx$^{balb\text{-}stz}$ (Figure 45A and C). Thus, we demonstrate that iECs are not responsible for improved graft revascularization in the absence of PTP-1B.

Expression of VEGF-A, in the absence of PTP-1B, is independent of HIF activation.

To attain a deeper understanding of the increased expression of VEGF-A by ß-cells lacking PTP-1B we performed an *in vitro* ELISA to quantify the secretion and content of VEGF-A in PTP-1B$^{-/-}$ and PTP-1B$^{+/+}$ islets after 48h in culture. To do so, an *in vitro*, 48h secretome was collected and analyzed together with the islets lysates. Results showed that PTP-1B$^{-/-}$ islets presented a relative VEGF-A secretion per VEGF-A content that was 1.92-fold higher than in PTP-1B$^{+/+}$ islets (Figure 46A).
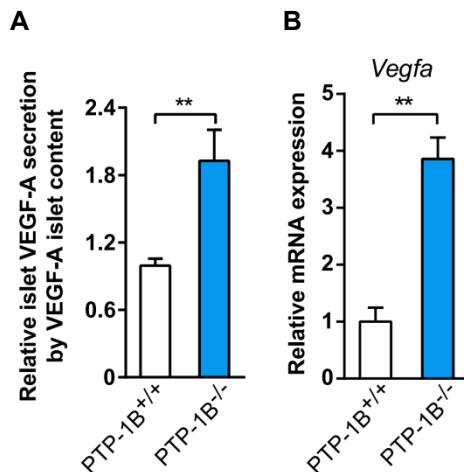
Figure 46: A. Relative VEGF-A in vitro secretion of PTP-1B$^{+/+}$ (n=6) and PTP-1B$^{-/-}$ (n=6) islets determine by ELISA; VEGF-A secretion was normalized by VEGF-A content. B. Expression of Vegfa in PTP-1B$^{+/+}$ (n=9) and PTP-1B$^{-/-}$ (n=9) islets; Data presented as Mean ± SEM. n.s., not significant,*$p<0.05$,**$p<0.01$,***$p<0.001$ by Student's t-test.

Gene expression analysis also revealed a 3.9-fold increase in *Vegfa* expression by PTP-1B^{-/-} islets (Figure 46B). Furthermore, IHC-IF analysis of isolated islets revealed that 92% of all ß-cells from PTP-1B^{-/-} islets were positive for VEGF-A (Figure 47A and B).
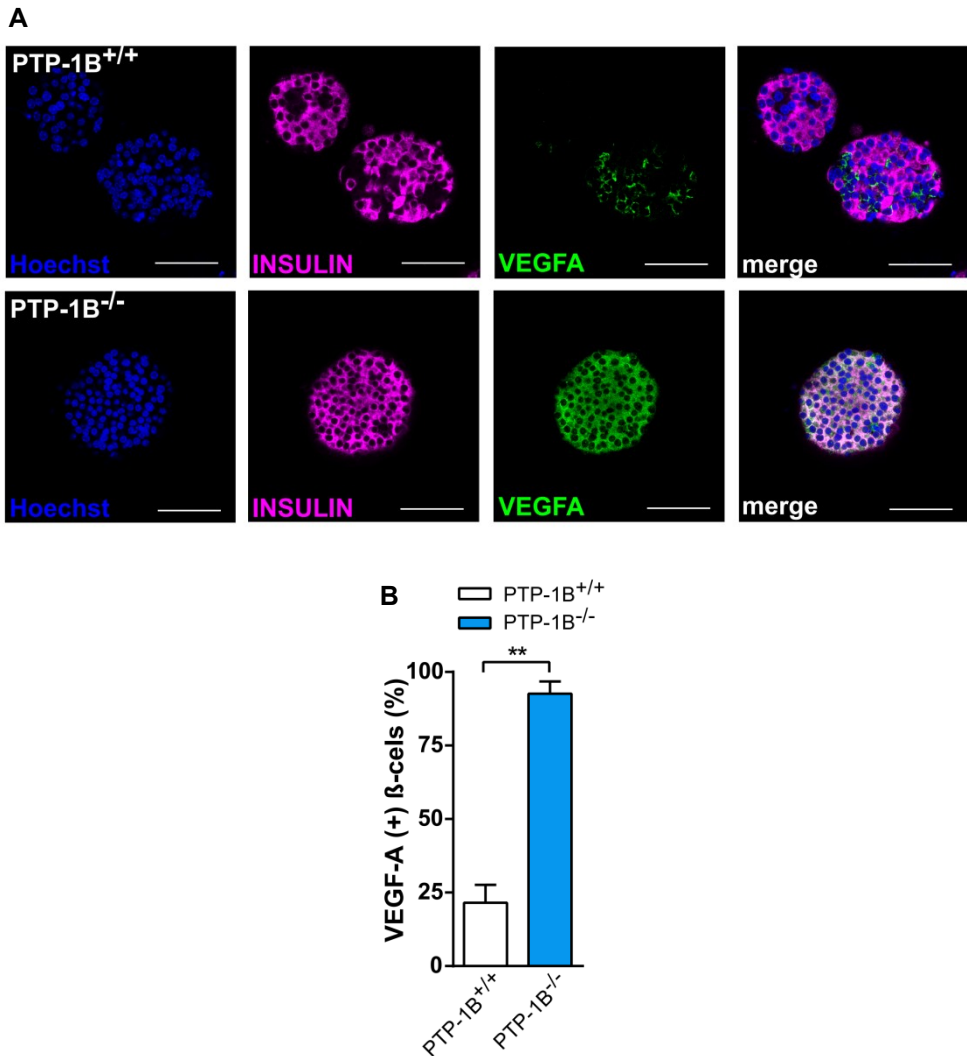
Figure 47 A. Representative images from the immunofluorescence staining of VEGFA (green) and INSULIN (magenta) in whole isolated islets cultures 2 days; colocalization of VEGF-A and ß-cells is showed on the right panels (merge; nuclei stained using Hoescht): top panels are relative to PTP-1B^{+/+} islets, bottom panels

are relative to PTP-1B$^{-/-}$ islets; scale bars, 25μm. B. Quantification of immunofluorescent colocalization of positive VEGF-A/INSULIN in PTP-1B$^{+/+}$ (n= 14) and PTP-1B$^{-/-}$ (n=14) islets. Data presented as Mean ± SEM. n.s., not significant,**p<0.01, by Student's t-test.

In order to evaluate if PTP-1B$^{-/-}$ islets presented higher levels of hypoxia than the controls, islets from PTP-1B$^{+/+}$ and PTP-1B$^{-/-}$ mice were isolated, and *Hif1a* expression was assessed following 2 days of culture. Gene expression assay revealed no differences between genotypes (Figure 48), demonstrating that HIF-alpha plays no role in PTP-1B mediated-*Vegfa* expression. Furthermore, the expression of PGC1α and ERRα was analyzed. Data showed an upregulation of *Ppargc1a* and *Esrra* (Figure 48)*, revealing the modulation of the PGC1α/ERRα pathway by PTP-1B.
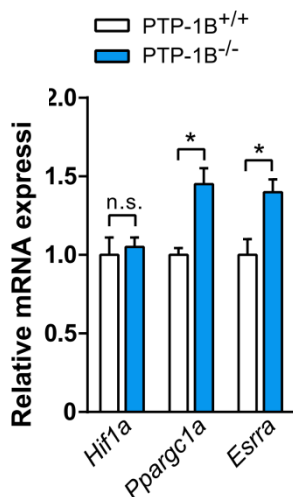
Figure 48 Gene expression of HIF1a, Ppargc1a and Esrra in PTP-1B$^{+/+}$ (n=9) and PTP-1B$^{-/-}$ (n=9) islets. Data presented as Mean ± SEM. n.s., not significant,*p<0.05, by Student's t-test.

The absence of PTP-1B triggers VEGF-A expression and secretion under nutrient deprivation via the PGC1α/ERRα axis.

As cells express *Vegfa* in response to nutrient deprivation, by activating PGC1α and ERRα[66], we cultured islets isolated from PTP-1B^{+/+}and PTP-1B^{-/-} mice in standard complete medium and under nutrient deprivation (Hank's balanced salt solution, Hbss), for two days and then assessed the gene expression of *Hif1a, Vegfa, Ppargc1a* and *Esrra*. When cultured in Hbss, no differences were observed between PTP-1B^{+/+} and PTP-1B^{-/-} islets regarding *Hif1a* expression, proving that nutrient deprivation does not activate this transcription factor (Figure 49A). However, *Vegfa, Ppargc1a,* and *Esrra* gene expression were found significantly increased in PTP-1B^{-/-} islets (Figure 49A), suggesting the modulation of this pathway by PTP-1B under nutrient deprivation. Outstandingly, when comparing PTP-1B^{-/-} gene expression between standard complete medium and nutrient deprivation conditions, we found that under nutrient deprivation, islets dramatically increased the expression of *Vegfa, Ppargc1a,* and *Esrra* (Figure 49B).
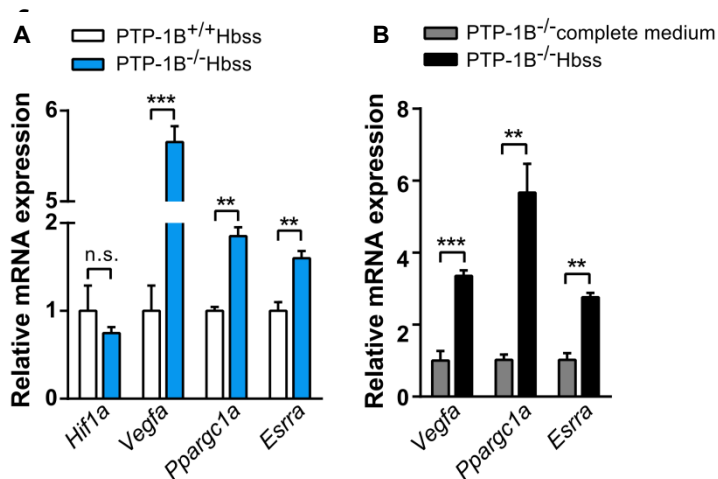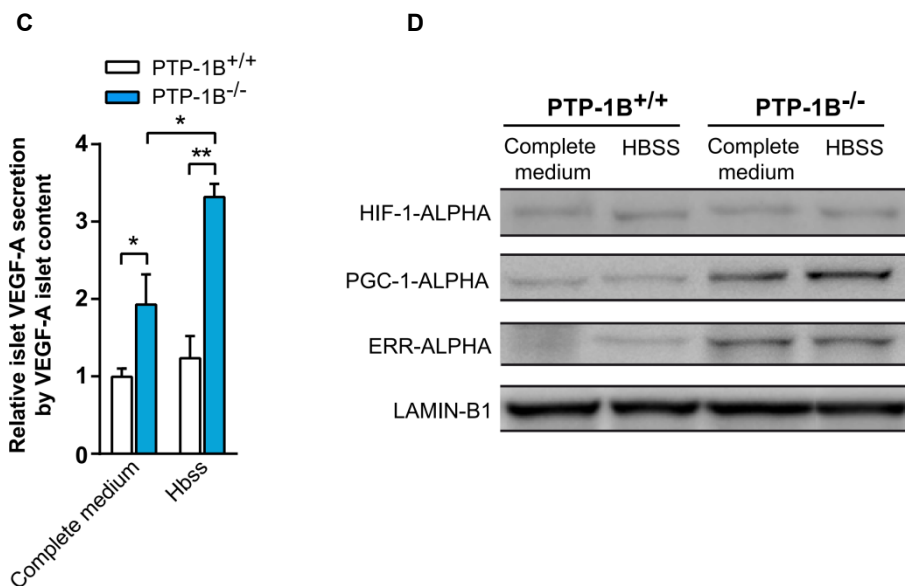
Figure 49 A. Expression of Hif1a, Vegfa, Ppargc1a and Esrra in PTP-1B^{+/+} (n=10) and PTP-1B^{-/-} (n=10) islets cultured 2 days in Hank's balanced salt solution (Hbss). B. Expression of Vegfa, Ppargc1a and Esrra in PTP-1B^{-/-} cultured in complete medium (n=10) and Hbss (n=10) for 2 days. C. Relative VEGF-A in vitro secretion of PTP-1B^{+/+} and PTP-1B^{-/-} islets cultured in complete medium (n=6/genotype) and in Hbss (n=6/genotype). D. Immunoblot for the proteins, HIF-1-ALPHA (120kDa), PGC-1-ALPHA (105kDa) and ERR-ALPHA (52 kDa), in nuclear extracts of PTP-1B^{+/+} and PTP-1B^{-/-} islets cultured either in complete medium or Hbss (n=2); housekeeping protein: LAMIN-B1. Data presented as Mean ± SEM. n.s., not significant,$*p<0.05,**p<0.01,***p<0.001$ by Student's t-test in (A, B and C) ;$*p<0.05, **p<0.01$ by two-way ANOVA in (C).

Using the same culture conditions, we measured VEGF-A secretion by ELISA, and found that was consistent with the previous observations; under both conditions, PTP-1B^{-/-} islets secreted significantly more VEGF-A then PTP-1B^{+/+} islets (Figure 49C). No differences were found, in relation to VEGF-A secretion, between PTP-1B^{+/+} islets cultured under complete medium and nutrient deprivation (Figure 49C). Taking these results into account, it is clear that, regarding gene expression, the lack of PTP-1B

triggers *Vegfa* expression and secretion, independently of *Hif1a*, but positively correlates with the increased expression of *Ppargc1a* and *Esrra*, a mechanism potentiated by the low nutritional environment surrounding islets. In order to validate the effect of the absence of PTP-1B in VEGF-A secretion, we cultured PTP-1B$^{-/-}$ and PTP-1B$^{+/+}$ in complete medium and in Hbss for 48h, and we analyzed protein levels of islets nuclear protein extracts by western blotting (with LaminB1 used as the housekeeping protein). In Figure 49D, we observed no changes in HIF1α protein levels between controls and PTP-1B$^{-/-}$islets in any of the conditions studied. By contrast, PTP-1B$^{-/-}$ islets exhibited increased levels of expression PGC1α and ERRα in complete medium and Hbss when compared to PTP-1B$^{+/+}$ islets.

Silencing PTP-1B in INS1E cells and rat islets upregulate VEGF-A expression and PGC-1-ALPHA/ERR-ALPHA signaling

Since it was possible to correlate expression and secretion of VEGFA with the increase in gene and protein levels of PGC1α and ERRα, in mice, we aim to confirm if this pathway is conserved in other species like rat and human. The first approach was to silence PTP-1B in a rat cell line: INS1E cells, using Dharmacon's Accell siRNA technology. This siRNA technology allows cell transfection, without the need to use toxic transfection reagents. INS1E cells were incubated 72h with PTPN1 targeting siRNA (PTPN1-siRNA), according to manufacturer recommendations and protocols. In parallel, a GAPDH targeting siRNA was used as a positive transfection control. After 72h, transfected and control (not transfected) cells were cultured, for 48h, in complete medium or in Hbss. Gene expression was performed using quantitative real-time PCR. In relation to the efficiency and extension of the transfection, it was possible to achieve an 80% reduction in both, Ptpn1 gene expression and Gapdh positive control (Figure 41).
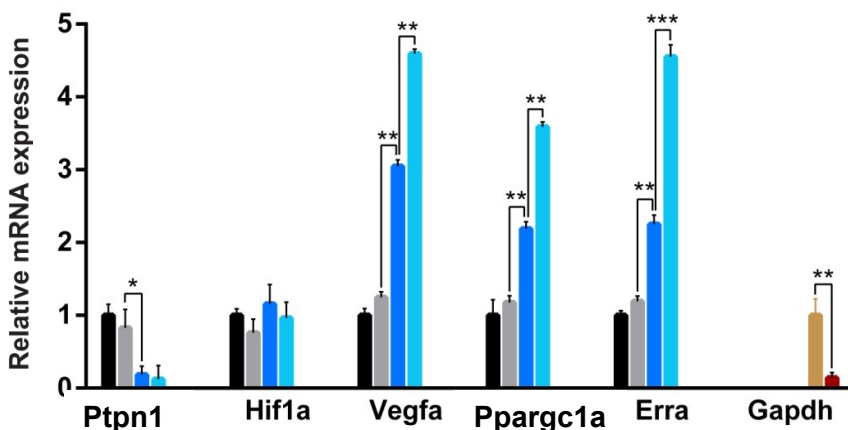
Figure 50: Silencing PTP-1B in INS1En cells: gene expression of cells, under nutrient deprivation. PTP-1B was silenced in INS1E cells using a siRNA; a positive control targeting GAPDH was used. mRNA levels of Ptpn1 Hif1a, Vegfa, Ppargc1a and *Erra* were evaluated by quantitative real-time PCR, using as housekeeping gene *actb (Beta-actin)*. Statistics: n=8; variance analysis: one-way ANOVA:*p<0.05; **p<0.01; ***p<0.001.

The downregulation in Ptpn1 expression in INS1E cells cultured in complete medium was followed by a 3 fold increase in Vegfa gene expression, a 2.1 fold increase in Pgc1a and a 2.2 fold increase in Erra gene expressions when compared with controls (Figure 50). Outstandingly, this transfected cells, cultured in HBSS, lead to a more dramatic increase in Vegfa, Ppargc1a and Erra gene expression (4.2 fold, 3.6 fold and 4.5 fold respectively) in relation to their control condition (Figure 50). These results confirm the conservation of this pathway in rat cells.

Vegfa expression mechanism in rat islets with Ptp-1b silenced.

PTP-1B was silenced in Wistar rat islets, accordingly with the previous protocol used in INS1E cells. Since islets are compact cellular structures, they were pre-incubated in a dilute solution of trypsin (50mg/mL or 2.1μM; dilution optimized in previous experiments). Incubation with diluted trypsin will increase the distance between islet cells, without compromise islet structure, allowing siRNA to diffuse into the core of the islet. In order to evaluate the diffusion of siRNA throughout the islets, we incubate islets, for 72h with a non-targeting siRNA with GFP, fixed them and visualize siRNA diffusion using confocal microscopy.

In Figure 51 it's possible to visualize four representative images from different cell layers acquired from different islet. SiRNA diffusion was not equal for all islets; neither reaches 100% of islet's cells, but all used islets presented positive GFP labeling. In general, siRNA-GFP reached the islet's core and infected 60 to 85% of total islet cells, and only in a small percentage of islets, positive-eGPF labeling was detected in few cells, (7-15% of total islet cells).
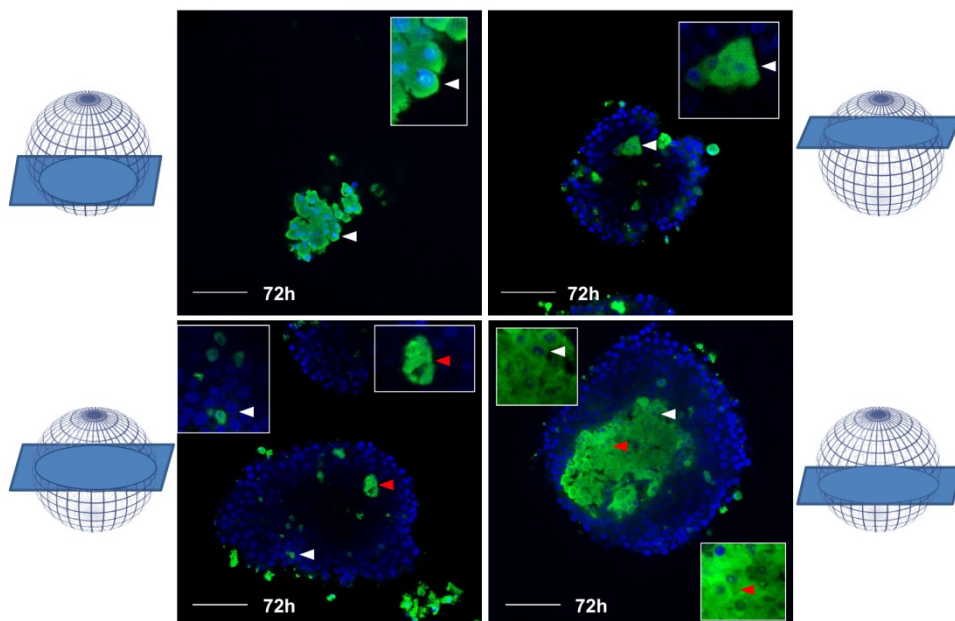
Figure 51: Diffusion of siRNA within rat islets. A non-targeted siRNA with GFP was used to evaluate the diffusion of the siRNA under the conditions used for silencing Ptp-1b. Islets were incubated 72h with non-targeting eGFP-siRNA, according to the manufacturer recommendations. Confocal microscopy was used to assess siRNA's GFP fluorescence (green), within different cell layers of the islets. After 72h of incubation, islets were fixed in Paraformaldehyde 4% and mounted with mounting medium with DAPI (in order to stain nuclei, blue). In order to represent de diversity in siRNA diffusion, four images of the different cell layer,

from four different islets were chosen. Zoomed sections of the images (white and red pointers, zoom 3x) are present in each image.

Following this transfection protocol, we silenced PTP-1B in rat islets, incubating these, for 72h, with the Dharmacon's Accell siRNA technology specific for rat PTPN1 gene. In parallel, a Gapdh targeting siRNA was used, as a positive transfection control. After 72h, transfected and control (transfected with scramble-siRNA) islets were culture, for 48h, in complete medium or in Hbss. Gene expression was assessed, through quantitative real-time PCR Figure 52)
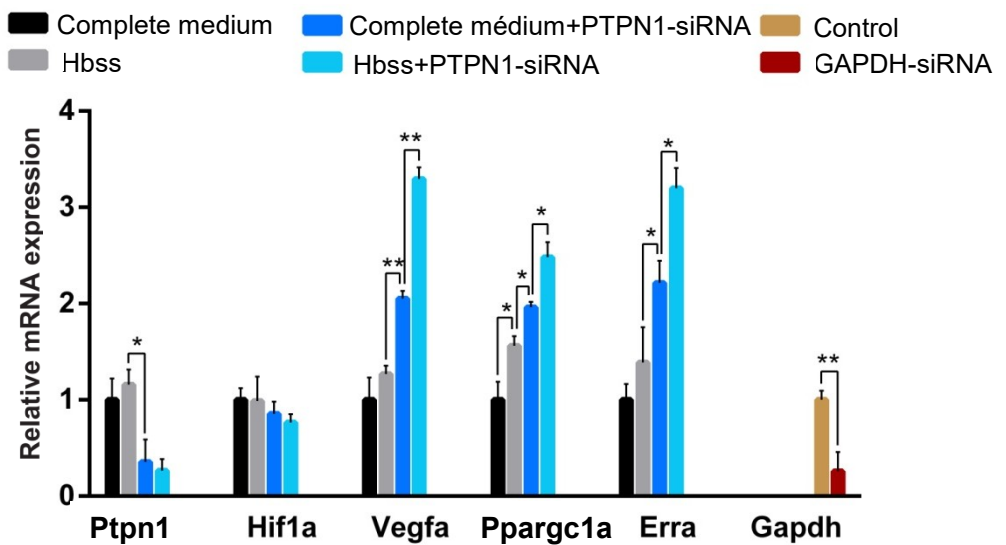
Figure 52 Silencing PTP-1B in rat islets: gene expression of islets, under nutrient deprivation. A positive control is targeting Gapdh used. mRNA levels of Ptpn1, Hif1a, Vegfa, Ppargc1a, and *Erra* were evaluated by quantitative real-time PCR; housekeeping gene: *ßactin*. Statistics: n=8; variance analysis: one-way ANOVA:*$p < 0.05$; **$p < 0.01$.

In relation to the efficiency and extension of the transfection, it was possible to achieve a 64% reduction in Ptpn1 gene expression and a 74% reduction in the expression of Gapdh positive control (Figure 52). Moreover, succeeding Ptpn1 silencing in islets cultured in complete medium, it was observed a 2 fold increase in Vegfa gene expression, followed by a 1.9 fold increase in Ppargc1a and a 2 fold increase in Erra gene expressions, when compared to controls (Figure 52). Furthermore and as expected, by the results obtained in INS1E cells, transfected islets, cultured in Hbss, lead to a more dramatic increase in Vegfa, Pgc1a and Erra gene expression (3.3 fold, 2.5 fold, and 3.2 fold respectively) in relation to their control condition (Figure 52). These results support the conservation of this pathway in rat islets.

Silencing PTP-1B in human islets induces VEGF-A expression through PGC-1-ALPHA/ERR-ALPHA signaling

Lastly, we aimed at investigating whether the modulation of VEGF-A by PTP-1B was conserved in human islets. Therefore, we obtained human islet from cadaveric donors in a total of 4 batches. In order to check batch purity, we stained a random sample with dithizone (DTZ). The average purity calculated for the 4 batches was 95.5% (± 1.3%). Islet viability was also assessed by a CFDA/PI am staining. Figure 53 represents the maximum projection image of fluorescent CFDA/PI in islets from two different batches. The average total viability calculated was 85.0% (±7.5%).
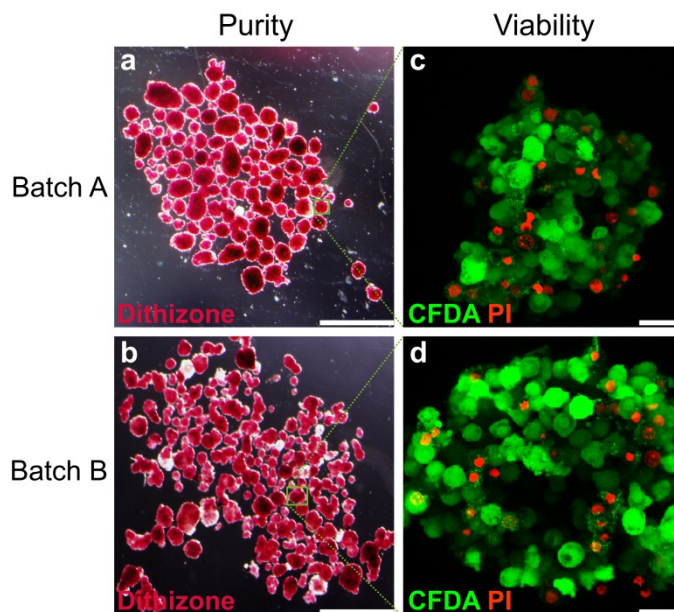
Figure 53: Human islets batches purity and viability. A, B. Representative images of the relative purity of the human islets batches (left column, batch A, top; batch B, bottom). A sample of each batch was stained with dithizone (pink), which stains zinc, accumulated mainly in the secretory vesicles of islet ß-cells. Scale bars: 1mm. C, D. Representative maximum projection of in vivo immunofluorescence staining of CFDA (viable cell marker, green) and PI (dead cells, nuclei staining,

red), on human islets from batch A (top) and batch B (bottom). Images obtained using confocal microscopy, scale bars:15 μm.

Silencing PTP-1B in human islets using siRNA technology

Our first approach was to silence PTP-1B in human islets using Dharmacon's Accell siRNA technology, according to the protocol established with rat islet. A non-targeting siRNA with eGFP was used to evaluate the diffusion of the siRNA throughout the islets. Figure 54 features four representative images: the two islets on the left represent negative control, while the two islets on the right represent islets incubated with siRNA. Negative control islets presented a weak fluorescent signal, which was attributed to auto-fluorescence. On the other hand, islets incubated with siRNA displayed strong eGFP fluorescence in the core of the islet, indicating a successful protocol for increasing siRNA diffusion. siRNA diffusion was not equal for all islets; neither group reached 100% of islet cells, but all used islets presented positive GFP labeling. Overall, it was observed that siRNA-GFP reached between 52 and 87% of total islet cells.
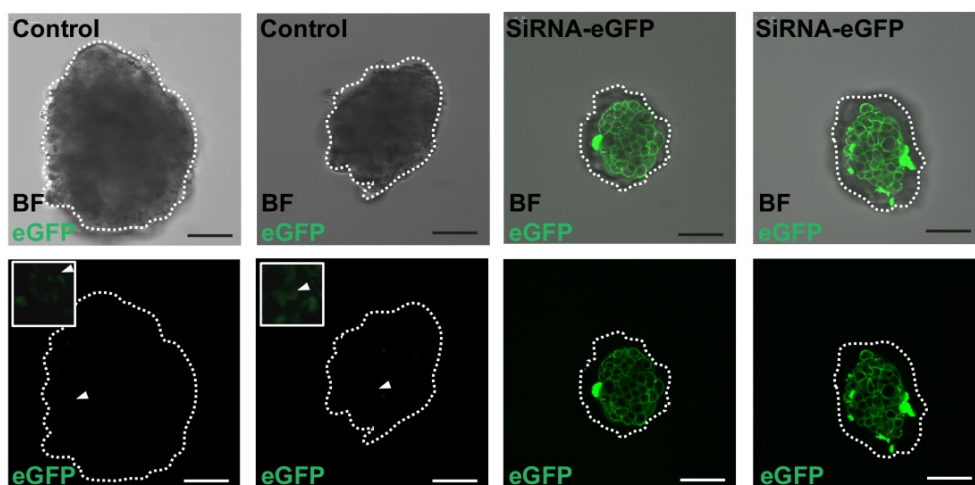
Figure 54: Representative immunofluorescence images of non-targeting, positive control, siRNA coupled with eGFP (siRNA-eGFP) in human islets (72h of exposure). Top panels: a merger between bright field and immunofluorescence, using as settings the excitation (488nm) and emission (517nm) wavebands of the eGFP molecule. A bottom panels: immunofluorescence images using eGFP previous settings. From left to right: column 1,2: control, human islets; column 3,4: human islets exposed to siRNA-eGFP; scale bars 50 µm.

To evaluate the extension of the downregulation of PTP-1B we assessed PTP-1B protein levels by IHC-IF and western blot, 48h after the transfection protocol. The IHC-IF analysis (Figure 55A and B) revealed an average decrease of 57% in PTP-1B positive staining in ß-cells within human islets transfected with PTPN1-siRNA comparing with islets PTP-1B transfected with a scramble-siRNA (control). Moreover, analyzing control and PTPN1-siRNA protein extracts by western blot revealed a decrease in PTP-1B protein level in PTPN1-siRNA, confirming a successful downregulation of PTP-1B (Figure 55C)

A
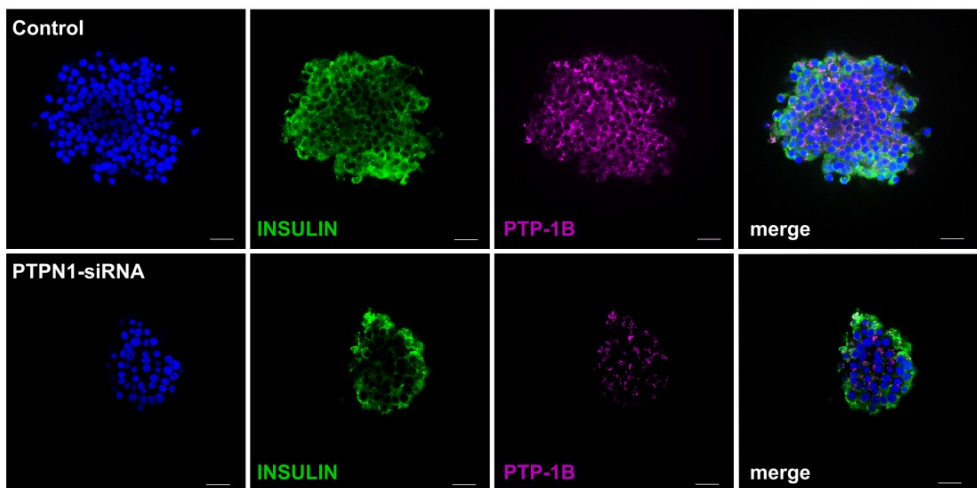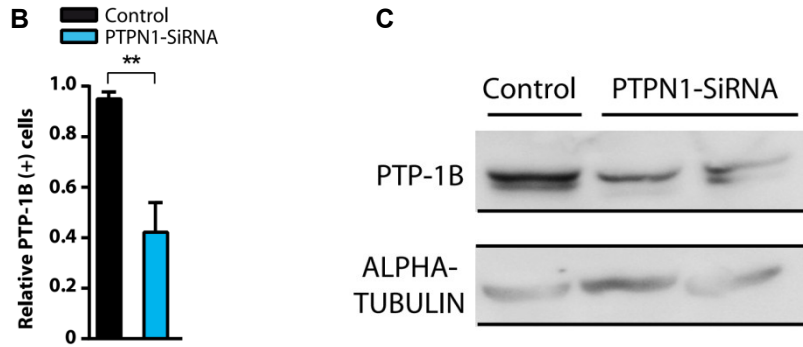
Figure 55: PTP-1B downregulation in human islets. A. Representative images from the immunofluorescence staining of PTP-1B (magenta) and INSULIN (green) in human islets following siRNA-PTPN1 silencing protocol. Top panels are relative to control human islet incubated with scramble-siRNA , bottom panels are relative to PTPN1-siRNA islets; B. Relative immunofluorescence quantification of PTP-1B/INSULIN staining in PTPN1-siRNA (n=8) and control islets n=8). C. Immunoblot for the proteins, PTP-1B (50kDa), AlPHA-TUBULIN (50kDa) in cell extracts of control and PTPN1-siRNA; Data presented as Mean ± SEM.,**$p<0.01$, by Student's t-test; scale bars, 25µm.

The obtained results indicate that we successfully downregulate PTP-1B in human islets. In addition to these results, gene expression was analyzed by quantitative real-time PCR. As a positive control for the transfection, we used GAPDH-siRNA. Gene expression analysis revealed a reduction in *PTPN1* expression between 30 and 50% and a reduction between 25 to 78% in *GAPDH* expression (Figure 56A and B). Along with the silencing of *PTPN1*, throughout the different batches, a significant increase of 1.4- to 3-fold in *VEGFA* expression was observed, followed by a 1.2- to 1.6-fold increase in *PPARGC1A* expression and a 1.3- to 2.8-fold increase in *ESRRA* expression. *HIF1A* expression did not present any modifications (Figure 56A and B). For these reasons, it was possible to confirm that the lack of PTP-1B triggers *VEGFA* expression through modulation of the PGC1α/ERRα pathway in human islets.
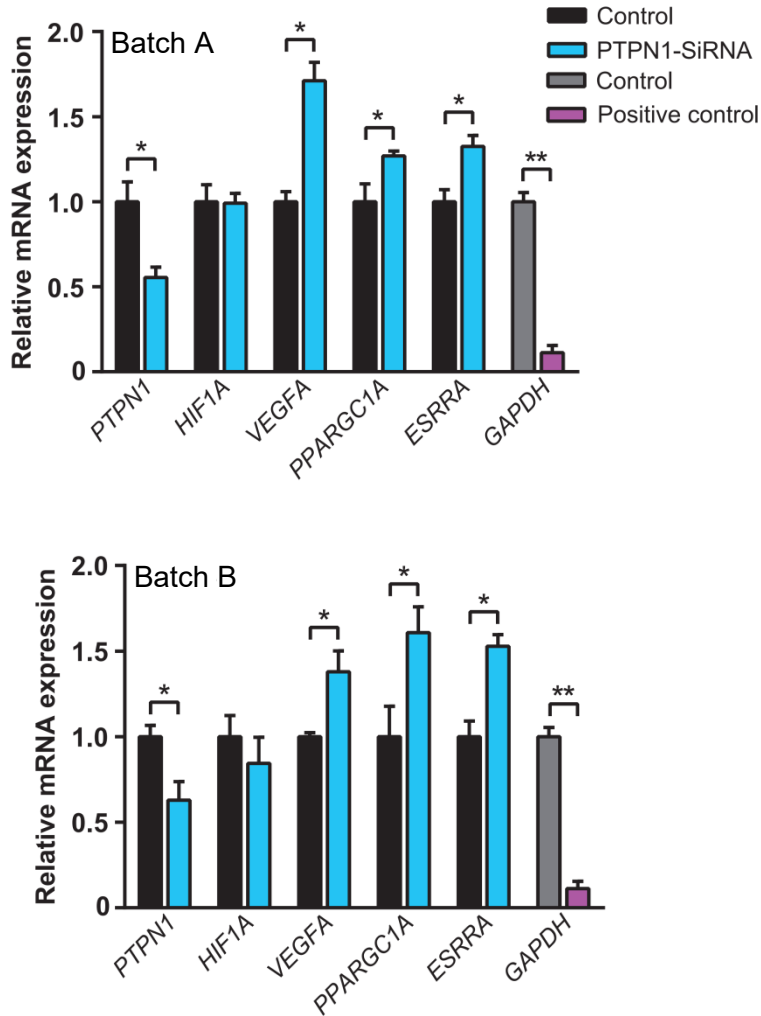
Figure 56: Expression of PTPN1, HIF1A, VEGFA, PPARGC1A and ESRRA in control human islets (n=6) and PTPN1-SiRNA islets (72h of exposure; n=6), results from two batches are represented. Expression of GAPDH (positive control) was compared against control islets (n=6); Data presented as Mean ± SEM. *p<0.05,**p<0.01 by Student's t-test. Gene expression assays were performed in four different batches

To assess if the downregulation of PTP-1B in human islets results in an increase in VEGF-A secretion, we performed an *in vitro* 48h secretion

assay analyzed by ELISA to quantify the secretion of VEGF-A in control and PTPN1-siRNA islets after 48h in culture. To do so, 48h secretome was collected and analyzed together with the islets lysates. Results showed that PTP-1B$^{-/-}$ islets presented a relative VEGF-A secretion per VEGF-A content that was 6-fold higher than in PTPN1-siRNA islets (Figure 57).
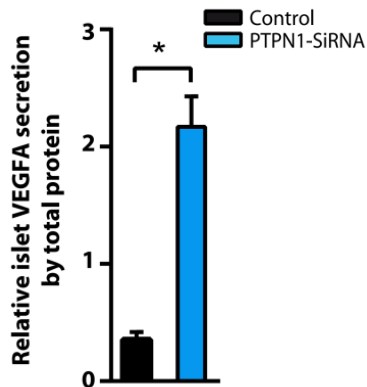
Figure 57: Relative *in vitro* secretion of VEGFA from control and PTPN1-siRNA islets (n=4) quantified by ELISA; VEGF-A secretion was normalized by total protein content. Data presented as Mean ± SEM (x10^5), *p<0.05 by Student's t-test.

Silencing PTP-1B in human islets using shRNA Lentivirus particles

Our previous results demonstrate that the signaling events by which the downregulation of PTP-1B induces VEGFA upregulation and secretion are conserved in human islets. Therefore we aimed to investigate whether it is possible to increase human islet-graft revascularization, after silencing PTP-1B. To achieve this, we use Short hairpin RNA lentiviral particles (shRNA LV) to silence PTPN1 gene. shRNA LV represents a more effective strategy for sustaining the downregulation of a gene in islets[296–298], when compared with siRNAs, moreover it is demonstrated that it does not affect islet function[296–298]. Therefore, using this technology allows evaluating the effect of PTP-1B silencing in the revascularization of human islet-grafts, after 8 days of transplant, where revascularization reaches its maximum.

This way, human islets were infected with a shRNA LV for human PTPN1 (shPTPN1 LV) with a pGFP vector, to monitor the transfection efficiency. After infection, the islets were maintained for 8 days, where the transfection was monitored. Transduced eGPF was monitored after 2 and 8 days following infection. ShPTPN1 LV islets presented high levels of transduction GFP 2 days following infection, on the contrary, at day 8 the number of cells presenting GFP fluorescence decreased (Figure 58), meaning the reduction of the transduction and therefore the possible downregulation of PTP-1B.
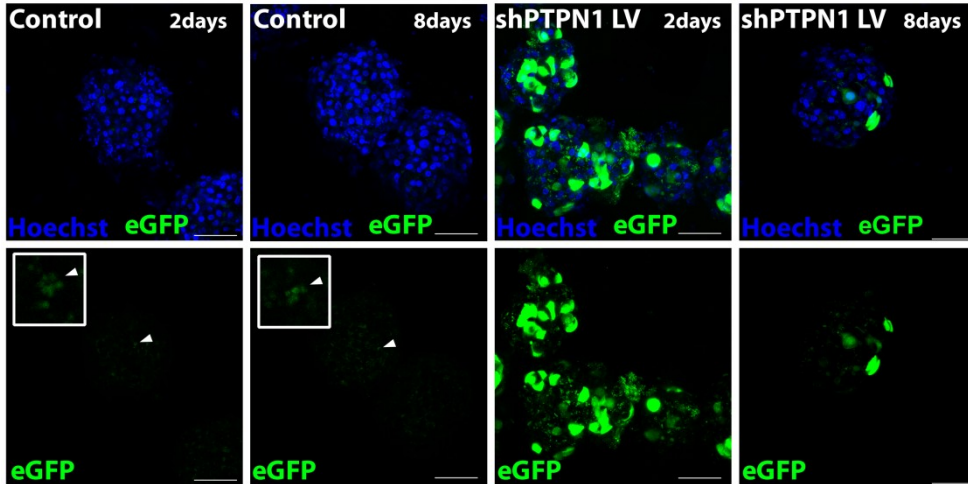
Figure 58: Representative fluorescence images of transduced eGFP in islets infected with shPTPN1 LV and control non-infected islets. Top panels: a merge between Hoechst/eGFP fluorescence, using as settings the excitation (488nm) and emission (517nm) wavebands for the eGFP molecule. A bottom panels: immunofluorescence images using eGFP previous settings. From left to right: column 1,2: control, human islets; column 3,4: human islets infected with shPTPN1 LV; scale bars 50 μm.

In order to understand the extension and duration of the downregulation of PTP-1B following the infection the infection, we analyzed protein levels of PTP-1B by western blot in protein extracts from shPTPN1 LV and scramble (infected by scramble shRNA LV) 2 and 8 days after the infection. Immunoblot reveals that 2 days following infection shPTPN1 LV islets presented a strong downregulation of PTP-1B when compared to control islets. However, eight days following infection, the protein levels of PTP-1B are almost normalized (Figure 59).
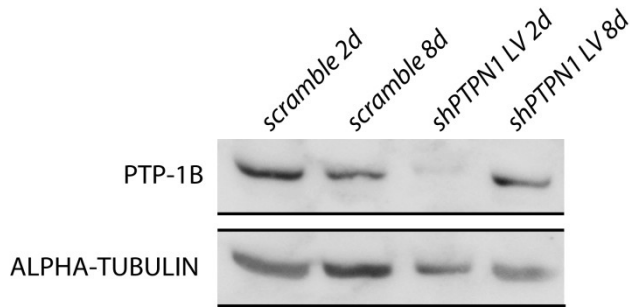
Figure 59: Immunoblot for the proteins, PTP-1B (50kDa), AlPHA-TUBULIN (50kDa) in cell extracts of control and shPTPN1 LV and scramble (scramble shRNA LV), 2 and 8 days after infection.

To assess if the downregulation of PTP-1B in human islets results in an increase in VEGF-A secretion we performed an *in vitro* secretion assay analyzed by ELISA to quantify the secretion of VEGF-A in control and in shPTPN1 LV islets cultured for 2 and 8 days. To do so, 48h secretome was collected and analyzed together with the islets lysates. Results showed that PTP-1B$^{-/-}$ islets presented a relative VEGF-A secretion per VEGF-A content that was 7-fold higher than in shPTPN1 LV after 2 days of culture. VEGF-A secretion levels decreased after 8 days of culture but sustained a 60% higher level of VEGF-A secretion than scramble islets (Figure 60).
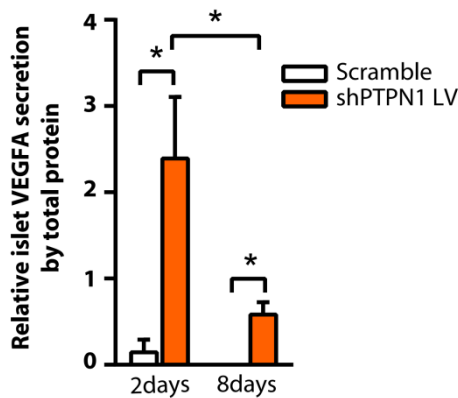
Figure 60: Relative *in vitro* secretion of VEGFA from control (scramble shRNA LV) and shPTPN1 LV islets (n=4) quantified by ELISA; VEGF-A secretion was

normalized by total protein content. Data presented as Mean ± SEM ($x10^5$), *p<0.05 by two way ANOVA.

The results obtained in this study support that targeting human islet PTP-1B improves VEGFA secretion, through a PGC1α/ERRα axis. In this sense, we design a small pilot study to investigate if this improvement was translated into an enhanced human islet-graft revascularization after silencing PTP-1B. We transplant 150 human islets infected with shPTPN1 LV (n=3 mice, 4 islets*animal) or scramble (n=2mice, 4 islet*mice) into the ACE of a small number of NSG mice, and assessed *in vivo* islet-graft functional revascularization by the end of 8 days, by two-photon microscopy. We found that 8 days following transplantation, shPTPN1 LV islet-graft present improved revascularization than scramble islet-graft (Figure 61). Curiously, and in contrast with previous *in* vitro results, infected islets display high levels of GFP fluorescence 8 days after infection, meaning that transduction is sustained over more time than in *vitro* conditions.
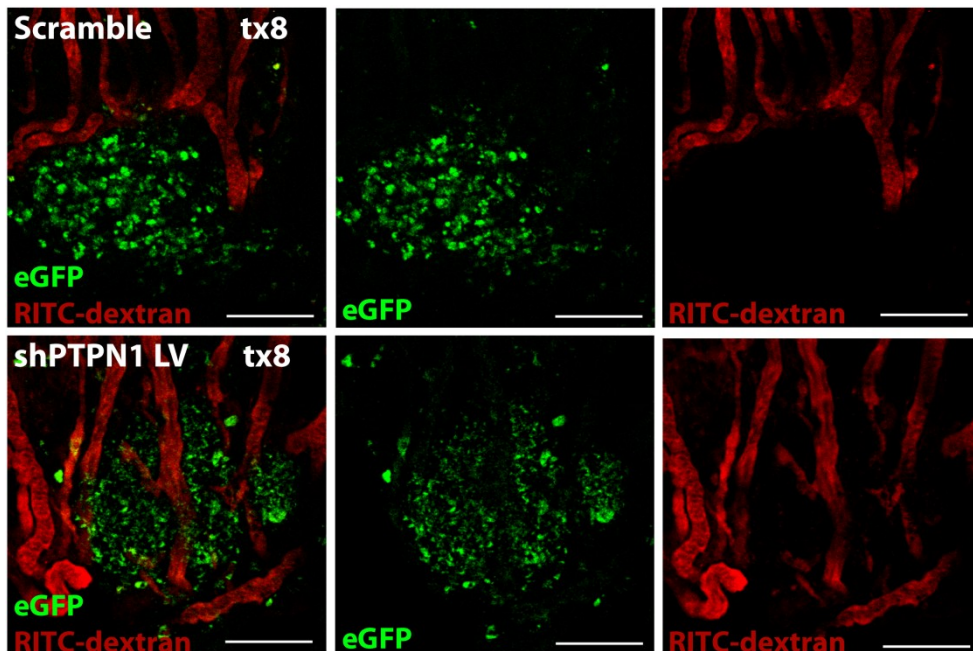
Figure 61: Absence of PTP-1B in human islet-graft improves graft revascularization. Representative in vivo images of functional vessels (in red, RITC-dextran labeling), and graft's transduced eGFP in scramble and shPTPN1 LV islets 8 days following transplantation, using two-photon microscopy; scale bars, 25µm.

Based on all these data, we propose a model whereby VEGF-A expression is enhanced via the PGC1α/ERRα axis in transplanted PTP-1B-/- islets (fig. 6). Briefly, in the presence of an external stimulus such as nutrient deprivation, the absence or downregulation of PTP-1B promotes an increase in PGC-1-α gene and protein levels through still unknown mechanisms. In turn, PGC1α increases the expression of orphan nuclear receptor ERRα, and PGC1α/ERRα dimers recognize and bind several conserved sites at the VEGF-A promoter, inducing the expression of the *VEGFA* gene. Increased *Vegfa* gene expression results in an increase in both protein and secretion levels of VEGF-A by islets. Lastly, VEGFA interacts with its receptor, VEGFR2, in endothelial cells, activating the signaling pathway of angiogenesis towards the islets.

Figure 62: Proposed scheme: PTP-1B enhances VEGF-A expression via PGC-1α/ERRα signaling in islet transplantation. During an external stimulus like nutrient deprivation, the absence or downregulation of PTP-1B (1) promotes the increase of PGC-1-ALPHA gene and protein level. (2) and the expression of ERR-ALPHA. (3) PGC-1-ALPHA/ERR-ALPHA complex is known to recognize several conserved sites at the VEGFA promoter (4), inducing its expression (5) and increasing its secretion (6). In ECs VEGF-A is known to interact with its receptor, VEGFR2, inducing angiogenesis.

Discussion

Islet transplantation as a potential treatment for type 1 diabetes fails mainly due to a deficient survival of the islet graft. Poor revascularization is mainly responsible for early graft loss and represents one of the major issues affecting long-term graft survival[123,303,304]. Searching for new targets to facilitate islet revascularization may lead to improved future results in cell transplantation[305].

Despite its potential, the clinical use of islet transplantation for treatment of T1D remains limited by post-transplantation challenges[123,303], being one of the main issues, graft's poor revascularization. Islets native architecture is characterized by a dense vessel network that, delivers oxygen, hormones, glucose, and nutrients to islet's cells allowing them to function correctly[33]. This vascular network is severed when islets are isolated for transplantation[123], and even though islets freely revascularize[122,129,130], they do not reach the levels of vascularization present in endogenous pancreatic islets[136,306], which results in the impairment of grafts function and survival. Altogether, the lack of a proper vascular network account as the primary responsible for early graft loss[124,136,307]. Therefore we focused on the searching of new ways to improve islet-grafts vascular network representing a step forward to improve the outcome of transplantation.

Sodium tungstate appears as a potent treatment, due to its low toxicity, high biodisponibility and to its high affinity to inhibit protein tyrosine phosphatases.Sodium tungstate has the potential to inhibit endothelial cell PTPs and potentiate VEGF-A-induced angiogenesis. In EC, tyrosine phosphorylation of the VEGFR2 and the adhesion molecule VE-cadherin constitute a crucial initial signaling event by which VEGF-A stimulates angiogenesis. Thus inhibiting VEGFR2 dephosphorylation, by inhibiting regulatory PTPs activity, will potentiate VEGFA-dependent receptor

dimerization and autophosphorylation. The result is the upregulation of unique downstream signaling pathways, which are linked to different angiogenic-liked cellular signals such as proliferation, migration, survival, and permeability[252,253]

Apart from this sodium tungstate is known to have a significant effect on several pathways that can improve transplantation outcome, islet-graft revascularization, survival, and even function, converting this inorganic salt in an excellent candidate to be tested. For instance, treatment with sodium tungstate can reduce the adaptive immune responses, which are a major barrier to successful transplantation. Rejection is caused by immune responses to alloantigens on the graft, which are proteins that vary from individual to individual within a species, and are thus perceived as foreign by the recipient. Sodium tungstate is an inhibitor of the molybdenum-containing enzymes such as (XO)[308,309], a ubiquitous enzyme that is part of the purine biosynthetic pathway that catalyzes the conversion of hypoxanthine to xanthine and finally uric acid. XO is also a well-known producer of reactive oxygen species (ROS) that contribute to host defenses in microbial infection models [310–312]; In addition, Maemura et al. describer that XO-dependent ROS have a central role in antigen presentation and cell maturation of Kupffer cells and other professional antigen-presenting cells (APC) [313], this suggests that sodium tungstate inhibition of XO in mice could delay, or partially impair the adaptive immune response and thus the blood-mediated inflammatory response[313], that destroys islet-grafts.

Sodium tungstate is also known to improve pancreatic beta cell function by restoring glucose-induced insulin secretion, as the treatment shown to improve dose-dependently insulin secretion, which may favor islet graft function. Moreover, sodium tungstate treatment was shown to decrease the expression of several genes involved in the mitochondrial apoptotic

pathway and inflammatory response in islets lacking IRS-2, indicating that sodium tungstate primarily targets β-cell death mechanisms through activation of endogenous kinases[195]. And finally, sodium tungstate treatment increases proliferation[172,176–178]. A transcriptomic analysis of pancreas from STZ-diabetic rats has revealed that ERK1/2 has been shown to participate in Sodium tungstate-induced proliferation of INS-1E cells. Since Rkip inhibits Raf-1 kinase, which phosphorylates MEK, which in turn phosphorylates ERK1/2, Sodium tungstate-induced normalization of Rkip expression leads to an increase in the MAPK pathway activity, favoring proliferation, and thus promoting islet-graft replication and graftß-cell mass expantion[176]. In addition, sodium tungstate is involved in the phosphorylation of PDX-1, which is involved in pancreas development, insulin expression, and β-cell functionality. In fact, sodium tungstate treatment augments the number of insulin and PDX-1 positive cells[172,200]. For all these reasons sodium tungstate treatment is a potential treatment to improve islet transplantation. However, and due to the risk of sodium tungstate treatment improve, also, insulin sensitivity, or induce pancreas regeneration as shown in STZ-induced diabetes models, the effects of this treatment on islets graft could be masked. Therefore we supplied 0.5mg/mL of sodium tungstate in the drinking water, ¼ of the standard concentration used in those studies[163,164,171,172,175].

Despite the potential to ameliorate islet transplantation at several levels. The principal effect observed was the improvement in islet-graft revascularization and the decrease in graft's cell death. The mechanism by which tungstate promotes revascularization in islet-grafts is unknown. It is possible that this effect may be the product of the inhibition of several phosphatases[170,314] from graft's cells or the overall effect on the recipient[315]. Une promising phosphatase inhibited by tungstate is PTP-1B[180,316,317], that was demonstrated to be the negative regulator of angiogenesis signiling[256]. In this sense, by transplanting islet from PTP-1B$^{-/-}$ we were able to study

whether tungstate was acting through the inhibition of PTP-1B in donor endothelial cells that play an essential role in the early stages of graft revascularization and survival[301,302,318]. We demonstrate that the PTP-1B knock-out grafts together with tungstate treatment achieve similar levels of revascularization and reduced graft's cell death as PTP-1B knock-out grafts without treatment and as PTP-1B wild-type grafts after with tungstate treatment. We propose that this improved revascularization is the main contributor to enhanced survival and function of PTP-1B$^{-/-}$ islet grafts. Although we cannot completely rule out improved ß-cell function due to loss of PTP-1B in our transplants, the experiments conducted with PTP-1B$^{-/-}$ islets *in vitro* demonstrate that they exhibit similar apoptosis rates and glucose-induced insulin secretion to controls.

PTP-1B emerges as a potential target with the ability to negatively modulate critical signaling pathways, such as cell proliferation and angiogenesis[256,300]; it was demonstrated to be the negative regulator of the phosphorylation of VEGFR2 upon the coupling of VEGFA and VE-CADHERIN[256]. The activation of signaling pathways leading to the upregulation of various critical angiogenic enzymes involved in ECs proliferation, migration[246] and loss of cell-cell contacts[247] are decisive for the success of new approaches aiming the improvement of islet-graft revascularization. In this study, we demonstrate that the absence of islet PTP-1B increases functional graft vascularization by increasing the number of newly formed vessel branches and total graft vessel area. Furthermore, we propose that this improved revascularization is the main contributor to enhanced survival and function of PTP-1B$^{-/-}$ islet grafts. Although we cannot completely rule out improved ß-cell function due to loss of PTP-1B in our transplants, the experiments conducted with PTP-1B$^{-/-}$ islets *in vitro* demonstrate that they exhibit similar apoptosis rates and glucose-induced insulin secretion to controls.

A number of mechanisms could explain improved revascularization in PTP-1B^{-/-} islet grafts[51,269,302] and in sodium tungstate treatment. As graft revascularization begins 2-4 days after islet transplantation[130,133], donor-intraislet endothelial cells engage a central role in the early stages of angiogenesis and vasculogenesis[301,302,318]. It is possible that in the absence or inhibition of PTP-1B, IECs might impulse early stages of revascularization, promoting a quicker re-establishment of blood vessels and improving islet-graft function and survival. Furthermore, since isolated PTP-1B^{-/-} islets present an upregulation of several EC markers as well as reduced EC loss in culture, we considered the possibility that donor PTP-1B^{-/-} iECs contributed to the increased functional vasculature in grafts[269,302,319]. Our study revealed that iECs disappeared by the end of 7 days. Although it is known that in culture, islets may alter the expression of several markers, or even insulin content and secretion[320,321], we did not find any differences between PTP-1B^{+/+} and PTP-1B^{-/-} in insulin secretion or apoptosis. Even though, we cannot exclude the possibility that other fundamental markers that could influence islet function could be modified during culture, our hypothesis, where iEC play a determining role on PTP-1B-/- final, improved revascularization was ruled out after we observed that mice transplanted with PTP-1B-/- without ECs still exhibited improved levels of revascularization.

The mechanisms underlying islet revascularization in the absence of PTP-1B are unknown, although a number of factors may be implicated[51]. One possibility was that islets lacking PTP-1B released more pro-angiogenic signals than control islets. Our study revealed that PTP-1B^{-/-} islet grafts expressed and secreted more VEGF-A, an angiogenic cytokine that stimulates extraembryonic blood vessel formation[49,50,322] than control grafts favors this notion. One may suggest that a similar effect on revascularization could be obtained by using previous strategies based on the overexpression or direct administration of VEGFA to islets[144–146]. These

therapies, however, have demonstrated induced hyper-revascularization of the grafts associated with a loss of ß-cell mass and, consequently, impaired graft function. In this sense, our approach differs from previous ones and offers a significant advantage, as we demonstrate that improved revascularization, by modulating VEGFA expression, was not associated with deleterious effects on ß-cell number or function in grafts. Of note, the increment in VEGF-A expression observed in the grafts from our study was not translated into a decrease in relative ß-cell population, as the improved observed was accredited to a decrease in graft cell death. With this observation, we may hypothesize that, instead of directly activating VEGF-A expression, like in other studied therapies, PTP-1B may act indirectly through a signaling pathway.

The mechanism by which PTP-1B enhances VEGF-A expression is still unknown and constitutes a potential breakthrough. Cells express and secret VEGF-A in response to numerous stimuli, such as hypoxia[60,62,319,323] or nutrient deprivation[66]. The *Vegfa* promoter is known to have several binding sites to multiple transcription factors[60,62,319] here the best known and the described factor is the hypoxia-inducible factor 1 (HIF1) and the primary hypoxia sensor, HIF1α[324]. However, our data show that HIF1α (primary hypoxia sensor) is not responsible for the upregulation of VEGF-A in islets lacking PTP-1B.

A study conducted by Arany et al. described a HIF1-independent regulation of VEGF-A[66]. Here, they demonstrated that cells express VEGF-A in response to ischemia and nutrient deprivation independently of HIF but by increasing PGC1α expression and coactivation of ERRα expression. This pathway can be activated in transplanted islets, since that, by restoring a proper vascular network, the graft suffered from hypoxia, ischemia or nutrient deprivation, depending on the milieu of each transplantation site[140,323,325]. Here we showed that PTP-1B^{-/-} islets presented higher levels

of *Ppargc1a* and *Esrra* mRNAs and higher amounts of their respective proteins, suggesting that this axis may be responsible for increased *Vegfa* expression. Importantly, downregulation of PTP-1B had similar effects in human islets, which is in agreement with the predicted conservation of 6 out of 11 binding sites recognized by ERRα between the mouse, rat and human *VEGFA genes*[66]. We also showed that the upregulation of PGC1α/ERRα in islets was enhanced in response to nutrient deprivation. As our work is focused on the study of islet graft revascularization, the used transplantation site is the anterior chamber of the eye. This is an ideal site, as it allows for non-invasive in vivo imaging of the graft[326], offers a reduced immune reaction[273] and constitutes a highly vascularized site[327]. As the major component of the anterior chamber of the eye, the aqueous humor (AH) serves as the graft milieu. This humor is a dynamic fluid composed not only by organic and inorganic salts but also by carbohydrates, glutathione, urea, amino acids, proteins, oxygen, carbon dioxide and water[327,328]. The AH is capable of sensing blood plasma changes, such as in glucose and oxygen[327,329]. When compared with plasma content, AQ content differs; the most significant difference is in the concentration of protein (around 200 times less, in the case of humans) and the quality of those proteins: most AH proteins are intrinsic glycoproteins[327,328]. In conclusion, it is possible to predict the occurrence of nutrient deprivation or even ischemia in islets transplanted into the anterior chamber of the eye, and therefore it is highly possible that during the early stages of the PTP-1B^{-/-}islet-grafts revascularization the signaling events leading to the upregulation of PGC1α/ERRα and VEGFA secretion were potentiated as demonstrated by this work.

PGC-1α has been identified as a tissue-specific coactivator of nuclear receptors[330,331] . The expression of PGC-1α is most well-known in tissues with high energy demands, similar to the expression pattern of ERRα[330,332]. PGC-1α mRNA levels are induced in response to signals that relay

metabolic needs, such as exposure to cold, fasting, and physical exercise[330,333]. In addition, an increase in PGC-1α levels seems sufficient to induce cellular pathways necessary for energy metabolism, including adaptive thermogenesis, mitochondrial biogenesis, and fatty acid oxidation[331,334,335]. This is accomplished by the interaction of PGC-1α with transcription factors, which recruit PGC-1α to target DNA regulatory sequences and enable the induction of relevant genes. Transcription factors that guide PGC-1α action to specific genes include nuclear receptors[336]. PGC-1α regulates ERRα function[332] and expression. PGC-1α interacts physically with ERRα, enabling it to activate transcription[332,336,337] of programs of fatty acid oxidation and oxidative phosphorylation[66,68–70]. It was also found that the first intron of the Vegfa gene contains a putative enhancer region in which several conserved Erra-binding sites are recognized by Erra and coactivated by PGC1α to elicit the robust induction of Vegfa transcription.

Curiously, PGC-1α induces the expression of VEGFA in numerous retinal cells, and PGC-1α expression is strongly induced during postnatal retinal development, coincident with VEGFA expression and angiogenesis[338]. *PGC-1α−/−* mice have a significant reduction of early retinal vascular outgrowth and reduced density of capillaries and number of main arteries and veins as adults. Moreover, *PGC-1α−/−* mice subjected to oxygen-induced retinopathy had decreased expression of VEGFA and were protected against pathological neovascularization. These results demonstrate that PGC-1α regulates VEGFA in the retina and is required for normal vessel development[338]. Islets transplanted into the anterior chamber of the eye are revascularized through angiogenesis from vessels majority from the iris, but also from the retina[339]. If PTP-1B inhibition can activate this signaling, this could be a partial explanation, for sodium tungstate effect on islet-graft revascularization. The relation between the VEGFA-induced PGC1α/ERRα signaling and PTP-1B in ß-cell, or any type of cell,

has never been described. Whether PTP-1B interact with one or both transcription factors directly, or via phosphotyrosine-mediated inhibition of an intermediary, is not known, and it is worth more profound research.

In order to establish PTP-1B as a groundbreaking and suitable target for cell transplantation, it was essential to study the conservation of these signaling events first in rats and then in human islets. Because islets are compact cellular structures that make difficult the access of molecules to its core, silencing PTP-1B was optimized using to methods, siRNA and shRNA Lentivirus infection. Both were suitable to silence PTP-1B in human or rat islets. However, shRNA LV particle represents a more effective strategy for sustaining the downregulation of a gene in islets[296–298], without affecting islet function[296–298] when compared with siRNAs. Therefore the siRNA was preferred to assessed gene and protein levels the shRNA LV was used in a physiological model, were human islets silenced for PTP-1B were transplanted in NSG mice. Our study demonstrated for the first time that targeting the downregulation of PTP-1B in human islets improves VEGF-A expression and secretion by modulating the PGC1α/ERRα axis, resulting in an improved islet-graft revascularization.

Based on all these data, we propose a model whereby VEGF-A expression is enhanced via the PGC1α/ERRα axis in transplanted PTP-1B^{-/-} islets (Figure 6). Briefly, in the presence of an external stimulus such as nutrient deprivation, the absence or downregulation of PTP-1B promotes an increase in PGC-1-α gene and protein levels through still unknown mechanisms. In turn, PGC1α increases the expression of orphan nuclear receptor ERRα, and PGC1α/ERRα dimers recognize and bind several conserved sites at the VEGF-A promoter, inducing the expression of the *VEGFA* gene. Increased *Vegfa* gene expression results in an increase in both protein and secretion levels of VEGF-A by islets. Lastly, VEGFA interacts with its receptor, VEGFR2, in endothelial cells, activating the signaling pathway of angiogenesis towards the islets.

These results support PTP-1B as a new potential key target in the improvement of islet graft revascularization by establishing a proof-of-concept that can lead to improving future results, thereby eliminating a critical stumbling block to islet transplantation and for cell replacement therapy. In fact, nowadays more islets have been transplanted to reverse hyperglycemia because a considerably high number of donor islets are lost due to the injuries from enzymatic/mechanical-mediated damage during isolation and lack of oxygen and nutrient supply during the slow reestablishment of blood supply to the transplanted islets. If this significant loss of donor islets can be avoided, then more diabetic recipients can be transplanted, and better insulin-independence rates will be achieved with the same number of currently available donors. Interventional strategies to improve islet engraftment by gene therapy could have a dramatic impact on the number of patients that might benefit from this therapy and could affect long-term graft survival[340]. Nevertheless, it is important to emphasize that to effectively reversing and cure type 1 diabetes, the studies and data from different therapeutical fields must come together and converge into a multidisciplinary approach.

Summary

✓ Sodium tungstate is a potential drug to be used to improve islet-graft revascularization in type 1 diabetes;

✓ Sodium tungstate treatment improves islet-graft revascularization without compromising graft-ß cell compartment, by a mechanism mediated by PTP-1B;

✓ Targeting PTP-1B is a potential therapy to improve islet-graft revascularization, without compromising graft's ß-cell compartment;

✓ Improved revascularization by targeting islet PTP-1B is independent of intra-islet endothelial cells;

✓ The mechanism by which PTP-1B improves islet-graft revascularization is based on the fine modulation of, graft ß-cell's, VEGFA expression and secretion by upregulating HIF1A-independent PGC1α/ERRα signaling;

✓ The conservation of these signal event in human islets unlocks a new paradigm for the improvement of islet transplantation;

Conclusions

Inhibiting Protein tyrosine phosphorylation, we found a new model to develop strategies for improving islet transplantation, like the treatment with sodium tungstate. Even though we can not discard multiples effects of sodium tungstate treatment in the recipient, we conclude that sodium tungstate improves grafts revascularization, and survival without compromising graft's ß-cell population, through a mechanism mediated by the inhibition of PTP-1B.

Additionally here we conclude that targeting PTP-1B in islets potentiates the upregulation of the ß-cell VEGF-A-induced PGC1α/ERRα signaling. This constitutes a new paradigm in the strategies to improve islet-graft revascularization as it allows islets to enhance revascularization without compromising ß-cell compartment and graft failure due to poor revascularization. These results support PTP-1B as a new potential key target in the improvement of islet graft revascularization by establishing a proof-of-concept that can lead to improving future results, thereby eliminating a critical stumbling block to islet transplantation. Nevertheless, in order to reverse type 1 diabetes, effort from all fields of expertise must come together in a multidisciplinary effort to overcome and cure this burden disease.

List of publications and most relevant communications

Peer-review publications

Hugo Figueiredo[1,2], Ana Lucia C. Figueroa[1,2], Ainhoa Garcia[1,3], Christophe Broca[4], Anne Wojtusciszyn[4,5,6], Rosa Gasa[1,3], Rita Malpique[1*], Ramon Gomis[1-3,7*]

Targeting pancreatic beta-cell PTP-1B improves islet graft revascularization and transplant outcome. (2017)

Submitted to the **Science Translational Medicine** (under second revision)

[1] Diabetes and Obesity Research Laboratory, August Pi i Sunyer Biomedical Research Institute (IDIBAPS), Rosselló 149-153, 08036 Barcelona, Spain

[2] University of Barcelona, Barcelona, Spain

[3] Centro de Investigación Biomédica en Red de Diabetes y Enfermedades Metabólicas Asociadas (CIBERDEM), Spain

[4] Laboratory of Cell Therapy for Diabetes (LTCD), Institute of Regenerative Medicine and Biotherapy, (IRMB), University Hospital of Montpellier, Saint Eloi Hospital, Montpellier, France

[5] INSERM U1191, Institute of Functional Genomics (IGF), CNRS UMR5203, Montpellier University, Montpellier, France

[6] Department of Endocrinology, Diabetes and Nutrition, University Hospital of Montpellier, Lapeyronie Hospital, Montpellier, France

[7] Department of Endocrinology and Nutrition, Hospital Clinic of Barcelona, Barcelona, Spain

Hugo Figueiredo[1,2]*, Rita Malpique[1]*, Ainhoa Garcia[1,3], Ramon Gomis[1,2,3,4].

Oral administration of sodium tungstate improves islet-graft revascularization and survival (2018).

Submitted to **American Journal of Transplantation**

[1] Diabetes and Obesity Research Laboratory, August Pi i Sunyer Biomedical Research Institute (IDIBAPS), Rosselló 149-153, 08036 Barcelona, Spain

[2] The University of Barcelona, Barcelona, Spain

[3] Centro de Investigación Biomédica en Red de Diabetes y Enfermedades Metabólicas Asociadas (CIBERDEM), Spain

[4] Department of Endocrinology and Nutrition, Hospital Clinic of Barcelona, Barcelona, Spain

Oral Communication

XXV Congreso Nacional de la Sociedad Española de Diabetes | from 3-5 April 2014 | Pamplona, Spain

Oral Presentation title: **The impact of PTP1B on the survival and revascularization of transplanted islets grafts"**

Authors (BY ORDER OF SIGNATURE): Hugo Figueiredo1,2, Ainhoa Garcia1,2, Rebeca Fernandez1,2, Hanan Farghaly1, Ramon Gomis1,2, Rita Malpique1,2

1Diabetes and Obesity - IDIBAPS - Hospital Clínic, Barcelona, Spain, 2CIBERDEM, Barcelona, Spain,

49th EASD Annual Meeting | from 23 - 27 September 2013 | Barcelona, Spain

Oral presentation Title:**"PTP1B a key player in the improvement of survival of transplanted islet grafts"**

Authors (BY ORDER OF SIGNATURE): Hugo Figueiredo1,2, Ainhoa Garcia1,2,

Rebeca Fernandez1,2, Hanan Farghaly1,3, Ramon Gomis1,2, Rita Malpique1,2

1Diabetes and Obesity - IDIBAPS - Hospital Clínic, Barcelona, Spain, 2CIBERDEM, Barcelona, Spain, 3Faculty of Medicine, Assiut, Egypt

───

Posters

51st EASD Annual Meeting | from 14 - 18 September 2015 | Stockholm, Sweden

Poster Title: "Protein tyrosine phosphatase 1B is a novel target on the improvement of islet graft's revascularisation".

Authors (BY ORDER OF SIGNATURE): **Hugo Figueiredo**, Ana Lucia Castillo Figueroa, Ainhoa Garcia, Rebeca Fernandez-Ruiz, Hanan.S.M. Farghaly, Rita Malpique, Ramon. Gomis;

49th EASD Annual Meeting | from 23 - 27 September 2013 | Barcelona, Spain

PosterTitle:"Impact of the peripancreatic adipose tissue on beta-cell adaptation to obesity: an integrated, multi-platform analysis".

Authors (BY ORDER OF SIGNATURE): Rita Malpique, **Hugo Figueiredo**, Sandra Rebuffat, Maria Vinaixa, Oscar Yanes, Xavier Correig, Sílvia Barceló-Batllori, Susana G. Kalko, Ramon Gomis;

48th EASD Annual Meeting | from 1 - 5 October 2012 | Berlin, Germany

PosterTitle:"Is PTP1B involved in the protective effect of tungstate on transplanted islets grafts?".

Authors (BY ORDER OF SIGNATURE): **H. Figueiredo**, A. Garcia, H.S.M. Farghaly, R. Fernandez, A. Novials, R. Gomis, R. Malpique

References

1.   WHO | Diabetes mellitus. *WHO* (2010). at <http://www.who.int/mediacentre/factsheets/fs138/en/>

2.   IDF diabetes atlas - Across the globe 8th Edition. at <http://www.diabetesatlas.org/across-the-globe.html>

3.   Van Belle, T. L., Coppieters, K. T. & Von Herrath, M. G. Type 1 Diabetes: Etiology, Immunology, and Therapeutic Strategies. *Physiol. Rev.* **91,** 79–118 (2011).

4.   Patterson, C. C. *et al.* Trends in childhood type 1 diabetes incidence in Europe during 1989–2008: evidence of non-uniformity over time in rates of increase. *Diabetologia* **55,** 2142–2147 (2012).

5.   Todd, J. A. Etiology of Type 1 Diabetes. *Immunity* **32,** 457–467 (2010).

6.   Naylor, R., Knight Johnson, A. & del Gaudio, D. *Maturity-Onset Diabetes of the Young Overview*. *GeneReviews*® (1993). at <http://www.ncbi.nlm.nih.gov/pubmed/29792621>

7.   Naylor, R. N., Greeley, S. A. W., Bell, G. I. & Philipson, L. H. Genetics and pathophysiology of neonatal diabetes mellitus. *J. Diabetes Investig.* **2,** 158–169 (2011).

8.   Bishay, R. H. & Greenfield, J. R. A review of maturity onset diabetes of the young (MODY) and challenges in the management of glucokinase-MODY. *Med. J. Aust.* **205,** 480–485 (2016).

9.   Skowera, A. *et al.* CTLs are targeted to kill β cells in patients with type 1 diabetes through recognition of a glucose-regulated preproinsulin epitope. *J. Clin. Invest.* **118,** 3390–402 (2008).

10.   Wang, Z., Xie, Z., Lu, Q., Chang, C. & Zhou, Z. Beyond

Genetics: What Causes Type 1 Diabetes. *Clin. Rev. Allergy Immunol.* **52,** 273–286 (2017).

11. Noble, J. A. Immunogenetics of type 1 diabetes: A comprehensive review. *J. Autoimmun.* **64,** 101–112 (2015).

12. Mathis, D., Vence, L. & Benoist, C. β-Cell death during progression to diabetes. *Nature* **414,** 792–798 (2001).

13. Klöppel, G., Löhr, M., Habich, K., Oberholzer, M. & Heitz, P. U. Islet pathology and the pathogenesis of type 1 and type 2 diabetes mellitus revisited. *Surv. Synth. Pathol. Res.* **4,** 110–25 (1985).

14. Jerram, S. T., Dang, M. N. & Leslie, R. D. The Role of Epigenetics in Type 1 Diabetes. *Curr. Diab. Rep.* **17,** 89 (2017).

15. Redondo, M. J., Steck, A. K. & Pugliese, A. Genetics of type 1 diabetes. *Pediatr. Diabetes* **19,** 346–353 (2018).

16. Risch, N. Assessing the role of HLA-linked and unlinked determinants of disease. *Am. J. Hum. Genet.* **40,** 1–14 (1987).

17. Saberzadeh-Ardestani, B. *et al.* Type 1 Diabetes Mellitus: Cellular and Molecular Pathophysiology at A Glance. *Cell J.* **20,** 294–301 (2018).

18. Katsarou, A. *et al.* Type 1 diabetes mellitus. *Nat. Rev. Dis. Prim.* **3,** 17016 (2017).

19. Viskari, H. R. *et al.* Maternal first-trimester enterovirus infection and future risk of type 1 diabetes in the exposed fetus. *Diabetes* **51,** 2568–71 (2002).

20. Orešič, M. *et al.* Cord Serum Lipidome in Prediction of Islet Autoimmunity and Type 1 Diabetes. *Diabetes* **62,** 3268–3274 (2013).

21. Eringsmark Regnéll, S. & Lernmark, Å. The environment and the origins of islet autoimmunity and Type 1 diabetes. *Diabet.*

Med. **30,** 155–160 (2013).

22. La Torre, D. *et al.* Decreased Cord-Blood Phospholipids in Young Age-at-Onset Type 1 Diabetes. *Diabetes* **62,** 3951–3956 (2013).

23. Lund-Blix, N. A. *et al.* Infant Feeding and Risk of Type 1 Diabetes in Two Large Scandinavian Birth Cohorts. *Diabetes Care* **40,** 920–927 (2017).

24. Hyöty, H. Viruses in type 1 diabetes. *Pediatr. Diabetes* **17,** 56–64 (2016).

25. Filippi, C. M. & von Herrath, M. G. Viral trigger for type 1 diabetes: pros and cons. *Diabetes* **57,** 2863–71 (2008).

26. Beyerlein, A., Donnachie, E., Jergens, S. & Ziegler, A.-G. Infections in Early Life and Development of Type 1 Diabetes. *JAMA* **315,** 1899 (2016).

27. Rewers, M. & Ludvigsson, J. Environmental risk factors for type 1 diabetes. *Lancet (London, England)* **387,** 2340–2348 (2016).

28. Pandol, S. J. *The Exocrine Pancreas*. *The Exocrine Pancreas* (Morgan & Claypool Life Sciences, 2010). doi:10.4199/C00026ED1V01Y201102ISP014

29. Ionescu-Tirgoviste, C. *et al.* A 3D map of the islet routes throughout the healthy human pancreas. *Sci. Rep.* **5,** 14634 (2015).

30. Kilimnik, G., Kim, A., Jo, J., Miller, K. & Hara, M. Quantification of pancreatic islet distribution in situ in mice. *Am. J. Physiol. Metab.* **297,** E1331–E1338 (2009).

31. Jansson, L. *et al.* Pancreatic islet blood flow and its measurement. *Ups. J. Med. Sci.* **121,** 81–95 (2016).

32. Konstantinova, I. & Lammert, E. Microvascular development : learning from pancreatic islets. *BioEssays* **26,** 1069–1075

(2004).

33. Ballian, N. & Brunicardi, F. C. Islet vasculature as a regulator of endocrine pancreas function. *World J. Surg.* **31,** 705–14 (2007).

34. Cabrera, O. *et al.* The unique cytoarchitecture of human pancreatic islets has implications for islet cell function. *Proc. Natl. Acad. Sci. U. S. A.* **103,** 2334–9 (2006).

35. Roscioni, S. S., Migliorini, A., Gegg, M. & Lickert, H. Impact of islet architecture on β-cell heterogeneity, plasticity and function. *Nat. Rev. Endocrinol.* **12,** 695–709 (2016).

36. Kim, A. *et al.* Islet architecture: A comparative study. *Islets* **1,** 129–36 (2009).

37. Weir, G. C. & Bonner-Weir, S. Islets of Langerhans: the puzzle of intraislet interactions and their relevance to diabetes. *J. Clin. Invest.* **85,** 983–7 (1990).

38. Abdulreda, M. H., Caicedo, A. & Berggren, P.-O. A NATURAL BODY WINDOW TO STUDY HUMAN PANCREATIC ISLET CELL FUNCTION AND SURVIVAL. *CellR4-- repair, Replace. Regen. reprogramming* **1,** 111–122 (2013).

39. Hogan, M. F. & Hull, R. L. The islet endothelial cell: a novel contributor to beta cell secretory dysfunction in diabetes. *Diabetologia* **60,** 952–959 (2017).

40. Lammert, E., Cleaver, O. & Melton, D. Induction of Pancreatic Differentiation by Signals from Blood Vessels. *Science (80-.).* **294,** 564–567 (2001).

41. El-Gohary, Y. *et al.* Three-Dimensional Analysis of the Islet Vasculature. *Anat. Rec. Adv. Integr. Anat. Evol. Biol.* **295,** 1473–1481 (2012).

42. Nyman, L. R. *et al.* Real-time, multidimensional in vivo imaging used to investigate blood flow in mouse pancreatic islets. *J. Clin. Invest.* **118,** 3790–7 (2008).

43. In't Veld, P. & Marichal, M. in *Advances in experimental medicine and biology* **654,** 1–19 (2010).

44. Kamba, T. *et al.* VEGF-dependent plasticity of fenestrated capillaries in the normal adult microvasculature. *Am. J. Physiol. Circ. Physiol.* **290,** H560–H576 (2006).

45. Källskog, Ö. *et al.* Lymphatic Vessels in Pancreatic Islets Implanted Under the Renal Capsule of Rats. *Am. J. Transplant.* **6,** 680–686 (2006).

46. Cao, Z. & Wang, X. The endocrine role between β cells and intra-islet endothelial cells. *Endocr. J.* **61,** 647–54 (2014).

47. Henderson, J. R. & Moss, M. C. A morphometric study of the endocrine and exocrine capillaries of the pancreas. *Q. J. Exp. Physiol.* **70,** 347–56 (1985).

48. Lifson, N., Lassa, C. V. & Dixit, P. K. Relation between blood flow and morphology in islet organ of rat pancreas. *Am. J. Physiol. Metab.* **249,** E43–E48 (1985).

49. Brissova, M. *et al.* Pancreatic Islet Production of Vascular Endothelial Growth Factor-A Is Essential for Islet Vascularization, Revascularization, and Function. *Diabetes* **55,** 2974–2985 (2006).

50. Yancopoulos, G. D. *et al.* Vascular-specific growth factors and blood vessel formation. *Nature* **407,** 242–8 (2000).

51. Vasir, B. *et al.* Gene expression of VEGF and its receptors Flk-1/KDR and Flt-1 in cultured and transplanted rat islets. *Transplantation* **71,** 924–35 (2001).

52. Inoue, M., Hager, J. H., Ferrara, N., Gerber, H.-P. & Hanahan, D. VEGF-A has a critical, nonredundant role in angiogenic switching and pancreatic beta cell carcinogenesis. *Cancer Cell* **1,** 193–202 (2002).

53. Lammert, E. *et al.* Role of VEGF-A in vascularization of pancreatic islets. *Curr. Biol.* **13,** 1070–4 (2003).

54. Iwashita, N. *et al.* Impaired insulin secretion in vivo but enhanced insulin secretion from isolated islets in pancreatic beta cell-specific vascular endothelial growth factor-A knockout mice. *Diabetologia* **50,** 380–9 (2007).

55. Zhang, N. *et al.* Elevated vascular endothelial growth factor production in islets improves islet graft vascularization. *Diabetes* **53,** 963–70 (2004).

56. Büchler, P. *et al.* Hypoxia-inducible factor 1 regulates vascular endothelial growth factor expression in human pancreatic cancer. *Pancreas* **26,** 56–64 (2003).

57. Gorden, D. L., Mandriota, S. J., Montesano, R., Orci, L. & Pepper, M. S. Vascular endothelial growth factor is increased in devascularized rat islets of Langerhans in vitro. *Transplantation* **63,** 436–43 (1997).

58. Berra, E. *et al.* HIF prolyl-hydroxylase 2 is the key oxygen sensor setting low steady-state levels of HIF-1 in normoxia. *EMBO J.* **22,** 4082–4090 (2003).

59. Forsythe, J. A. *et al.* Activation of vascular endothelial growth factor gene transcription by hypoxia-inducible factor 1. *Mol. Cell. Biol.* **16,** 4604–13 (1996).

60. Mueller, M. D. *et al.* Regulation of vascular endothelial growth factor (VEGF) gene transcription by estrogen receptors alpha and beta. *Proc. Natl. Acad. Sci. U. S. A.* **97,** 10972–7 (2000).

61. Osera, C. *et al.* Induction of *VEGFA* mRNA translation by CoCl$_2$ mediated by HuR. *RNA Biol.* **12,** 1121–1130 (2015).

62. Pagès, G. & Pouysségur, J. Transcriptional regulation of the Vascular Endothelial Growth Factor gene--a concert of activating factors. *Cardiovasc. Res.* **65,** 564–73 (2005).

63. Semenza, G. Signal transduction to hypoxia-inducible factor 1. *Biochem. Pharmacol.* **64,** 993–8 (2002).

64. Perry, M.-C., Dufour, C. R., Tam, I. S., B'chir, W. & Giguère, V.

Estrogen-Related Receptor-α Coordinates Transcriptional Programs Essential for Exercise Tolerance and Muscle Fitness. *Mol. Endocrinol.* **28,** 2060–2071 (2014).

65. Stein, R. A., Gaillard, S. & McDonnell, D. P. Estrogen-related receptor alpha induces the expression of vascular endothelial growth factor in breast cancer cells. *J. Steroid Biochem. Mol. Biol.* **114,** 106–12 (2009).

66. Arany, Z. *et al.* HIF-independent regulation of VEGF and angiogenesis by the transcriptional coactivator PGC-1alpha. *Nature* **451,** 1008–12 (2008).

67. Willy, P. J. *et al.* Regulation of PPARgamma coactivator 1alpha (PGC-1alpha) signaling by an estrogen-related receptor alpha (ERRalpha) ligand. *Proc. Natl. Acad. Sci. U. S. A.* **101,** 8912–7 (2004).

68. Huss, J. M., Torra, I. P., Staels, B., Giguère, V. & Kelly, D. P. Estrogen-related receptor alpha directs peroxisome proliferator-activated receptor alpha signaling in the transcriptional control of energy metabolism in cardiac and skeletal muscle. *Mol. Cell. Biol.* **24,** 9079–91 (2004).

69. Kressler, D., Schreiber, S. N., Knutti, D. & Kralli, A. The PGC-1-related Protein PERC Is a Selective Coactivator of Estrogen Receptor α. *J. Biol. Chem.* **277,** 13918–13925 (2002).

70. Schreiber, S. N., Knutti, D., Brogli, K., Uhlmann, T. & Kralli, A. The Transcriptional Coactivator PGC-1 Regulates the Expression and Activity of the Orphan Nuclear Receptor Estrogen-Related Receptor α (ERRα). *J. Biol. Chem.* **278,** 9013–9018 (2003).

71. Cines, D. B. *et al.* Endothelial cells in physiology and in the pathophysiology of vascular disorders. *Blood* **91,** 3527–61 (1998).

72. Narayanan, S. *et al.* Intra-islet endothelial cell and β-cell crosstalk: Implication for islet cell transplantation. *World J.*

Transplant. **7,** 117–128 (2017).

73. Johansson, Å. *et al.* Endothelial cell signalling supports pancreatic beta cell function in the rat. *Diabetologia* **52,** 2385–2394 (2009).

74. Eichmann, A. & Simons, M. VEGF signaling inside vascular endothelial cells and beyond. *Curr. Opin. Cell Biol.* **24,** 188–193 (2012).

75. Hoeben, A. *et al.* Vascular endothelial growth factor and angiogenesis. *Pharmacol. Rev.* **56,** 549–80 (2004).

76. Kostromina, E., Wang, X. & Han, W. Altered Islet Morphology but Normal Islet Secretory Function In Vitro in a Mouse Model with Microvascular Alterations in the Pancreas. *PLoS One* **8,** e71277 (2013).

77. Nikolova, G. *et al.* The Vascular Basement Membrane: A Niche for Insulin Gene Expression and β Cell Proliferation. *Dev. Cell* **10,** 397–405 (2006).

78. Copenhaver, M. & Hoffman, R. P. Type 1 diabetes: where are we in 2017? *Transl. Pediatr.* **6,** 359–364 (2017).

79. Atkinson, M. A., Eisenbarth, G. S. & Michels, A. W. Type 1 diabetes. *Lancet (London, England)* **383,** 69–82 (2014).

80. Nathan, D. M. *et al.* Intensive Diabetes Treatment and Cardiovascular Disease in Patients with Type 1 Diabetes. *N. Engl. J. Med.* **353,** 2643–2653 (2005).

81. Fiorina, P., Shapiro, A. M. J., Ricordi, C. & Secchi, A. The Clinical Impact of Islet Transplantation. *Am. J. Transplant.* **8,** 1990–1997 (2008).

82. Maffi, P. *et al.* Risks and Benefits of Transplantation in the Cure of Type 1 Diabetes: Whole Pancreas Versus Islet Transplantation. A Single Center Study. *Rev. Diabet. Stud.* **8,** 44–50 (2011).

83. Duke, D. C. *et al.* Distal technologies and type 1 diabetes management. *Lancet Diabetes Endocrinol.* **6,** 143–156 (2018).

84. Agarwal, A. & Brayman, K. Update on Islet Cell Transplantation for Type 1 Diabetes. *Semin. Intervent. Radiol.* **29,** 090–098 (2012).

85. Hering, B. J. *et al.* Phase 3 Trial of Transplantation of Human Islets in Type 1 Diabetes Complicated by Severe Hypoglycemia. *Diabetes Care* **39,** 1230–1240 (2016).

86. Shapiro, A. M. M. J. *et al.* Islet transplantation in seven patients with type 1 diabetes mellitus using a glucocorticoid-free immunosuppressive regimen. *N. Engl. J. Med.* **343,** 230–8 (2000).

87. Scharp, D. W. *et al.* Insulin independence after islet transplantation into type I diabetic patient. *Diabetes* **39,** 515–8 (1990).

88. Shapiro, A. M. J. *et al.* International Trial of the Edmonton Protocol for Islet Transplantation. *N. Engl. J. Med.* **355,** 1318–1330 (2006).

89. Ryan, E. A. *et al.* Five-year follow-up after clinical islet transplantation. *Diabetes* **54,** 2060–9 (2005).

90. Fiorina, P. *et al.* Long-term beneficial effect of islet transplantation on diabetic macro-/microangiopathy in type 1 diabetic kidney-transplanted patients. *Diabetes Care* **26,** 1129–36 (2003).

91. Shapiro, A. M. J. Strategies toward single-donor islets of Langerhans transplantation. *Curr. Opin. Organ Transplant.* **16,** 627–631 (2011).

92. Posselt, A. M. *et al.* Islet Transplantation in Type 1 Diabetics Using an Immunosuppressive Protocol Based on the Anti-LFA-1 Antibody Efalizumab. *Am. J. Transplant.* **10,** 1870–1880 (2010).

93. Matsumoto, S. Clinical allogeneic and autologous islet cell transplantation: update. *Diabetes Metab. J.* **35,** 199–206 (2011).

94. Campbell, P. M. *et al.* High Risk of Sensitization After Failed Islet Transplantation. *Am. J. Transplant.* **7,** 2311–2317 (2007).

95. Olack, B. J. *et al.* Sensitization to HLA antigens in islet recipients with failing transplants. *Transplant. Proc.* **29,** 2268–9 (1997).

96. Dahlbäck, B. Blood coagulation. *Lancet* **355,** 1627–1632 (2000).

97. Moberg, L. *et al.* Production of tissue factor by pancreatic islet cells as a trigger of detrimental thrombotic reactions in clinical islet transplantation. *Lancet (London, England)* **360,** 2039–45

98. Mandrup-Poulsen, T., Bendtzen, K., Nielsen, J. H., Bendixen, G. & Nerup, J. Cytokines cause functional and structural damage to isolated islets of Langerhans. *Allergy* **40,** 424–9 (1985).

99. Kaufman, D. B. *et al.* Effect of 15-deoxyspergualin on immediate function and long-term survival of transplanted islets in murine recipients of a marginal islet mass. *Diabetes* **43,** 778–83 (1994).

100. Nagata, M., Mullen, Y., Matsuo, S., Herrera, M. & Clare-Salzler, M. Destruction of islet isografts by severe nonspecific inflammation. *Transplant. Proc.* **22,** 855–6 (1990).

101. Versteeg, H. H., Peppelenbosch, M. P. & Spek, C. A. The pleiotropic effects of tissue factor: a possible role for factor VIIa-induced intracellular signalling? *Thromb. Haemost.* **86,** 1353–9 (2001).

102. Harlan, D. M., Kenyon, N. S., Korsgren, O., Roep, B. O. & Immunology of Diabetes Society. Current Advances and Travails in Islet Transplantation. *Diabetes* **58,** 2175–2184

(2009).

103. Shapiro, A. M. J. State of the Art of Clinical Islet Transplantation and Novel Protocols of Immunosuppression. *Curr. Diab. Rep.* **11,** 345–354 (2011).

104. Pickup, J. C., Zhi, Z.-L., Khan, F., Saxl, T. & Birch, D. J. S. Nanomedicine and its potential in diabetes research and practice. *Diabetes. Metab. Res. Rev.* **24,** 604–610 (2008).

105. Rao, P. V. & Gan, S. H. Recent Advances in Nanotechnology-Based Diagnosis and Treatments of Diabetes. *Curr. Drug Metab.* **16,** 371–5 (2015).

106. Desai, T. & Shea, L. D. Advances in islet encapsulation technologies. *Nat. Rev. Drug Discov.* **16,** 338–350 (2016).

107. Marek, N. *et al.* Coating Human Pancreatic Islets With CD4+CD25highCD127− Regulatory T Cells as a Novel Approach for the Local Immunoprotection. *Ann. Surg.* **254,** 512–519 (2011).

108. Duprez, I. R., Johansson, U., Nilsson, B., Korsgren, O. & Magnusson, P. U. Preparatory studies of composite mesenchymal stem cell islets for application in intraportal islet transplantation. *Ups. J. Med. Sci.* **116,** 8–17 (2011).

109. He, S. *et al.* MSCs promote the development and improve the function of neonatal porcine islet grafts. *FASEB J.* **32,** 3242–3253 (2018).

110. Arzouni, A. A., Vargas-Seymour, A., Nardi, N., J. F. King, A. & Jones, P. M. Using Mesenchymal Stromal Cells in Islet Transplantation. *Stem Cells Transl. Med.* (2018). doi:10.1002/sctm.18-0033

111. Hematti, P., Kim, J., Stein, A. P. & Kaufman, D. Potential role of mesenchymal stromal cells in pancreatic islet transplantation. *Transplant. Rev.* **27,** 21–29 (2013).

112. Soria, B. *et al.* Insulin-secreting cells derived from embryonic

stem cells normalize glycemia in streptozotocin-induced diabetic mice. *Diabetes* **49,** 157–62 (2000).

113. Soria, B., Montanya, E., Martín, F. & Hmadcha, A. A Role for the Host in the Roadmap to Diabetes Stem Cell Therapy. *Diabetes* **65,** 1155–1157 (2016).

114. Vanikar, A. V., Trivedi, H. L. & Thakkar, U. G. Stem cell therapy emerging as the key player in treating type 1 diabetes mellitus. *Cytotherapy* **18,** 1077–1086 (2016).

115. Pepper, A. R., Bruni, A. & Shapiro, A. M. J. Clinical islet transplantation. *Curr. Opin. Organ Transplant.* 1 (2018). doi:10.1097/MOT.0000000000000546

116. Aguayo-Mazzucato, C. & Bonner-Weir, S. Stem cell therapy for type 1 diabetes mellitus. *Nat. Rev. Endocrinol.* **6,** 139–148 (2010).

117. Stojanovic, I. *et al.* Cell-based Tolerogenic Therapy, Experience from Animal Models of Multiple Sclerosis, Type 1 Diabetes and Rheumatoid Arthritis. *Curr. Pharm. Des.* **23,** 2623–2643 (2017).

118. Rodriguez-Fernandez, S. *et al.* Phosphatidylserine-Liposomes Promote Tolerogenic Features on Dendritic Cells in Human Type 1 Diabetes by Apoptotic Mimicry. *Front. Immunol.* **9,** 253 (2018).

119. Serra, P. & Santamaria, P. Nanoparticle-based approaches to immune tolerance for the treatment of autoimmune diseases. *Eur. J. Immunol.* **48,** 751–756 (2018).

120. Clemente-Casares, X. *et al.* Expanding antigen-specific regulatory networks to treat autoimmunity. *Nature* **530,** 434–440 (2016).

121. Cobo-Vuilleumier, N. *et al.* LRH-1 agonism favours an immune-islet dialogue which protects against diabetes mellitus. *Nat. Commun.* **9,** 1488 (2018).

122. Jansson, L. & Carlsson, P.-O. P.-O. Graft vascular function after transplantation of pancreatic islets. *Diabetologia* **45,** 749–763 (2002).

123. Davalli, A. M. *et al.* Vulnerability of Islets in the Immediate Posttransplantation Period: Dynamic Changes in Structure and Function. *Diabetes* **45,** 1161–7 (1996).

124. Biarnés, M. *et al.* β-Cell Death and Mass in Syngeneically Transplanted Islets Exposed to Short- and Long-Term Hyperglycemia. *Diabetes* **51,** 66–72 (2002).

125. Miao, G. *et al.* Dynamic Production of Hypoxia-Inducible Factor-1α in Early Transplanted Islets. *Am. J. Transplant.* **6,** 2636–2643 (2006).

126. Andersson, A. *et al.* Promoting islet cell function after transplantation. *Cell Biochem. Biophys.* **40,** 55–64 (2004).

127. Lau, J. *et al.* Implantation site-dependent dysfunction of transplanted pancreatic islets. *Diabetes* **56,** 1544–50 (2007).

128. Carlsson, P.-O. Influence of microenvironment on engraftment of transplanted β-cells. *Ups. J. Med. Sci.* **116,** 1–7 (2011).

129. Menger, M. D., Yamauchi, J. & Vollmar, B. Revascularization and microcirculation of freely grafted islets of Langerhans. *World J. Surg.* **25,** 509–15 (2001).

130. Vajkoczy, P., Menger, M. D., Simpson, E. & Messmer, K. Angiogenesis and vascularization of murine pancreatic islet isografts. *Transplantation* **60,** 123–7 (1995).

131. Carlsson, P.-O. O., Palm, F., Andersson, A. & Liss, P. Markedly decreased oxygen tension in transplanted rat pancreatic islets irrespective of the implantation site. *Diabetes* **50,** 489–95 (2001).

132. Carmeliet, P. Angiogenesis in health and disease. *Nat. Med.* **9,** 653–660 (2003).

133. Menger, M. D. *et al.* Angiogenesis and hemodynamics of microvasculature of transplanted islets of Langerhans. *Diabetes* **38 Suppl 1,** 199–201 (1989).

134. Bruni, A., Gala-Lopez, B., Pepper, A. R., Abualhassan, N. S. & Shapiro, A. J. Islet cell transplantation for the treatment of type 1 diabetes: recent advances and future challenges. *Diabetes. Metab. Syndr. Obes.* **7,** 211–23 (2014).

135. Mattsson, G., Jansson, L. & Carlsson, P.-O. Decreased vascular density in mouse pancreatic islets after transplantation. *Diabetes* **51,** 1362–6 (2002).

136. Carlsson, P.-O., Palm, F. & Mattsson, G. Low revascularization of experimentally transplanted human pancreatic islets. *J. Clin. Endocrinol. Metab.* **87,** 5418–23 (2002).

137. Brissova, M. & Powers, A. C. Revascularization of transplanted islets: can it be improved? *Diabetes* **57,** 2269–71 (2008).

138. Olsson, R. & Carlsson, P.-O. Better vascular engraftment and function in pancreatic islets transplanted without prior culture. *Diabetologia* **48,** 469–76 (2005).

139. Lau, J. *et al.* Beneficial role of pancreatic microenvironment for angiogenesis in transplanted pancreatic islets. *Cell Transplant.* **18,** 23–30 (2009).

140. Pepper, A. R. *et al.* Revascularization of transplanted pancreatic islets and role of the transplantation site. *Clin. Dev. Immunol.* **2013,** 352315 (2013).

141. Mattsson, G., Carlsson, P.-O., Olausson, K. & Jansson, L. Histological markers for endothelial cells in endogenous and transplanted rodent pancreatic islets. *Pancreatology* **2,** 155–162 (2002).

142. Lau, J. & Carlsson, P.-O. Low Revascularization of Human

Islets When Experimentally Transplanted Into the Liver. *Transplantation* **87,** 322–325 (2009).

143. Johansson, Å., Olerud, J., Johansson, M. & Carlsson, P. O. Angiostatic factors normally restrict islet endothelial cell proliferation and migration: Implications for islet transplantation. *Transpl. Int.* (2009). doi:10.1111/j.1432-2277.2009.00939.x

144. Cai, Q. *et al.* Enhanced expression of VEGF-A in β cells increases endothelial cell number but impairs islet morphogenesis and β cell proliferation. *Dev. Biol.* **367,** 40–54 (2012).

145. Brissova, M. *et al.* Islet microenvironment, modulated by vascular endothelial growth factor-A signaling, promotes β cell regeneration. *Cell Metab.* **19,** 498–511 (2014).

146. Agudo, J. *et al.* Vascular endothelial growth factor-mediated islet hypervascularization and inflammation contribute to progressive reduction of β-cell mass. *Diabetes* **61,** 2851–61 (2012).

147. Gebe, J. A., Preisinger, A., Gooden, M. D., D'Amico, L. A. & Vernon, R. B. Local, Controlled Release In Vivo of Vascular Endothelial Growth Factor Within a Subcutaneous Scaffolded Islet Implant Reduces Early Islet Necrosis and Improves Performance of the Graft. *Cell Transplant.* **27,** 531–541 (2018).

148. Staels, W. *et al.* Vegf-A mRNA transfection as a novel approach to improve mouse and human islet graft revascularisation. *Diabetologia* (2018). doi:10.1007/s00125-018-4646-7

149. Shimoda, M., Chen, S., Noguchi, H., Matsumoto, S. & Grayburn, P. A. In vivo non-viral gene delivery of human vascular endothelial growth factor improves revascularisation and restoration of euglycaemia after human islet transplantation into mouse liver. *Diabetologia* **53,** 1669–1679

(2010).

150. Lai, Y. *et al.* Vascular endothelial growth factor increases functional beta-cell mass by improvement of angiogenesis of isolated human and murine pancreatic islets. *Transplantation* **79,** 1530–6 (2005).

151. Narang, A. S. *et al.* Vascular Endothelial Growth Factor Gene Delivery for Revascularization in Transplanted Human Islets. *Pharm. Res.* **21,** 15–25 (2004).

152. Cheng, K. *et al.* Adenovirus-based vascular endothelial growth factor gene delivery to human pancreatic islets. *Gene Ther.* **11,** 1105–1116 (2004).

153. Lassner, E. & Schubert, W.-D. in *Tungsten* 255–282 (Springer US, 1999). doi:10.1007/978-1-4615-4907-9_6

154. Lassner, E., Newsletter, W. S.-I. & 2005, undefined. The History of Tungsten. *htp.www.itia.info* at <https://htp.www.itia.info/assets/files/newsletters/Newsletter_2 005_12.pdf>

155. Li, K. & Wang, C. *Tungsten*. (1955). at <http://krishikosh.egranth.ac.in/bitstream/1/11474/1/48194.pdf >

156. Goya, P., Martín, N. & Román, P. W for tungsten and wolfram. *Nat. Chem.* **3,** 336–336 (2011).

157. Domingo, J. L. Vanadium and Tungsten Derivatives as Antidiabetic Agents. *Biol. Trace Elem. Res.* **88,** 097–112 (2002).

158. Egloff, M.-P., Cohen, P. T. W., Reinemer, P. & Barford, D. Crystal Structure of the Catalytic Subunit of Human Protein Phosphatase 1 and its Complex with Tungstate. *J. Mol. Biol.* **254,** 942–959 (1995).

159. McCain, W. C. *et al.* Subchronic Oral Toxicity of Sodium Tungstate in Sprague-Dawley Rats. *Int. J. Toxicol.* **34,** 336–

345 (2015).

160. Le Lamer, S., Cros, G., Piñol, C., Fernández-Alvarez, J. & Bressolle, F. An application of population kinetics analysis to estimate pharmacokinetic parameters of sodium tungstate after multiple-dose during preclinical studies in rats. *Pharmacol. Toxicol.* **90,** 100–5 (2002).

161. Barberà, A. *et al.* Tungstate is an effective antidiabetic agent in streptozotocin-induced diabetic rats: a long-term study. *Diabetologia* **44,** 507–513 (2001).

162. Nagareddy, P. R., Vasudevan, H. & McNeill, J. H. Oral administration of sodium tungstate improves cardiac performance in streptozotocin-induced diabetic rats. *Can. J. Physiol. Pharmacol.* **83,** 405–411 (2005).

163. Muñoz, M. C. *et al.* Effects of tungstate, a new potential oral antidiabetic agent, in Zucker diabetic fatty rats. *Diabetes* **50,** 131–8 (2001).

164. Nocito, L., Zafra, D., Calbó, J., Domínguez, J. & Guinovart, J. J. Tungstate Reduces the Expression of Gluconeogenic Enzymes in STZ Rats. *PLoS One* **7,** e42305 (2012).

165. Domínguez, J. E. *et al.* The Antidiabetic Agent Sodium Tungstate Activates Glycogen Synthesis through an Insulin Receptor-independent Pathway. *J. Biol. Chem.* **278,** 42785–42794 (2003).

166. Le Lamer-Déchamps, S., Poucheret, P., Cros, G. & Bressolle, F. Influence of food and diabetes on pharmacokinetics of sodium tungstate in rat. *Int. J. Pharm.* **248,** 131–9 (2002).

167. Le Lamer, S. *et al.* Pharmacokinetics of sodium tungstate in rat and dog: a population approach. *J. Pharmacol. Exp. Ther.* **294,** 714–21 (2000).

168. in *The MAK-Collection for Occupational Health and Safety* 246–263 (Wiley-VCH Verlag GmbH & Co. KGaA, 2012).

doi:10.1002/3527600418.mb744033e0023

169. Leggett, R. W. A model of the distribution and retention of tungsten in the human body. *Sci. Total Environ.* **206,** 147–165 (1997).

170. Bertinat, R., Nualart, F., Li, X., Yáñez, A. J. & Gomis, R. Preclinical and Clinical Studies for Sodium Tungstate: Application in Humans. *J. Clin. Cell. Immunol.* **6,** (2015).

171. Barberà, A., Rodríguez-Gil, J. E. & Guinovart, J. J. Insulin-like actions of tungstate in diabetic rats. Normalization of hepatic glucose metabolism. *J. Biol. Chem.* **269,** 20047–53 (1994).

172. Fernández-Alvarez, J. *et al.* Stable and functional regeneration of pancreatic beta-cell population in nSTZ-rats treated with tungstate. *Diabetologia* **47,** 470–477 (2004).

173. Palanivel, R. & Sakthisekaran, D. Immunomodulatory effect of tungstate on streptozotocin-induced experimental diabetes in rats. *Ann. N. Y. Acad. Sci.* **958,** 382–6 (2002).

174. Amigó-Correig, M. *et al.* Anti-Obesity Sodium Tungstate Treatment Triggers Axonal and Glial Plasticity in Hypothalamic Feeding Centers. *PLoS One* **7,** e39087 (2012).

175. Claret, M. *et al.* Tungstate Decreases Weight Gain and Adiposity in Obese Rats through Increased Thermogenesis and Lipid Oxidation. *Endocrinology* **146,** 4362–4369 (2005).

176. Altirriba, J. *et al.* Molecular mechanisms of tungstate-induced pancreatic plasticity: a transcriptomics approach. *BMC Genomics* **10,** 406 (2009).

177. Rodríguez-Gallardo, J., Silvestre, R. A., Egido, E. M. & Marco, J. Effects of sodium tungstate on insulin and glucagon secretion in the perfused rat pancreas. *Eur. J. Pharmacol.* **402,** 199–204 (2000).

178. Oliveira, J. M. *et al.* Tungstate promotes β-cell survival in *Irs2* $^{-/-}$ mice. *Am. J. Physiol. Metab.* **306,** E36–E47 (2014).

179. Tonks, N. K. Protein tyrosine phosphatases: from genes, to function, to disease. *Nat. Rev. Mol. Cell Biol.* **7,** 833–46 (2006).

180. Bellomo, E., Birla Singh, K., Massarotti, A., Hogstrand, C. & Maret, W. The metal face of protein tyrosine phosphatase 1B. *Coord. Chem. Rev.* **327–328,** 70–83 (2016).

181. Zhang, Y.-L. & Zhang, Z.-Y. Low-Affinity Binding Determined by Titration Calorimetry Using a High-Affinity Coupling Ligand: A Thermodynamic Study of Ligand Binding to Protein Tyrosine Phosphatase 1B. *Anal. Biochem.* **261,** 139–148 (1998).

182. Torres, T. P. *et al.* Defective Glycogenesis Contributes Toward the Inability to Suppress Hepatic Glucose Production in Response to Hyperglycemia and Hyperinsulinemia in Zucker Diabetic Fatty Rats. *Diabetes* **60,** 2225–2233 (2011).

183. Zafra, D., Nocito, L., Domínguez, J. & Guinovart, J. J. Sodium tungstate activates glycogen synthesis through a non-canonical mechanism involving G-proteins. *FEBS Lett.* **587,** 291–296 (2013).

184. Mariappan, M. M., Shetty, M., Sataranatarajan, K., Choudhury, G. G. & Kasinath, B. S. Glycogen Synthase Kinase 3β Is a Novel Regulator of High Glucose- and High Insulin-induced Extracellular Matrix Protein Synthesis in Renal Proximal Tubular Epithelial Cells. *J. Biol. Chem.* **283,** 30566–30575 (2008).

185. Hauge, C. & Frödin, M. RSK and MSK in MAP kinase signalling. *J. Cell Sci.* **119,** 3021–3023 (2006).

186. Rodriguez-Hernandez, C. J., Guinovart, J. J. & Murguia, J. R. Anti-diabetic and anti-obesity agent sodium tungstate enhances GCN pathway activation through Glc7p inhibition. *FEBS Lett.* **586,** 270–276 (2012).

187. Puigserver, P. *et al.* Insulin-regulated hepatic gluconeogenesis through FOXO1–PGC-1α interaction. *Nature* **423,** 550–555

(2003).

188. Gurney, A. L., Park, E. A., Giralt, M., Liu, J. & Hanson, R. W. Opposing actions of Fos and Jun on transcription of the phosphoenolpyruvate carboxykinase (GTP) gene. Dominant negative regulation by Fos. *J. Biol. Chem.* **267,** 18133–9 (1992).

189. Yáñez, A. J. *et al.* Subcellular localization of liver FBPase is modulated by metabolic conditions. *FEBS Lett.* **577,** 154–158 (2004).

190. Bertinat, R. *et al.* Nuclear accumulation of fructose 1,6-bisphosphatase is impaired in diabetic rat liver. *J. Cell. Biochem.* **113,** 848–856 (2012).

191. Foster, J. D., Young, S. E., Brandt, T. D. & Nordlie, R. C. Tungstate: A Potent Inhibitor of Multifunctional Glucose-6-Phosphatase. *Arch. Biochem. Biophys.* **354,** 125–132 (1998).

192. Yoon, J. C. *et al.* Control of hepatic gluconeogenesis through the transcriptional coactivator PGC-1. *Nature* **413,** 131–138 (2001).

193. DeFronzo, R. A. & Tripathy, D. Skeletal Muscle Insulin Resistance Is the Primary Defect in Type 2 Diabetes. *Diabetes Care* **32,** S157–S163 (2009).

194. Yánez, A. J. *et al.* Broad expression of fructose-1,6-bisphosphatase and phosphoenolpyruvate carboxykinase provide evidence for gluconeogenesis in human tissues other than liver and kidney. *J. Cell. Physiol.* **197,** 189–197 (2003).

195. Oliveira, J. M. *et al.* Tungstate promotes β-cell survival in Irs2-/- mice. *Am. J. Physiol. Endocrinol. Metab.* **306,** E36-47 (2014).

196. Girón, M. D. *et al.* Modulation of glucose transporters in rat diaphragm by sodium tungstate. *FEBS Lett.* **542,** 84–8 (2003).

197. Stöckli, J., Fazakerley, D. J. & James, D. E. GLUT4

exocytosis. *J. Cell Sci.* **124,** 4147–4159 (2011).

198. Altirriba, J. *et al.* Molecular mechanisms of tungstate-induced pancreatic plasticity: a transcriptomics approach. *BMC Genomics* **10,** 406 (2009).

199. Barberà, A., Fernàndez-Alvarez, J., Truc, A., Gomis, R. & Guinovart, J. J. Effects of tungstate in neonatally streptozotocin-induced diabetic rats: mechanism leading to normalization of glycaemia. *Diabetologia* **40,** 143–9 (1997).

200. Yuan, H., Liu, H., Tian, R., Li, J. & Zhao, Z. Regulation of mesenchymal stem cell differentiation and insulin secretion by differential expression of Pdx-1. *Mol. Biol. Rep.* **39,** 7777–7783 (2012).

201. Carmona, M. C. *et al.* Dual effects of sodium tungstate on adipocyte biology: inhibition of adipogenesis and stimulation of cellular oxygen consumption. *Int. J. Obes.* **33,** 534–540 (2009).

202. Yang, Y., Mo, Z., Chen, K., He, H. & Xiong, J. [Effect of sodium tungstate on glucose metabolism in adipocytes]. *Zhong Nan Da Xue Xue Bao. Yi Xue Ban* **33,** 727–30 (2008).

203. Barceló-Batllori, S. *et al.* Integration of DIGE and Bioinformatics Analyses Reveals a Role of the Antiobesity Agent Tungstate in Redox and Energy Homeostasis Pathways in Brown Adipose Tissue. *Mol. Cell. Proteomics* **7,** 378–393 (2008).

204. Canals, I. *et al.* A Functional Leptin System Is Essential for Sodium Tungstate Antiobesity Action. *Endocrinology* **150,** 642–650 (2009).

205. Barceló-Batllori, S. *et al.* Target identification of the novel antiobesity agent tungstate in adipose tissue from obese rats. *Proteomics* **5,** 4927–4935 (2005).

206. Marty, N., Dallaporta, M. & Thorens, B. Brain Glucose Sensing, Counterregulation, and Energy Homeostasis.

Physiology **22,** 241–251 (2007).

207. Amigó-Correig, M. *et al.* Sodium tungstate regulates food intake and body weight through activation of the hypothalamic leptin pathway. *Diabetes, Obes. Metab.* **13,** 235–242 (2011).

208. Tonks, N. K. Protein tyrosine phosphatases: from genes, to function, to disease. *Nat. Rev. Mol. Cell Biol.* **7,** 833–846 (2006).

209. Bellomo, E., Birla Singh, K., Massarotti, A., Hogstrand, C. & Maret, W. The metal face of protein tyrosine phosphatase 1B. *Coord. Chem. Rev.* **327–328,** 70–83 (2016).

210. Alonso, A. *et al.* Protein Tyrosine Phosphatases in the Human Genome. *Cell* **117,** 699–711 (2004).

211. Frangioni, J. V., Beahm, P. H., Shifrin, V., Jost, C. A. & Neel, B. G. The nontransmembrane tyrosine phosphatase PTP-1B localizes to the endoplasmic reticulum via its 35 amino acid C-terminal sequence. *Cell* **68,** 545–560 (1992).

212. Barford, D., Das, A. K. & Egloff, M.-P. THE STRUCTURE AND MECHANISM OF PROTEIN PHOSPHATASES: Insights into Catalysis and Regulation. *Annu. Rev. Biophys. Biomol. Struct.* **27,** 133–164 (1998).

213. Özcan, A., Olmez, E. O. & Alakent, B. Effects of protonation state of Asp181 and position of active site water molecules on the conformation of PTP1B. *Proteins Struct. Funct. Bioinforma.* **81,** 788–804 (2013).

214. Brandão, T. A. S., Johnson, S. J. & Hengge, A. C. The molecular details of WPD-loop movement differ in the protein-tyrosine phosphatases YopH and PTP1B. *Arch. Biochem. Biophys.* **525,** 53–59 (2012).

215. Fauman, E. B., Yuvaniyama, C., Schubert, H. L., Stuckey, J. A. & Saper, M. A. The X-ray crystal structures of Yersinia tyrosine phosphatase with bound tungstate and nitrate.

Mechanistic implications. *J. Biol. Chem.* **271,** 18780–8 (1996).

216. Bakke, J. & Haj, F. G. Protein-tyrosine phosphatase 1B substrates and metabolic regulation. *Semin. Cell Dev. Biol.* **37,** 58–65 (2015).

217. Luo, J. & Cantley, L. C. Then Negative Regulation of Phosphoinositide 3-Kinase Signaling by p85 and Its Implication in Cancer. *Cell Cycle* **4,** 1309–1312 (2005).

218. Avruch, J. Insulin signal transduction through protein kinase cascades. *Mol. Cell. Biochem.* **182,** 31–48 (1998).

219. Elchebly, M. *et al.* Increased insulin sensitivity and obesity resistance in mice lacking the protein tyrosine phosphatase-1B gene. *Science* **283,** 1544–8 (1999).

220. Owen, C. *et al.* Inducible liver-specific knockdown of protein tyrosine phosphatase 1B improves glucose and lipid homeostasis in adult mice. *Diabetologia* **56,** 2286–2296 (2013).

221. Delibegovic, M. *et al.* Liver-Specific Deletion of Protein-Tyrosine Phosphatase 1B (PTP1B) Improves Metabolic Syndrome and Attenuates Diet-Induced Endoplasmic Reticulum Stress. *Diabetes* **58,** 590–599 (2009).

222. Delibegovic, M. *et al.* Improved Glucose Homeostasis in Mice with Muscle-Specific Deletion of Protein-Tyrosine Phosphatase 1B. *Mol. Cell. Biol.* **27,** 7727–7734 (2007).

223. Grant, L. *et al.* Myeloid-Cell Protein Tyrosine Phosphatase-1B Deficiency in Mice Protects Against High-Fat Diet and Lipopolysaccharide-Induced Inflammation, Hyperinsulinemia, and Endotoxemia Through an IL-10 STAT3-Dependent Mechanism. *Diabetes* **63,** 456–470 (2014).

224. Zabolotny, J. M. *et al.* Transgenic Overexpression of Protein-tyrosine Phosphatase 1B in Muscle Causes Insulin Resistance, but Overexpression with Leukocyte Antigen-

related Phosphatase Does Not Additively Impair Insulin Action. *J. Biol. Chem.* **279,** 24844–24851 (2004).

225. Haj, F. G., Zabolotny, J. M., Kim, Y.-B., Kahn, B. B. & Neel, B. G. Liver-specific Protein-tyrosine Phosphatase 1B (PTP1B) Re-expression Alters Glucose Homeostasis of PTP1B–/–Mice. *J. Biol. Chem.* **280,** 15038–15046 (2005).

226. Hummasti, S. & Hotamisligil, G. S. Endoplasmic Reticulum Stress and Inflammation in Obesity and Diabetes. *Circ. Res.* **107,** 579–591 (2010).

227. Kaufman, R. J. *et al.* The unfolded protein response in nutrient sensing and differentiation. *Nat. Rev. Mol. Cell Biol.* **3,** 411–421 (2002).

228. Su, Q. *et al.* Modulation of the Eukaryotic Initiation Factor 2 α-Subunit Kinase PERK by Tyrosine Phosphorylation. *J. Biol. Chem.* **283,** 469–475 (2008).

229. Krishnan, N., Fu, C., Pappin, D. J. & Tonks, N. K. H2S-Induced Sulfhydration of the Phosphatase PTP1B and Its Role in the Endoplasmic Reticulum Stress Response. *Sci. Signal.* **4,** ra86-ra86 (2011).

230. Agouni, A. *et al.* Liver-specific deletion of protein tyrosine phosphatase (PTP) 1B improves obesity- and pharmacologically induced endoplasmic reticulum stress. *Biochem. J.* **438,** 369–378 (2011).

231. Bettaieb, A. *et al.* Protein Tyrosine Phosphatase 1B Deficiency Potentiates PERK/eIF2α Signaling in Brown Adipocytes. *PLoS One* **7,** e34412 (2012).

232. Bettaieb, A. *et al.* Differential Regulation of Endoplasmic Reticulum Stress by Protein Tyrosine Phosphatase 1B and T Cell Protein Tyrosine Phosphatase. *J. Biol. Chem.* **286,** 9225–9235 (2011).

233. Jain, R. *et al.* Pharmacological inhibition of Eph receptors

enhances glucose-stimulated insulin secretion from mouse and human pancreatic islets. *Diabetologia* **56,** 1350–1355 (2013).

234. Haj, F. G. *et al.* Regulation of Signaling at Regions of Cell-Cell Contact by Endoplasmic Reticulum-Bound Protein-Tyrosine Phosphatase 1B. *PLoS One* **7,** e36633 (2012).

235. Liu, S. *et al.* Disruption of Protein-Tyrosine Phosphatase 1B Expression in the Pancreas Affects β-Cell Function. *Endocrinology* **155,** 3329–3338 (2014).

236. Zhang, Y. *et al.* Positional cloning of the mouse obese gene and its human homologue. *Nature* **372,** 425–432 (1994).

237. Ahima, R. S. & Osei, S. Y. Leptin signaling. *Physiol. Behav.* **81,** 223–241 (2004).

238. Tsou, R. C., Rak, K. S., Zimmer, D. J. & Bence, K. K. Improved metabolic phenotype of hypothalamic PTP1B-deficiency is dependent upon the leptin receptor. *Mol. Metab.* **3,** 301–312 (2014).

239. Zabolotny, J. M. *et al.* PTP1B regulates leptin signal transduction in vivo. *Dev. Cell* **2,** 489–95 (2002).

240. Cheng, A. *et al.* Attenuation of leptin action and regulation of obesity by protein tyrosine phosphatase 1B. *Dev. Cell* **2,** 497–503 (2002).

241. Bettaieb, A. *et al.* Protein Tyrosine Phosphatase 1B Regulates Pyruvate Kinase M2 Tyrosine Phosphorylation. *J. Biol. Chem.* **288,** 17360–17371 (2013).

242. Kayne, F. J. & Price, N. C. Amino acid effector binding to rabbit muscle pyruvate kinase. *Arch. Biochem. Biophys.* **159,** 292–6 (1973).

243. Nakamura, Y. *et al.* Role of Protein Tyrosine Phosphatase 1B in Vascular Endothelial Growth Factor Signaling and Cell-Cell Adhesions in Endothelial Cells. *Circ. Res.* **102,** 1182–1191

(2008).

244. Fernandez-Ruiz, R., Vieira, E., Garcia-Roves, P. M. & Gomis, R. Protein tyrosine phosphatase-1B modulates pancreatic β-cell mass. *PLoS One* **9,** e90344 (2014).

245. Liu, S. *et al.* Disruption of protein-tyrosine phosphatase 1B expression in the pancreas affects β-cell function. *Endocrinology* **155,** 3329–38 (2014).

246. Matsumoto, T. & Claesson-Welsh, L. VEGF receptor signal transduction. *Sci. STKE* **2001,** re21 (2001).

247. Wallez, Y., Vilgrain, I. & Huber, P. Angiogenesis: the VE-cadherin switch. *Trends Cardiovasc. Med.* **16,** 55–9 (2006).

248. Millauer, B. *et al.* High affinity VEGF binding and developmental expression suggest Flk-1 as a major regulator of vasculogenesis and angiogenesis. *Cell* **72,** 835–46 (1993).

249. Quinn, T. P., Peters, K. G., De Vries, C., Ferrara, N. & Williams, L. T. Fetal liver kinase 1 is a receptor for vascular endothelial growth factor and is selectively expressed in vascular endothelium. *Proc. Natl. Acad. Sci. U. S. A.* **90,** 7533–7 (1993).

250. Oelrichs, R. B., Reid, H. H., Bernard, O., Ziemiecki, A. & Wilks, A. F. NYK/FLK-1: a putative receptor protein tyrosine kinase isolated from E10 embryonic neuroepithelium is expressed in endothelial cells of the developing embryo. *Oncogene* **8,** 11–8 (1993).

251. Holmes, K., Roberts, O. L., Thomas, A. M. & Cross, M. J. Vascular endothelial growth factor receptor-2: Structure, function, intracellular signalling and therapeutic inhibition. *Cell. Signal.* **19,** 2003–2012 (2007).

252. Simons, M., Gordon, E. & Claesson-Welsh, L. Mechanisms and regulation of endothelial VEGF receptor signalling. *Nat. Rev. Mol. Cell Biol.* **17,** 611–625 (2016).

253. Koch, S. & Claesson-Welsh, L. Signal Transduction by Vascular Endothelial Growth Factor Receptors. *Cold Spring Harb. Perspect. Med.* **2,** a006502–a006502 (2012).

254. Sugano, M., Tsuchida, K. & Makino, N. A protein tyrosine phosphatase inhibitor accelerates angiogenesis in a rat model of hindlimb ischemia. *J. Cardiovasc. Pharmacol.* **44,** 460–5 (2004).

255. Tonks, N. K. PTP1B: from the sidelines to the front lines! *FEBS Lett.* **546,** 140–8 (2003).

256. Nakamura, Y. *et al.* Role of Protein Tyrosine Phosphatase 1B in Vascular Endothelial Growth Factor Signaling and Cell–Cell Adhesions in Endothelial Cells. *Circ. Res.* **102,** 1182–1191 (2008).

257. Chang, Y. Increase of PTP levels in vascular injury and in cultured aortic smooth muscle cells treated with specific growth factors. *AJP Hear. Circ. Physiol.* **287,** H2201–H2208 (2004).

258. Speier, S. *et al.* Noninvasive in vivo imaging of pancreatic islet cell biology. *Nat. Med.* **14,** 574–578 (2008).

259. Klaman, L. D. *et al.* Increased energy expenditure, decreased adiposity, and tissue-specific insulin sensitivity in protein-tyrosine phosphatase 1B-deficient mice. *Mol. Cell. Biol.* **20,** 5479–89 (2000).

260. Hayashi, K., Kojima, R. & Ito, M. Strain differences in the diabetogenic activity of streptozotocin in mice. *Biol. Pharm. Bull.* **29,** 1110–9 (2006).

261. Deeds, M. C. *et al.* Single dose streptozotocin-induced diabetes: considerations for study design in islet transplantation models. *Lab. Anim.* **45,** 131–40 (2011).

262. Rerup, C. C. Drugs producing diabetes through damage of the insulin secreting cells. *Pharmacol. Rev.* **22,** 485–518 (1970).

263. Weiss, R. B. Streptozocin: a review of its pharmacology, efficacy, and toxicity. *Cancer Treat. Rep.* **66,** 427–38 (1982).

264. Bennett, R. A. & Pegg, A. E. Alkylation of DNA in rat tissues following administration of streptozotocin. *Cancer Res.* **41,** 2786–90 (1981).

265. Bolzán, A. D. & Bianchi, M. S. Genotoxicity of streptozotocin. *Mutat. Res.* **512,** 121–34 (2002).

266. Lenzen, S. The mechanisms of alloxan- and streptozotocin-induced diabetes. *Diabetologia* **51,** 216–226 (2008).

267. Tjälve, H., Wilander, E. & Johansson, E. B. Distribution of labelled streptozotocin in mice: uptake and retention in pancreatic islets. *J. Endocrinol.* **69,** 455–6 (1976).

268. Karunanayake, E. H., Baker, J. R., Christian, R. A., Hearse, D. J. & Mellows, G. Autoradiographic study of the distribution and cellular uptake of (14C) - streptozotocin in the rat. *Diabetologia* **12,** 123–8 (1976).

269. Nyqvist, D. *et al.* Donor islet endothelial cells in pancreatic islet revascularization. *Diabetes* **60,** 2571–7 (2011).

270. Speier, S. *et al.* Noninvasive high-resolution in vivo imaging of cell biology in the anterior chamber of the mouse eye. *Nat. Protoc.* **3,** 1278–86 (2008).

271. Adeghate, E. Host-graft circulation and vascular morphology in pancreatic tissue transplants in rats. *Anat. Rec.* **251,** 448–59 (1998).

272. Adeghate, E. & Donáth, T. Morphological findings in long-term pancreatic tissue transplants in the anterior eye chamber of rats. *Pancreas* **5,** 298–305 (1990).

273. Cousins, S. W., McCabe, M. M., Danielpour, D. & Streilein, J. W. Identification of transforming growth factor-beta as an immunosuppressive factor in aqueous humor. *Invest. Ophthalmol. Vis. Sci.* **32,** 2201–11 (1991).

274. Niederkorn, J. Y. Immune privilege in the anterior chamber of the eye. *Crit. Rev. Immunol.* **22,** 13–46 (2002).

275. Becker, H. M., Chen, M., Hay, J. B. & Cybulsky, M. I. Tracking of leukocyte recruitment into tissues of mice by in situ labeling of blood cells with the fluorescent dye CFDA SE. *J. Immunol. Methods* **286,** 69–78 (2004).

276. Wang, X.-Q., Duan, X.-M., Liu, L.-H., Fang, Y.-Q. & Tan, Y. Carboxyfluorescein diacetate succinimidyl ester fluorescent dye for cell labeling. *Acta Biochim. Biophys. Sin. (Shanghai).* **37,** 379–85 (2005).

277. Dumitriu, I. E. *et al.* 5,6-Carboxyfluorescein Diacetate Succinimidyl Ester-Labeled Apoptotic and Necrotic as Well as Detergent-Treated Cells Can Be Traced in Composite Cell Samples. *Anal. Biochem.* **299,** 247–252 (2001).

278. Abdulreda, M. H., Caicedo, A. & Berggren, P.-O. Transplantation into the anterior chamber of the eye for longitudinal, non-invasive in vivo imaging with single-cell resolution in real-time. *J. Vis. Exp.* e50466 (2013). doi:10.3791/50466

279. Leibiger, I. B. & Berggren, P.-O. Intraocularin vivoimaging of pancreatic islet cell physiology/pathology. *Mol. Metab.* **6,** 1002–1009 (2017).

280. Cahalan, M. D., Parker, I., Wei, S. H. & Miller, M. J. Two-photon tissue imaging: seeing the immune system in a fresh light. *Nat. Rev. Immunol.* **2,** 872–880 (2002).

281. Denk, W., Strickler, J. H. & Webb, W. W. Two-photon laser scanning fluorescence microscopy. *Science* **248,** 73–6 (1990).

282. Leathers, T. D. in *Biopolymers Online* (eds. Vandamme, E. J., De Baets, S. & Steinbüchel, A.) (Wiley-VCH Verlag GmbH & Co. KGaA, 2005). doi:10.1002/3527600035.bpol5012

283. Shedd, D. P. Dextran and Its Use in Colloidal Infusion

Solutions. *Yale J. Biol. Med.* **30,** 75 (1957).

284. Bellhorn, M. B., Bellhorn, R. W. & Poll, D. S. Permeability of fluorescein-labelled dextrans in fundus fluorescein angiography of rats and birds. *Exp. Eye Res.* **24,** 595–605 (1977).

285. Vérant, P., Serduc, R., Van Der Sanden, B., Rémy, C. & Vial, J.-C. A Direct Method for Measuring Mouse Capillary Cortical Blood Volume Using Multiphoton Laser Scanning Microscopy. *J. Cereb. Blood Flow Metab.* **27,** 1072–1081 (2007).

286. Egawa, G. *et al.* Intravital analysis of vascular permeability in mice using two-photon microscopy. *Sci. Rep.* **3,** 1932 (2013).

287. Pollack, A. & Ciancio, G. Cell cycle phase-specific analysis of cell viability using Hoechst 33342 and propidium iodide after ethanol preservation. *Methods Cell Biol.* **33,** 19–24 (1990).

288. Aerts, J., Nys, J. & Arckens, L. A Highly Reproducible and Straightforward Method to Perform In Vivo Ocular Enucleation in the Mouse after Eye Opening. *J. Vis. Exp.* e51936–e51936 (2014). doi:10.3791/51936

289. Schmucker, C. & Schaeffel, F. A paraxial schematic eye model for the growing C57BL/6 mouse. *Vision Res.* **44,** 1857–1867 (2004).

290. Schmucker, C. & Schaeffel, F. In vivo biometry in the mouse eye with low coherence interferometry. *Vision Res.* **44,** 2445–2456 (2004).

291. Zhou, X. *et al.* Biometric measurement of the mouse eye using optical coherence tomography with focal plane advancement. *Vision Res.* **48,** 1137–1143 (2008).

292. Brelje, T. C., Scharp, D. W. & Sorenson, R. L. Three-dimensional imaging of intact isolated islets of Langerhans with confocal microscopy. *Diabetes* **38,** 808–14 (1989).

293. Ricordi, C., Lacy, P. E., Finke, E. H., Olack, B. J. & Scharp, D. W. Automated method for isolation of human pancreatic islets. *Diabetes* **37,** 413–20 (1988).

294. Bucher, P. *et al.* Assessment of a novel two-component enzyme preparation for human islet isolation and transplantation. *Transplantation* **79,** 91–7 (2005).

295. Murdoch, T. B., McGhee-Wilson, D., Shapiro, A. M. J. & Lakey, J. R. T. Methods of Human Islet Culture for Transplantation. *Cell Transplant.* **13,** 605–617 (2004).

296. Jimenez-Moreno, C. M. *et al.* A Simple High Efficiency Intra-Islet Transduction Protocol Using Lentiviral Vectors. *Curr. Gene Ther.* **15,** 436–46 (2015).

297. Li, F. & Mahato, R. I. RNA interference for improving the outcome of islet transplantation. *Adv. Drug Deliv. Rev.* **63,** 47–68 (2011).

298. Bertrand, J.-R. *et al.* Comparison of antisense oligonucleotides and siRNAs in cell culture and in vivo. *Biochem. Biophys. Res. Commun.* **296,** 1000–4 (2002).

299. Bettaieb, A. *et al.* Differential regulation of endoplasmic reticulum stress by protein tyrosine phosphatase 1B and T cell protein tyrosine phosphatase. *J. Biol. Chem.* **286,** 9225–35 (2011).

300. Lanahan, A. A. *et al.* PTP1b Is a Physiologic Regulator of Vascular Endothelial Growth Factor Signaling in Endothelial Cells. *Circulation* **130,** 902–9 (2014).

301. Brissova, M. *et al.* Intraislet endothelial cells contribute to revascularization of transplanted pancreatic islets. *Diabetes* **53,** 1318–25 (2004).

302. Nyqvist, D., Köhler, M., Wahlstedt, H. & Berggren, P.-O. Donor islet endothelial cells participate in formation of functional vessels within pancreatic islet grafts. *Diabetes* **54,** 2287–93

(2005).

303. Liljebäck, H., Grapensparr, L., Olerud, J. & Carlsson, P.-O. Extensive Loss of Islet Mass beyond the First Day after Intraportal Human Islet Transplantation in a Mouse Model. *Cell Transplant.* **25,** 481–489 (2016).

304. Del Toro-Arreola, A., Robles-Murillo, A. K., Daneri-Navarro, A. & Rivas-Carrillo, J. D. The role of endothelial cells on islet function and revascularization after islet transplantation. *Organogenesis* **12,** 28–32 (2016).

305. Fotino, N., Fotino, C. & Pileggi, A. Re-engineering islet cell transplantation. *Pharmacol. Res.* **98,** 76–85 (2015).

306. Morini, S. *et al.* Revascularization and remodelling of pancreatic islets grafted under the kidney capsule. *J. Anat.* **210,** 565 (2007).

307. Plesner, A. & Verchere, C. B. Advances and challenges in islet transplantation: islet procurement rates and lessons learned from suboptimal islet transplantation. *J. Transplant.* **2011,** 979527 (2011).

308. Osterburg, A. R. *et al.* Oral tungstate (Na $_2$ WO $_4$) exposure reduces adaptive immune responses in mice after challenge. *J. Immunotoxicol.* **11,** 148–159 (2014).

309. Pacher, P., Nivorozhkin, A. & Szabó, C. Therapeutic Effects of Xanthine Oxidase Inhibitors: Renaissance Half a Century after the Discovery of Allopurinol. *Pharmacol. Rev.* **58,** 87–114 (2006).

310. Vorbach, C., Harrison, R. & Capecchi, M. R. Xanthine oxidoreductase is central to the evolution and function of the innate immune system. *Trends Immunol.* **24,** 512–7 (2003).

311. Umezawa, K., Akaike, T., Fujii, S., … M. S.-I. and & 1997, undefined. Induction of nitric oxide synthesis and xanthine oxidase and their roles in the antimicrobial mechanism against

Salmonella typhimurium infection in mice. *Am Soc Microbiol* at
<http://iai.asm.org/content/65/7/2932.short>

312. Wright, R. M. *et al.* Mononuclear Phagocyte Xanthine Oxidoreductase Contributes to Cytokine-Induced Acute Lung Injury. *Am. J. Respir. Cell Mol. Biol.* **30,** 479–490 (2004).

313. Maemura, K. *et al.* Reactive oxygen species are essential mediators in antigen presentation by Kupffer cells. *Immunol. Cell Biol.* **83,** 336–343 (2005).

314. Stankiewicz, P. J. & Gresser, M. J. Inhibition of phosphatase and sulfatase by transition-state analogues. *Biochemistry* **27,** 206–12 (1988).

315. Guandalini, G. S. *et al.* Tissue distribution of tungsten in mice following oral exposure to sodium tungstate. *Chem. Res. Toxicol.* **24,** 488–93 (2011).

316. Sarmiento, M., Zhao, Y., Gordon, S. J. & Zhang, Z. Y. Molecular basis for substrate specificity of protein-tyrosine phosphatase 1B. *J. Biol. Chem.* **273,** 26368–74 (1998).

317. Huyer, G. *et al.* Mechanism of inhibition of protein-tyrosine phosphatases by vanadate and pervanadate. *J. Biol. Chem.* **272,** 843–51 (1997).

318. Linn, T. *et al.* Angiogenic capacity of endothelial cells in islets of Langerhans. *FASEB J.* **17,** 881–3 (2003).

319. Lopez, P., Wagner, K.-D., Hofman, P. & Van Obberghen, E. RNA Activation of the Vascular Endothelial Growth Factor Gene (VEGF) Promoter by Double-Stranded RNA and Hypoxia: Role of Noncoding VEGF Promoter Transcripts. *Mol. Cell. Biol.* **36,** 1480–93 (2016).

320. London, N. J., Swift, S. M. & Clayton, H. A. Isolation, culture and functional evaluation of islets of Langerhans. *Diabetes Metab.* **24,** 200–7 (1998).

321. Sabek, O. M., Marshall, D. R., Penmetsa, R., Scarborough, O.

& Gaber, A. O. Examination of Gene Expression Profile of Functional Human Pancreatic Islets After 2-Week Culture. *Transplant. Proc.* **38,** 3678–3679 (2006).

322. Boker, A. *et al.* Human islet transplantation: update. *World J. Surg.* **25,** 481–6 (2001).

323. McCall, M. & Shapiro, A. M. J. Update on islet transplantation. *Cold Spring Harb. Perspect. Med.* **2,** a007823 (2012).

324. Ahluwalia, A. & Tarnawski, A. S. Critical role of hypoxia sensor--HIF-1α in VEGF gene activation. Implications for angiogenesis and tissue injury healing. *Curr. Med. Chem.* **19,** 90–7 (2012).

325. Warnock, G. L. *et al.* An odyssey of islet transplantation for therapy of type 1 diabetes. *World J. Surg.* **31,** 1569–76 (2007).

326. Ali, Y. *et al.* The anterior chamber of the eye is a transplantation site that supports and enables visualisation of beta cell development in mice. *Diabetologia* **59,** 1007–11 (2016).

327. Goel, M., Picciani, R. G., Lee, R. K. & Bhattacharya, S. K. Aqueous humor dynamics: a review. *Open Ophthalmol. J.* **4,** 52–9 (2010).

328. Haddad, A., Laicine, E. M. & de Almeida, J. C. Origin and renewal of the intrinsic glycoproteins of the aqueous humor. *Graefe's Arch. Clin. Exp. Ophthalmol. = Albr. von Graefes Arch. für Klin. und Exp. Ophthalmol.* **229,** 371–9 (1991).

329. Aihara, M., Lindsey, J. D. & Weinreb, R. N. Aqueous humor dynamics in mice. *Invest. Ophthalmol. Vis. Sci.* **44,** 5168–73 (2003).

330. Puigserver, P. & Spiegelman, B. M. Peroxisome Proliferator-Activated Receptor-γ Coactivator 1α (PGC-1α): Transcriptional Coactivator and Metabolic Regulator. *Endocr. Rev.* **24,** 78–90 (2003).

331. Puigserver, P. *et al.* A cold-inducible coactivator of nuclear receptors linked to adaptive thermogenesis. *Cell* **92,** 829–39 (1998).

332. Schreiber, S. N., Knutti, D., Brogli, K., Uhlmann, T. & Kralli, A. The Transcriptional Coactivator PGC-1 Regulates the Expression and Activity of the Orphan Nuclear Receptor Estrogen-Related Receptor α (ERRα). *J. Biol. Chem.* **278,** 9013–9018 (2003).

333. Knutti, D. & Kralli, A. PGC-1, a versatile coactivator. *Trends Endocrinol. Metab.* **12,** 360–5 (2001).

334. Lehman, J. J. *et al.* Peroxisome proliferator–activated receptor γ coactivator-1 promotes cardiac mitochondrial biogenesis. *J. Clin. Invest.* **106,** 847–856 (2000).

335. Wu, Z. *et al.* Mechanisms Controlling Mitochondrial Biogenesis and Respiration through the Thermogenic Coactivator PGC-1. *Cell* **98,** 115–124 (1999).

336. Schreiber, S. N. *et al.* The estrogen-related receptor alpha (ERRalpha) functions in PPARgamma coactivator 1alpha (PGC-1alpha)-induced mitochondrial biogenesis. *Proc. Natl. Acad. Sci. U. S. A.* **101,** 6472–7 (2004).

337. Huss, J. M., Kopp, R. P. & Kelly, D. P. Peroxisome Proliferator-activated Receptor Coactivator-1α (PGC-1α) Coactivates the Cardiac-enriched Nuclear Receptors Estrogen-related Receptor-α and -γ. *J. Biol. Chem.* **277,** 40265–40274 (2002).

338. Saint-Geniez, M. *et al.* PGC-1α regulates normal and pathological angiogenesis in the retina. *Am. J. Pathol.* **182,** 255–65 (2013).

339. Li, G. *et al.* Multifunctional *in vivo* imaging of pancreatic islets during diabetes development. *J. Cell Sci.* **129,** 2865–2875 (2016).

340. Wang, X. *et al.* Improving islet engraftment by gene therapy. *J. Transplant.* **2011,** 594851 (2011).